INFORMATION TO USERS

This manuscript has been reproduced from the microfilm master. UMI films the text directly from the original or copy submitted. Thus, some thesis and dissertation copies are in typewriter face, while others may be from any type of computer printer.

The quality of this reproduction is dependent upon the quality of the copy submitted. Broken or indistinct print, colored or poor quality illustrations and photographs, print bleedthrough, substandard margins, and improper alignment can adversely affect reproduction.

In the unlikely event that the author did not send UMI a complete manuscript and there are missing pages, these will be noted. Also, if unauthorized copyright material had to be removed, a note will indicate the deletion.

Oversize materials (e.g., maps, drawings, charts) are reproduced by sectioning the original, beginning at the upper left-hand corner and continuing from left to right in equal sections with small overlaps.

ProQuest Information and Learning
300 North Zeeb Road, Ann Arbor, MI 48106-1346 USA
800-521-0600

POST-ELASTIC BEHAVIOR

OF BOLTED CONNECTIONS IN WOOD

by

Nourhene Kharouf

May 2001

Department of Civil Engineering and Applied Mechanics
McGill University
Montreal, Canada

A thesis submitted to the Faculty of Graduate Studies and Research
in partial fulfilment of the requirements for
the degree of Doctor of Philosophy

© Nourhene Kharouf, 2001

National Library of Canada
Acquisitions and Bibliographic Services
395 Wellington Street
Ottawa ON K1A 0N4
Canada

Bibliothèque nationale du Canada
Acquisitions et services bibliographiques
395, rue Wellington
Ottawa ON K1A 0N4
Canada

Your file Votre référence

Our file Notre référence

The author has granted a non-exclusive licence allowing the National Library of Canada to reproduce, loan, distribute or sell copies of this thesis in microform, paper or electronic formats.

L'auteur a accordé une licence non exclusive permettant à la Bibliothèque nationale du Canada de reproduire, prêter, distribuer ou vendre des copies de cette thèse sous la forme de microfiche/film, de reproduction sur papier ou sur format électronique.

The author retains ownership of the copyright in this thesis. Neither the thesis nor substantial extracts from it may be printed or otherwise reproduced without the author's permission.

L'auteur conserve la propriété du droit d'auteur qui protège cette thèse. Ni la thèse ni des extraits substantiels de celle-ci ne doivent être imprimés ou autrement reproduits sans son autorisation.

0-612-70060-7

Canada

To the Memory of my Father

ABSTRACT

A nonlinear finite element model is developed to study the behavior of single- and double-bolted timber connections with relatively low member thickness-to-fastener diameter ratios. These structural joints tend to fail in a brittle fashion. The established model is capable of predicting the post-elastic deformations of the connections locally and globally, and the unequal load fractions transferred by each bolt in a two-fastener connection.

The ADINA software package is used to generate the model. The problem presents two types of non-linearity. The first is due to geometric effects caused by increased sliding contact between the bolts and the oversized holes in the wood member. Contact is simulated using the Lagrange Multiplier algorithm available in ADINA. This algorithm enforces the compatibility of surface displacements at the wood member which is the contactor surface, and Coulomb frictional conditions over the contact segments, with a coefficient of friction of 0.7. The second non-linearity results from the material post-elastic behavior adjacent to the contact points. A plasticity-based compressive constitutive material model is developed to represent wood as elasto-plastic orthotropic according to the Hill yield criterion in regions of bi-axial compression. Linear elastic orthotropic response is applied otherwise. The model is incorporated as a user-supplied material model of ADINA to carry out the analysis.

The performance of the program and the effectiveness of the elasto-plastic material model are first verified with examples from the literature. Thereafter, numerical

simulations of the post-elastic deformations of one- and two-bolt connections are compared to experimental results from tensile tests undertaken on glued-laminated timber connections with stocky bolts and subject to monotonic loading. Characterization tests are undertaken to obtain stiffness and strength for compression and tension parallel and perpendicular to grain, and shear, required as input in the new material model. Five configurations of single-bolt connections and four configurations of double-bolt connections have been tested with different combinations of end distance, edge distance, and spacing between bolts. Reasonable agreement is found between numerical and experimental load vs. strains obtained using single axis strain gages and strain rosettes mounted in regions of stress concentrations. The model is capable of tracing the post-elastic global deformation as obtained from experimental load vs. displacements of LVDT's mounted on specimens. The non-linearity of these load-slip curves is primarily caused by the inelastic wood deformation beneath the bolts at low load levels. This behavior explains the redistribution of load proportions among the bolts in a double-bolt connection. Under test configurations forces are unequally shared between the bolts even at the ultimate load. As a consequence, joint capacity as estimated with the proposed elasto-plastic material model is bounded by the so-called European Yield Model, which assumes equal load distribution among the bolts at ultimate, and the linear elastic model. Observed shear-out brittle failures of wood bolted connections are believed to be caused by excessive combined shear and tension perpendicular to grain along the sides of the contact zone.

RÉSUMÉ

L'auteure a développé un modèle d'élément fini non linéaire pour l'analyse des connexions boulonnées simples et doubles de pièces en bois avec faible rapport épaisseur/diamètre du boulon, sous charge statique monotone. Ces connexions ont tendance à avoir un mode de rupture fragile. Le modèle proposé est capable de prédire l'évolution des déformations post-élastiques locales et globales de ces connexions, ainsi que la redistribution de la proportion de la charge résistée par chaque boulon dans les connexions à deux boulons.

Le modèle a été développé à l'aide du logiciel d'analyse commercial ADINA. Le problème combine des non linéarités de nature géométrique et constitutive. Les non linéarités géométriques proviennent du glissement et du contact entre les boulons et les surfaces des trous dans lesmembrures en bois. Le phénomène de contact est modélisé par un algorithme basé sur la méthode des multiplicateurs de Lagrange disponible dans ADINA. Cet algorithme établit la compatibilité des déplacements des surfaces en contact, à la surface de la pièce en bois, et impose les conditions de frottement de type Coulomb (avec coefficient de frottement de 0.7) sur les segments en contact. Les non linéarités constitutives dans le bois se manifestent dans les régions avoisinantes aux surface de contact avec le boulon. L'auteure a développé un modèle constitutif original pour le comportement en compression du bois dans ces régions. Le modèle est de type élasto-plastique orthotrope selon la règle de plasticité de Hill dans le domaine de la compression bi-axiale. Le modèle linéaire élastique orthotrope classique s'applique pour

les autres domaines de contraintes. Ce modèle est intégré dans ADINA pour l'analyse par éléments finis des connexions boulonnées.

La performance du programme ainsi que la précision du modèle élasto-plastique orthotrope proposé ont d'abord été vérifiées à partir de résultats expérimentaux obtenus par d'autres chercheurs et publiés dans la littérature technique. Par la suite, des simulations numériques ont été faites pour des modèles correspondant à des nouveaux spécimens de connexions boulonnées de plaques en bois lamellé-collé, testés sous charge de traction monotone. Des tests de caractérisation du matériau ont été faits afin d'obtenir des valeurs représentatives pour les divers paramètres du modèle proposé, tels la rigidité et résistance en traction et en compression dans les directions orthotropes principales ainsi qu'en cisaillement. Cinq agencements de connexions à un boulon et quatre agencements de connexions à deux boulons ont été testés avec diverses combinaisons de distance au bout, distance au bord et espacement entre les boulons. Des jauges de déformation simples ainsi que des rosettes ont été utilisées à la surface des pièces en bois, dans les régions à concentration de contraintes, et des transducteurs à voltage linéaire (LVDT) ont été installés pour mesurer l'historique des déplacements des pièces connectées en fonction de la charge appliquée. Les résultats obtenus par modélisation numérique concordent bien avec les mesures expérimentales des déformations. Le modèle d'analyse peut également reproduire le comportement post-élastique non linéaire global obtenu lors des tests pour les déplacements en fonction de la charge. Ces non linéarités résultent des déformations inélastiques du bois au contact des boulons à des niveaux de charge relativement faibles. Ce comportement explique aussi la redistribution des efforts entre les boulons prédite par le modèle

numérique pour les connexions à deux boulons. Toutefois, même au niveau de la charge ultime, la distribution des efforts entre les deux boulons reste inégale. Ainsi, la capacité de la connexion estimée à l'aide du modèle élasto-plastique non linéaire proposé se situe entre la valeur prédite par le modèle de rupture européen (*European Yield Model*), qui suppose une redistribution égale de la charge à tous les boulons à l'ultime, et celle prédite selon le modèle linéaire élastique. L'auteure explique également que les ruptures de connexion par déchirement d'une bande derrière les boulons sont initiées par des fortes contraintes combinées de cisaillement et traction perpendiculaire au grain du bois au droit des côtés des zones de contact avec le boulon.

ACKNOWLEGEMENTS

The author wants to express her deepest gratitude to her thesis supervisor, Professor Ghyslaine McClure for her guidance, valuable comments, and continuous support and advice throughout her academic years at McGill University. The author also thanks her co-supervisor, Professor Ian Smith, for his assistance and valuable suggestions and comments on the research subject.

Special thanks are due to Dr. Mohammad Mohammad for undertaking the required experimental tests at the Structure Laboratory of the Royal Military College of Canada in Kingston, Ontario and providing the data in best delays.

The author wants to extend her thanks to the research team in the collaborative project on "Failure Mechanisms for Structural Connections in Wood-Fiber Composites": Dr. Pierre Quenneville, Dr. Donming Tan, Ms. Svetlana Vasic, and Ms. Maya Sawaya for their suggestions and constructive discussions during the collaborative project meetings.

The financial support provided by the Natural Science and Engineering Research Council in Canada and the Canadian Wood Council is greatly acknowledged.

Most of all, the author is indebted to her husband, Hazem for his support, critical comments on the subject and help, her daughter, Azza, and her son, Iyadh Mahmoud for their love and kindness. The author is grateful to her dear mother for her love and care, her parents in law for their support, and all her friends and family for their encouragement.

TABLE OF CONTENTS

LIST OF SYMBOLS

A	=	anisotropic strength parameters
a	=	flow vector
a_i	=	crack length including the intense energy region
C^e	=	elastic stiffness matrix
C^e	=	elasto-plastic stiffness matrix
$[D^e]$	=	elastic compliance matrix
D_t	=	characteristic length for tension
D_c	=	characteristic length for compression
$\{d\varepsilon\}$	=	total strain increment
$\{d\varepsilon^e\}$	=	elastic components of total strain increment
$\{d\varepsilon^p\}$	=	plastic components of total strain increment
$d\lambda$	=	plastic multiplier
d	=	bolt diameter
E_c	=	modulus of elasticity in compression
E_t	=	modulus of elasticity in tension
E_p	=	plastic modulus
E_T	=	Tangent modulus
e	=	end distance
f	=	yield function
$f(\sigma)$	=	probability of failure
G	=	shear modulus
G_p	=	plastic shear modulus
G_T	=	Tangent shear modulus
k	=	scalar parameter which stands for a reference yield stress
K	=	stress intensity factor
K_{Ic}	=	fracture toughness
l	=	member thickness
P	=	applied load

r	=	radius of the notch
s	=	spacing between the bolts
s_1, s_2	=	complex roots of characteristic equation in the stress function
S	=	shear strength
T	=	Traction
u	=	displacement
V_r	=	representative volume of the material
w	=	edge distance
α	=	origin of the yield surface
ε	=	strain
χ	=	termed hardening parameter
γ	=	shear strain
μ	=	friction coefficient
ν	=	Poisson's ratio
σ	=	stress
σ_e	=	effective stress
σ_c	=	compressive strength
σ_t	=	tensile strength
σ_0	=	unnotched strength
σ_c	=	critical stress
τ	=	shear stress
θ	=	polar coordinates of an element ahead of a crack tip
Π	=	resulting incremental potential
Π_t	=	incremental total potential
$\Sigma_K W_K$	=	total potential of the contact forces

Subscripts

i, j	=	positive integer indices
n, t	=	indices for normal and tangential directions

r, θ	=	indices for radial and tangential directions
a	=	average
c	=	critical
L,T,R	=	indices for longitudinal, tangential, and radial directions
//	=	parallel to grain
$\perp$	=	perpendicular to grain

Superscripts

(i)	=	iteration I

LIST OF FIGURES

LIST OF TABLES

CHAPTER 1

INTRODUCTION

The evolution of joints was central to wood technologies of even ancient societies. Today methods of joining may be adhesive bonding or mechanical fastening. In many situations, the latter method is preferred because of its capability for repeated assembly, ease of inspection, high reliability, and tolerance to the environment. Dowel-type fasteners include drift pins, bolts, lag screws, nails, spikes, and rivets, with nails or bolts being the most common types. Both nails and bolts are used to join thin or thick members. While these structural joints can, by design, provide the capacity for load transfer from one component to others, they are often the weakest links in wood structural systems (Foliente 1998). Premature failures of bolted connections are due to the inherent high stress concentrations around the loaded holes. Such stress concentrations are sites for initiation and propagation of fracture surfaces, which lead to brittle failure once cracks reach an unstable stage of development.

1.1 BACKGROUND: DESIGN OF BOLTED TIMBER CONNECTIONS

Contemporary timber design codes base the capacity of a single bolted connection on the so-called European Yield Model (EYM) (Johansen 1949). This model

incorporates the effects of wood embedment strength and bolt yielding to predict the connection failure load, assuming wood and the bolt to be ideal rigid plastic materials. It is presumed by the Canadian code, CSA Standard O86.1-94 (CSA 1994), "Engineering Design in Wood (Limit State Design)", that the specified minimum edge and end distance are adequate to insure a ductile failure mechanism (Figure 1.1). For joints with relatively large member thickness-to-bolt diameter ratios (slender bolts) a considerable amount of ductility is observed prior to failure, and the joint capacity is well predicted using EYM theory (Smith et al. 1998).

When there are multiple bolts in a connection, design rules assume that retention of a ductile failure behavior is possible provided that fasteners are spaced sufficiently apart. Because of this ductility, it is reasonable to assume that the load is equally shared among a serial row of fasteners. The load-carrying capacity of a multiple-fastener joint is then proportional to the number of fasteners and is equal to the sum of individual fastener capacities. This is particularly applicable to connections employing nails and slender bolts.

For connections with relatively small member thickness-to-bolt diameter ratios (using stocky bolts) and load being applied in the parallel-to-grain direction, the failure is generally brittle with no or limited ductility before reaching the ultimate load (Figure 1.2). This type of connections has many practical uses, especially in glued-laminated (glulam) timber construction. In this case, the EYM is not a reliable basis on which to predict joint capacity (Jorissen 1998). Moreover, it has been observed that the load is not uniformly distributed in a row of stocky bolts (Mohammad et al. 1997). The global

connection failure is brittle though individual bolts might exhibit some ductility prior to failure. As a result, the ultimate capacity of a multiple-bolted connection can be substantially less than the sum of individual joint capacities, as would be predicted by the EYM theory.

In the 1989 revision of the Canadian Standards Association, CSA 086.1 (CSA 1989) new modification factors were incorporated to account for premature brittle failures associated with sub-optimum loaded end distance and bolt group action in timber members. However, the basis of these factors is empirical due to the high number of parameters that influence the behavior of joints. These parameters include the variability of wood, the loading conditions, and the geometry of the connection. The development of these procedures is hampered by the complexity of the fastener interaction with such an anisotropic, non-homogeneous material, compounded by the tendency of the bolt to bend and the lack of a rational failure theory. Recent publications have identified an urgent need to change from the design by empirical and experience-based rules to design based on fundamental understanding of material behavior and mechanics principles (Bjorhovde and Saddarth 1992). This gave rise to the present study being part of a collaborative project on "Failure Mechanisms for Structural Connections in Wood-Fiber Composites". The research team consists of investigators from the University of New Brunswick in Fredericton, the Royal Military College of Canada in Kingston, Ontario, and McGill University in Montreal, Quebec.

1.2 OBJECTIVES AND SCOPE

The objective of this research work is to analyze the post-elastic behavior of bolted timber connections using stocky bolts under short-term static loading. Specifically, it is desired to:

i. Develop a finite element model of one- and two-bolt timber connections loaded parallel to grain. This model takes into account the nonlinear geometric effects caused by increased sliding contact between the member and the bolts.

ii. Propose a material model capable of tracing wood's post-elastic behavior beneath loaded bolts. The model is to be incorporated in a nonlinear finite element code to carry out the analysis.

iii. Undertake material characterization tests to determine the required input parameters for the program.

iv. Numerically predict the global deformation and local stresses and strains at discrete critical locations for different joint geometry.

v. Conduct an experimental investigation on the behavior of one- and two-bolt connections where the bolts load glulam timber members parallel to grain with different end distance, edge distance and spacing between the bolts.

vi. Examine the reliability of the finite element model by comparing numerical simulations to experimental measurements of local and global deformations and explaining the brittle failure mechanism.

vii. Determine the load proportions in a double-bolt timber connection in order to explain the interaction between the loaded hole boundaries and estimate the load-carrying capacity of the joint.

1.3 THESIS ORGANIZATION

The material presented in this thesis is separated into six different sections.

Chapter 1 "Introduction", explains the shortfalls in the design of bolted timber connections, which has motivated the present study, and presents the objectives of the thesis and its organization.

Chapter 2 "Literature Review: Modeling of Bolted Connections in Wood and Composites", selectively reviews existing literature on modeling joints in orthotropic materials, notably wood and advanced man-made composite materials. This includes stress analysis techniques and failure criteria. Conclusions are drawn concerning the limitations of existing connection models, and what is needed for a more rigorous approach.

Chapter 3 "Numerical Modeling of Bolted Connections", describes the nonlinear finite element model developed for one- and two-bolt timber connections. A description of the proposed material model for wood and its implementation in the finite element code is provided.

Chapter 4 "Experimental Procedure", outlines tests undertaken to characterize the material properties. An extensive experimental program of static tensile tests on single- and double-bolt connections in glulam timber is then presented.

Chapter 5 "Results and Discussion", is devoted to a discussion on the post- elastic behavior of one- and two-bolt connections. The numerical predictions of connection local and global deformations are compared to experimental data. Variation in load proportions among a row of two bolts loading a connection parallel to grain is determined as a function of applied load, which can provide an estimation of the capacity of the joint.

Chapter 6 "Conclusions" summarizes the results of the thesis, highlights some concluding remarks, and makes some recommendations for future work.

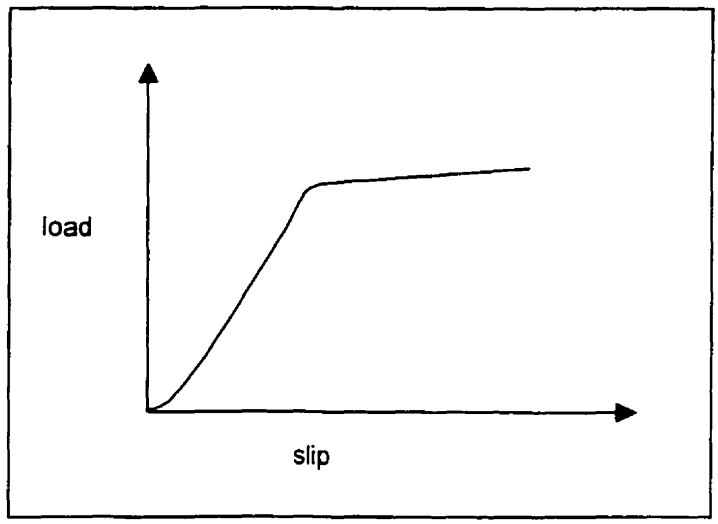

Figure 1. 1 Typical Load-Slip Response for a Connection Exhibiting a Ductile Failure Mechanism

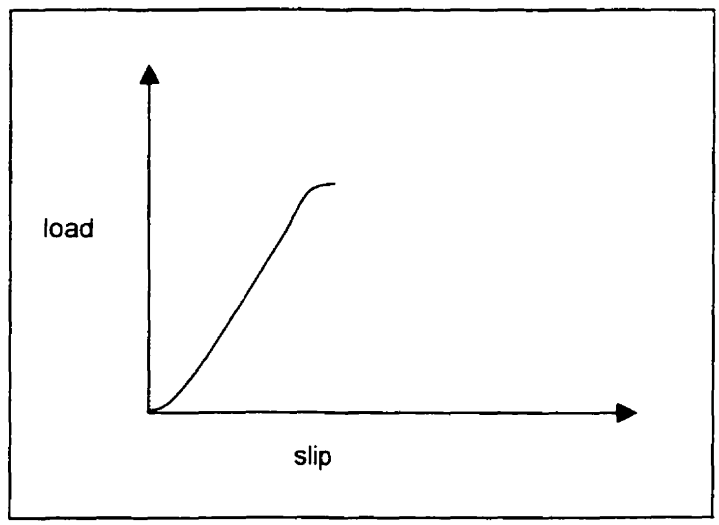

Figure 1. 2 Typical Load-Slip Response for a Connection Exhibiting a Brittle Failure Mechanism

CHAPTER 2

LITERATURE REVIEW: MODELING OF BOLTED CONNECTIONS IN WOOD AND COMPOSITES

2.1 INTRODUCTION

The problem of mechanical connections in orthotropic materials has been the subject of several past analytical and numerical studies. Some have been concerned with stress analysis. Others have extended the work to predict the strength of the joint. Most of the research has focused on the fundamental problem of a single bolt-hole loaded in tension. In this chapter, a review of the available literature is presented on solution techniques for stress analysis and failure criteria of connections in wood. Because of similarities in behavior and failure modes, the review will include structural joints in man-made fiber-reinforced composite materials. Their increasing use in advanced structures, especially in recent years, has led to extensive research in this area. This is not an exhaustive review, but rather its purpose is to point the way to a more appropriate approach in modeling wood bolted connections.

2.2 FAILURE MODES OF BOLTED JOINTS

The predominant failure modes that are observed in wood and composite materials are illustrated in Figure 2.1. The governing mode and failure load of a joint depend on factors such as the orientation of fibers in the members, the joint geometry (width and edge distance to diameter ratios w/d and e/d and member thickness), and clamping force (Arnold et al 1990; Harding and Fowkes 1984; Wilkinson and Rowlands 1981, Patton-Mallory et al. 1997). For a predictable design, a bearing failure is most desirable. It arises from compression damage over the loaded hole as the fastener bears against it (Fig. 2.1a). In practice, connection geometry often results in e/d and w/d ratios that are not sufficiently large to prevent brittle failures. Shear failures are induced by shear stress concentrations, resulting in shear plugs that are displaced parallel to the fibers (Fig. 2.1b). Cleavage failures are characterized by fracture initiating at the hole or at the end of a member and growing along the fibers (Fig. 2.1c). If the specimen width is too small, tension failures occur in the residual cross section (Fig. 2.1d). For multiple bolts, block shear failure may occur along a path involving tension on one plane and shear on a perpendicular plane (Fig. 2.1e).

2.3 STRESS ANALYSIS

In order to predict the strength of a joint, one must first determine the stress distribution in the region surrounding the bolt(s) in a joint. In the past, several analytical

solutions using the elasticity approach were carried out. These solutions were based on assumptions of: homogeneous linear elastic orthotropic material, infinite plates under plane stress, and a rigid pin fitting the hole perfectly. Green (1945) and Lekhnitskii (1968) were among the first to analyze the stress distribution around loaded holes in wood, assuming infinitely wide plate geometry. Later, finite geometry effects were included using boundary integration and collocation schemes (De Jong 1977).

2.3.1 Contact Modeling

Closed-form solutions become more complicated when any of the conditions assumed previously is removed. For this reason, numerical techniques based on the finite element method are used. In many studies, the contact area between the bolt and the hole was simplified as a semi-circle. In fact, either the contact pressure was assumed as a cosine function (Chang et al.1984; Wazczack and Cruse 1971), or the bolt was considered as a rigid frictionless pin with a radial displacement boundary condition (Agarwal 1980; Soni 1981). But several other investigators recognized the need to model the geometric non-linearity introduced by the variation of the contact area and by the sliding friction, which occurs on the contact surface. The inverse technique was first used (Mangalgiri and Dattaguru 1986; Naik and Cruse 1986; Ramamurthy 1989), where the contact conditions are specified by displacement constraint conditions. The disadvantage of this method is that the contact arc should be prescribed in

advance. Wilkinson and his collaborators (Wilkinson 1978, Wilkinson and Rowlands 1981, Wilkinson et al. 1981) developed a transformation matrix method that requires iterative matching of the contact nodes. With each load increment, the condition of contacting nodes with the surface of the bolt is checked. Then, sliding or fixation of the contacting nodes is determined.

Wilkinson's contact method was adopted by Moss (1984) for stress analysis around a single fastener in timber, and improved by Rahman and co-workers (Rahman 1981; Rahman and Rowlands 1993; Rowlands et al. 1982) for double-bolted joints in sitka-spruce. The determined compressive strains in the contact region for very thin members (0.6mm) matched Moiré experimental values away from the hole at loads lower than 30 percent of the ultimate connection strength. Gap elements have been used to represent the clearance between the hole and the bolt (Mohammadien et al. 1996; Bouchair and Vergne 1995). Such elements uncouple behavior between the normal and the tangential directions to model different contact conditions.

An alternative and more general approach is to enforce the contact conditions in the load-displacement formulation. The stiffnesses corresponding to the contact elements are introduced in the global stiffness matrix. Such contact algorithms are available in some finite element softwares such as ADINA (Automatic Dynamic Nonlinear Analysis).

2.3.2 Material Models

Most of the analyses were performed on the basis of linearly elastic material behavior. However wood exhibits nonlinear response when loaded beyond the elastic limit in compression. Such a situation is encountered in the contact region beneath the bolt. In order to simulate the nonlinear compressive response of wood in pinned joints, Chang (1983) used cubic spline interpolation of the experimental curve. Patton-Mallory (1997) modeled the nonlinear compression and shear stiffness using a trilinear stress-strain relationship. A major shortcoming of these models, however, is that they do not obey the laws of constitutive modeling in continuum media. Furthermore, there is no coupling between the material behavior in each direction.

Others attempted to model wood as elasto-plastic everywhere in a connection. In a study on a wood pinned-joint by Bouchair (1993), the evolution of plasticity according to Tsai flow criterion was found to take place at the end of the member first, then beneath the bolt for a perfect-fit pinned joint with e/d = 4. When a small clearance was introduced the non-linearity caused by a combination of contact and plasticity could not be handled by the model. To overcome the problem, a thin layer of wood behaving elastically was used around the hole (Bouchair and Vergne 1997). No verifications of the model were presented. In a recent study by Moses and Prion (1999), the plastic anisotropic material model with isotropic hardening available in ANSYS software was used to model connections in Douglas-Fir. Numerical simulations of load displacement curves were compared to earlier numerical predictions obtained by Patton Mallory. In

both of these studies, the assumption of elasto-plasticity everywhere in the wood member is inaccurate because it would result in theoretically "unrealistic" plastified regions due to combined compression/tension at the end of the member or combined tension/tension and shear on the hole-boundary, thus effecting the overall stress-state.

Large classes of fiber-reinforced composite materials exhibit nonlinear elastic behavior, primarily in shear. This problem is easier to handle since shear has an uncoupled behavior. The non-linearity is modeled by curve fitting the stress-strain relationship and using incremental methods (Petit and Waddoup 1969, Hashin et al. 1974, Sandhu 1976). Hahn and Tsai (1973) presented a constitutive equation for in-plane shear stress and strain of a composite lamina using a complementary strain energy density. The constitutive equation takes the following form:

$$\gamma = \frac{1}{G}\tau + \beta \tau^3 \qquad (2.1)$$

where γ is the shear strain, τ is the shear stress, G is the initial shear modulus and β is a non-linearity parameter which causes softening of the material as the level of stress is increased. Equation 2.1 was adopted to model nonlinear shear response in pinned-joint stress analysis (Chang et al. 1984, Lessard and Shokrieh 1995).

2.3.3 Three-dimensional Modeling

Members in bolted joints in man-made composites tend to be thin compared to those in bolted wood joints. A few researchers performed a three-dimensional analysis of thin composite joints to examine the influence of through-the-thickness clamping caused by tightening the bolt (Mathews et al. 1982) and the effect of the stacking sequence (Marshall et al. 1989, Shokrieh and Lessard 1996). A wood connection can be thick enough that the bolt bends significantly when the connection is loaded. In that case, a steel bolt is modeled using an elasto-plastic isotropic material model. Patton-Mallory et al. (1997) studied the three-dimensional mechanics of a single wood bolted connection. Their results showed that bending of the bolt becomes an issue for an aspect ratio (member thickness-to-bolt diameter ratio) l/d > 3, and affects the overall stress state. Another 3-D model was developed by Guan and Rodd (1996) to simulate the structural performance of a single moment transmitting timber joint made with a resin injected hollow steel dowel. Reasonable agreement was found between numerical load-deflection curves of the dowel and their experimental tests. The work was extended to model joints with four or eight hollow dowels (Guan and Rodd 1999). Moment rotation characteristics obtained from finite element modeling were correlated with experimental results and found to compare reasonably well.

2.4 FAILURE ANALYSIS

2.4.1 Strength Criteria

Early attempts at failure predictions for joint problems in orthotropic materials were mainly based on strength criteria ranging from uniaxial to polynomial failure theories. A review of proposed criteria is given by Nahas (1986). Waszczack and Cruse (1971) applied maximum strain, maximum stress and distortional energy criteria around the loaded hole in composite materials. A more convenient mathematical representation of failure that accounts for the interaction of stresses or strains is in terms of polynomials. Soni (1981) applied the quadratic failure criterion on a ply-by-ply basis until all plies had failed. The failure strength of the strongest ply at its weakest point was considered to correspond to the ultimate failure of a laminated joint. Chang et al. (1984) used the Yamada-Sun failure criterion on a characteristic curve. In their work on bolted joints in wood, Rahman et al. (1991) made a comparison between the capabilities of Tsai-Hill, Tsai-Wu, and Cowin criteria to predict the initiation of failure. Their numerically predicted strength (10 to 25 percent of the ultimate experimental strength) correlates with the physically observed and/or audible initiation of damage. In order to distinguish failure modes of bolted joints in laminated composites, the Hashin failure criterion was used (Chang and Chang 1987). It has distinct polynomials corresponding to the different failure modes: fiber tension, fiber compression, matrix tension, matrix compression and fiber-matrix shear failure. All the above theories could only predict failure initiation.

2.4.2 Fracture Mechanics Models

Experimental observations indicate that brittle failures of bolted joints in wood and composite materials initiate at the hole surface and propagate parallel to the fibers, as through-the-thickness cracks, for a short distance from or near the hole boundary. Several investigators then relied upon fracture mechanics models for solving the problem. A review of the fracture models applied to wood and composite materials is given by Kharouf et al. (1999).

Eisenmann (1975) used the inherent flaw model to predict the static strength of mechanical joints in laminates. This is a semi-empirical model in which fracture is assumed to occur once the stress evaluated at a characteristic distance from the notch reaches the unnotched strength. Eight equally spaced points are chosen on the fastener hole to account for the different lay-ups. The stress intensity factors K are calculated for various unit load conditions, and superposition is used to determine the final stress intensity factor at any location. It is assumed that a crack of length a_i (including the intense energy region) is extending radially at location i. The failure criterion $K = K_{Ic}$ is then applied. This fracture mechanics approach has been considered a very practical and reliable design method (Kedward and Whitney 1990). In another work by Schulz et al. (1995) the inherent flaw model was further extended to account for mixed-mode failure based on the maximum circumferential stress failure criterion. The crack was assumed to extend in the location where $\frac{\sigma_\theta}{\sigma_{\theta c}}$ is maximum. This was expressed as:

$$\frac{C_1K_1 + C_2K_2}{C_1K_{Ic}} < 1 \qquad (2.2)$$

where K_1 and K_2 are stress intensity factors for the opening mode and shearing mode, respectively, and C_1 and C_2 are trigonometric functions of θ, s_1 and s_2 (complex roots of the characteristic equation in the stress function). Comparison of predicted ultimate loads with the experiments for bolted joints in two laminates is illustrated on Figure 2.2.

The characteristic distance approach based on the point and average stress has been employed by numerous authors with moderate success (Jurf and Vinson 1990). Agarwal (1980) assumed that tension, bearing and shear failures occur if the average normal stress over some distance in the corresponding location equals the unnotched stress. This concept was extended by Chang et al. (1984) to a characteristic curve specified by the expression:

$$r_c(\theta) = \frac{D}{2} + D_t + (D_c - D_t \cos\theta) \qquad (2.3)$$

where D is the hole diameter, D_t and D_c are the characteristic lengths for tension and compression, determined experimentally. The location (angle θ) at which failure is detected, provides an estimate of the failure mode.

Progressive damage modeling was introduced by Chang and Chang (1989) using Hashin failure criterion to assess the extent and types of damage and predict ultimate strengths of pinned joints in composites. Only fiber/matrix net tension and shear-out were considered. Damage is implemented by reducing or vanishing the stiffnesses of damaged elements with an appropriate material degradation rule. They assumed that upon matrix cracking, only the transverse modulus of elasticity and Poisson's ratio reduce to zero. For fiber failure, the longitudinal and shear moduli reduce according to a Weibull distribution, while all other properties vanish. A few of their results are shown on Figure 2.3. Lessard and Shokrieh (1995) generalized their approach to include fiber/matrix compression failure and considered large deformation theory to improve convergence of the problem. Predicted final failure loads of graphite epoxy laminated pinned joints were within 20% of experimental values. Numerical damage progression could capture the failure modes observed with experimental X-rays.

In their analysis of timber bolted joints loaded perpendicular to the grain, Smith and Hu (1994) applied the concept of average normal stress over a finite area to predict the location and load at crack nucleation. A mixed fracture criterion was then adopted to analyze the growth of the crack. Their analysis predicted well the crack initiation, but the maximum load was well below the experimental failure load. The discrepancy was attributed to the post-peak stress softening due to transverse tension and shear that was not modeled. Daudeville et al. (1996) studied the cases of a bolt loading wood parallel or perpendicular to the grain. Principles of linear elastic fracture mechanics,

based on the energy release rate, were used to analyze the stable and unstable crack propagating along the grain. A mixed fracture criterion was applied where G_I and G_{II} (strain energies for the opening mode and shearing mode, respectively) were computed with the necessary work to close the crack in the x and y directions. The predicted load capacities were claimed to be comparable with the experimental values (values were averaged for all geometries studied, even though the differences in the corresponding load capacities were significant and the modes of failure different).

The finite small area fracture criterion has been proposed by Masuda (1998) to be applied to the problem of bolted connections loaded parallel to grain. It has a unified concept based on the LEFM and the classical strength criteria and is formulated as follows:

$$\varepsilon_{//}\left(\frac{\varepsilon_{//a}}{\varepsilon_{//c}}\right)^2 + \varepsilon_{\perp}\left(\frac{\varepsilon_{\perp a}}{\varepsilon_{\perp c}}\right)^2 + \gamma_{\perp}\left(\frac{\gamma_a}{\gamma_c}\right)^2 \geq 1 \qquad (2.4)$$

where ε_a is an average strain over an area of 1mm parallel to grain and 0.2~0.4mm perpendicular to grain. His theoretical results compared well with experimental tests for very short end distances (e/d) $\leq$ 3 where cleavage initiates from the end of the plate in loaded connections parallel to grain (Figure 2.4).

2.4.3 Probabilistic Models

Because of the wide variability observed in experiments of brittle structures, a statistical rather than a deterministic approach can be followed in analysis or design. This is based on the weakest link theory originally proposed by Weilbull (Weibull 1939). The model assumes that failure at the most critical flaw leads to total failure, where:

$$F(\sigma) = 1 - \exp\left(-\frac{1}{V_r}\int_V \frac{\sigma^b}{a} dV\right) \tag{2.5}$$

$F(\sigma)$ is the probability of failure of the element, V is the volume of the body, V_r is a representative volume of the material, b is a shape parameter, and a is a scale parameter. This model governs the initiation of cracks since it is controlled by the local stress at the most critical particle. Therefore, it is not a reliable method to describe the total failure of materials that undergo stable macroscopic crack growth.

In the recent work on wood bolted connections undertaken by Moses (2000), failure was predicted using the above probabilistic theory for integrated tensile stresses perpendicular to grain and a probability of failure of 0.5. However, the model did not succeed in predicting failure loads or modes observed in the experiments. The model predicted no failure for all tested geometries except one geometry with small edge and end distances (w/d=1.5, e/d=4). For integrated shear stresses, the threshold failure level

was much below the critical level, indicating that shear does not govern failure of the connections.

2.5 MODELING MULTIPLE BOLTED CONNECTIONS

In a multiple bolted connection, the load is not equally shared among the fasteners. This problem is encountered in composites as well as timber connections with stocky bolts. The load capacity is inversely related to the maximum load fraction, which occurs usually at either the first, last, or both bolts in a row of fasteners.

Simplified analytical load transfer models have been suggested. These spring models as shown on Figure 2.5 are based on the extensional stiffness of the members and load-slip characteristics of the bolt, either linear (Cramer 1968, Lantos 1969) or nonlinear (Wilkinson 1986). The major limitation of these models however is that no account is taken of the non-uniform stress distribution in the neighborhood of the loaded holes due to contact.

Numerical models using finite elements and assuming linear elastic orthotropic behavior for the members have given good predictions for particular geometries in composites (Griffin et al. 1994, Hassan et al. 1995). Results for bolted timber connections were conservative (Kharouf et al. 1998). In fact, even though the general failure of multi-bolted wood connections is brittle elastic, experiments show that there exists some ductility in the load-slip response of individual bolts. Eventually, the real load proportion is bounded by the EYM and the linear elastic model.

Smith et al. (1999) developed a semi-empirical hybrid elasto-plastic model for steel-wood-steel splice joints, in which each bolt is supported on a rigid-plastic spring. The model combines linear elastic finite element analysis and calibrated load-slip characteristics of single fasteners from tests (yield load and plastic limit slip). It was shown that the model gives good results for two and four bolts in a row loading timber parallel to grain (figure 2.6). It is believed that a finite element analysis, which incorporates inelastic deformation of wood around the holes at small load levels, would give better estimates of load proportioning between the bolts.

2.6 CONCLUSIONS

Numerical techniques based on finite element analysis proved to be efficient in modeling the contact problem in bolted connections in orthotropic materials. The interaction between the bolt and the hole cannot be limited to a pressure contact function, but should vary with the load increment and with the effect of sliding friction. Most of the available analyses of bolted connections are limited to two dimensions, assuming plane stress. This is particularly limiting in the case of thick timber connections as bolt bending can cause significant three-dimensional effects.

As yet, there is no failure theory with general applicability. Each theory appears to have been developed to predict the behavior of a given class of orthotropic materials depending on the associated fracture processes and failure modes. Strength criteria, ranging from uniaxial to multiaxial failure criteria, could predict the load and location of

failure initiation. Probabilistic models based on the weakest link theory were not successful in predicting the failure of bolted connections in wood. Fracture mechanics models, i.e. LEFM and semi-empirical models seem to be more appropriate to predict brittle failures. But these models need to be applied with caution by identifying the parameters that control initiation and propagation of cracking or damage.

In the case of bolted wood connections loaded parallel to grain, there is definitely a need for a constitutive bi-axial compressive material model in the contact region for an accurate stress analysis. The existing material models are not adequate. This model is also needed to get better estimates of the load transferred on individual bolts in the case of multi-bolted connections, and hence better predictions of the load capacity.

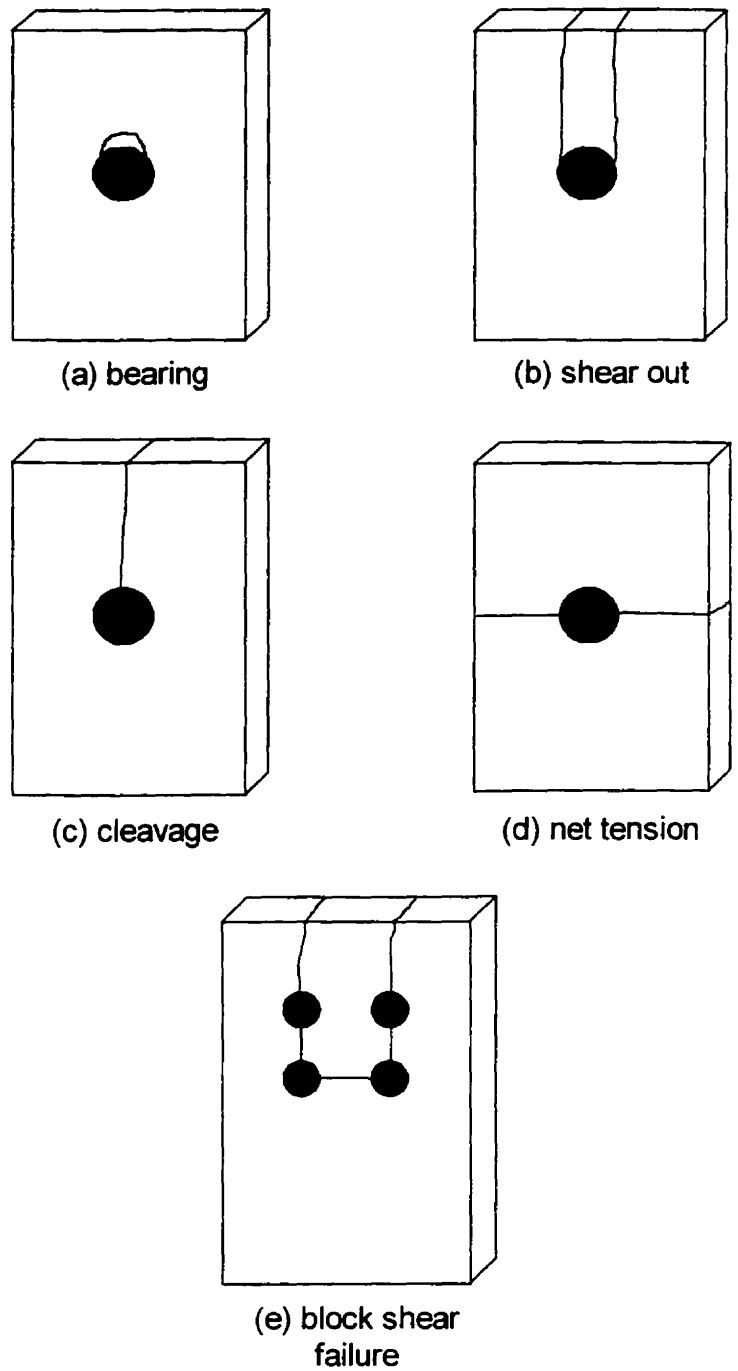

Figure 2.1 Typical failure mechanisms in bolted joints.

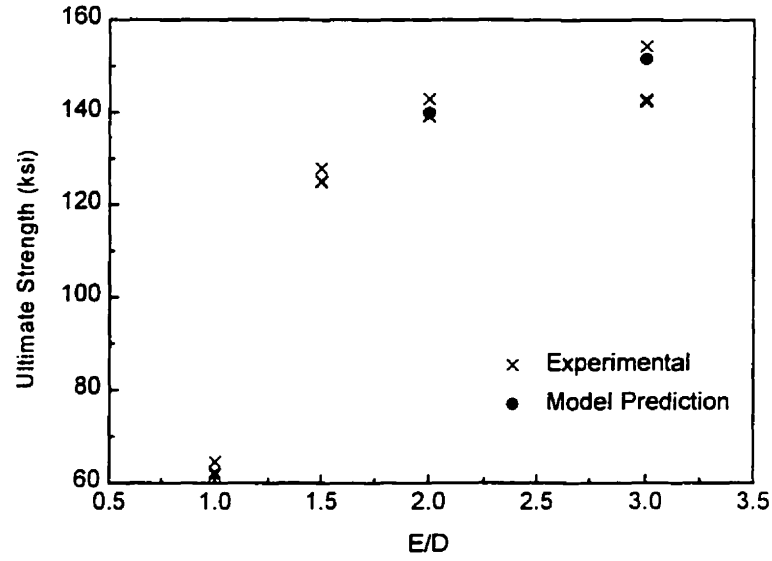

(a)

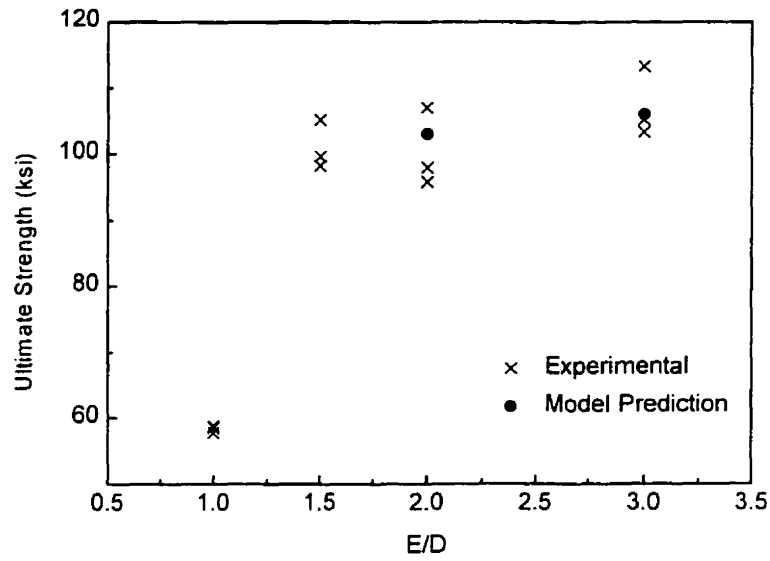

(b)

Figure 2. 2 Experimental versus model prediction for (a) Graphite-epoxy 42/50/8 (b) Graphite-epoxy 12/80/8 (Schulz et al. 1995).

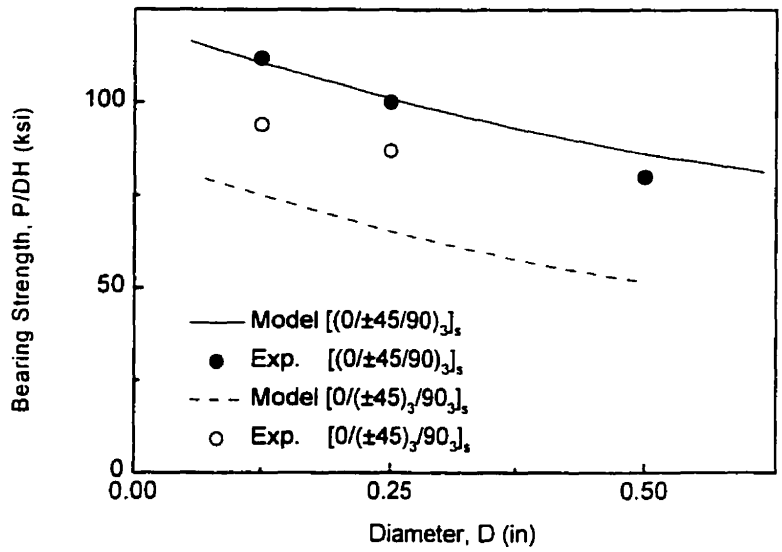

(a)

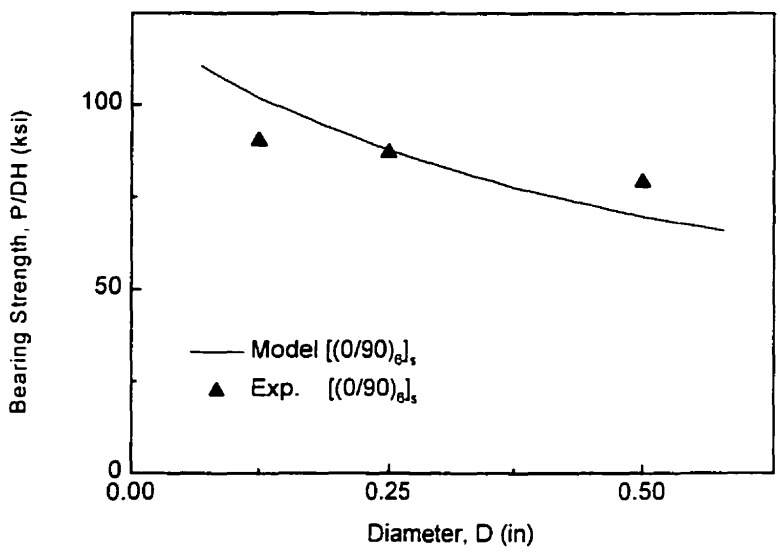

(b)

Figure 2. 3 Ultimate strengths of Fiberite T300/1034-C laminates containing a pin-loaded hole, comparisons between the results and the test data for (a) Net tension failure (b) Shear-out failure (Chang and Chang 1984).

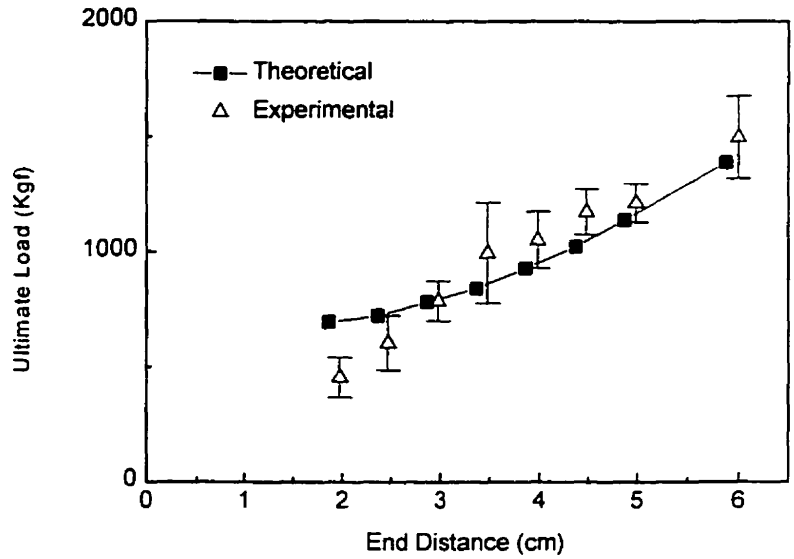

Figure 2. 4 Comparison between experimental and numerical results for wood bolted connections loaded // to grain where D=2cm (Masuda 1998).

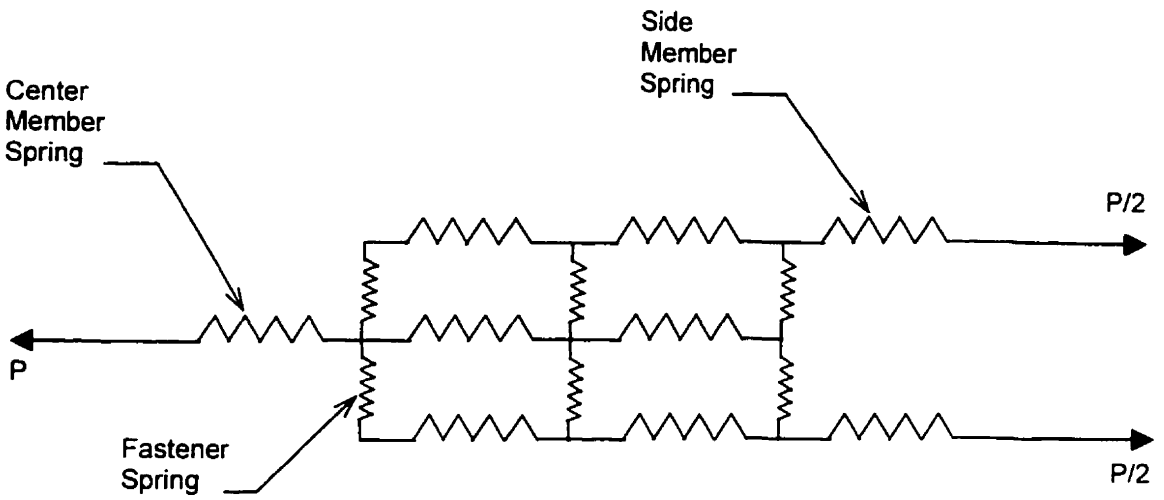

Figure 2. 5 Schematic of spring model for multiple fastener connections.

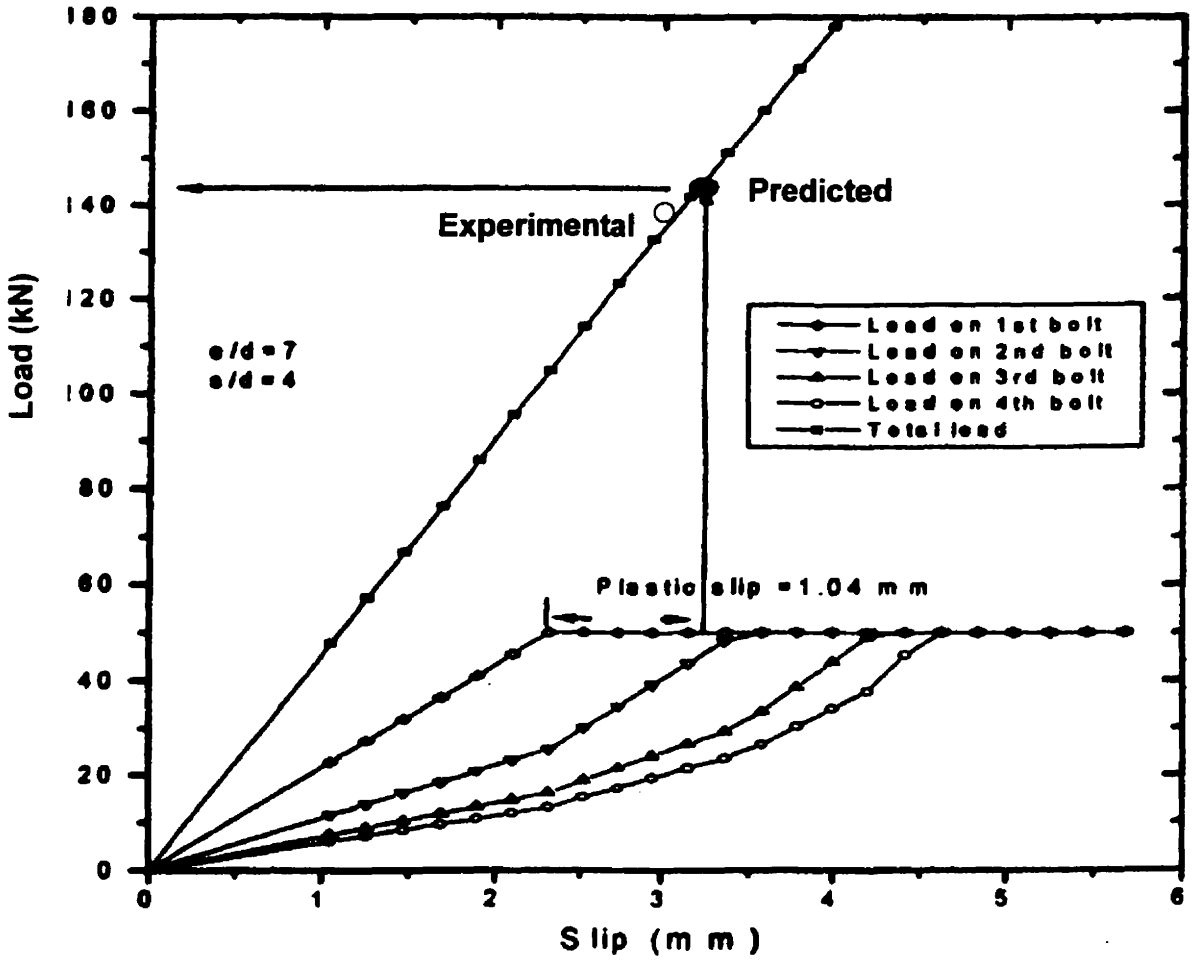

Figure 2. 6 Hybrid elasto-plastic FEM model applied to 4-bolts-in-a-row joint (Smith et al. 1999).

CHAPTER 3

NUMERICAL MODELING

3.1 INTRODUCTION

The mechanical behavior of wood connections with stocky bolts, i.e. when the arrangement results in a relatively low ratio of wood member thickness to bolt diameter, is very complex and is influenced by a number of geometric, material and loading parameters. The bolt-hole contact introduces high localized stress concentrations. Macroscopic observations have revealed that compressibility of wood in the contact zones play an important role in the development of brittle failures around holes (Rodd 1973). Moreover, Individual bolts in a multi- bolted connection do not necessarily contribute evenly to load carrying (Zahn 1991, Tan and Smith 1999). Insufficient knowledge of the stresses surrounding the bolt-loaded holes has inhibited improved design procedures, which are typically empirical.

In the present chapter, a two-dimentional finite element model of one and two-bolt timber connections loaded parallel to grain is presented. This model takes into account most of the complex aspects of the connection system. Nonlinear geometry due to increased sliding contact between the bolt and the holes is modeled. A plasticity-based constitutive compressive material model is developed to predict the nonlinear

wood behavior in the contact zones. The purpose of the model is to predict local and global deformation for wood members with different end, edge distance and spacing between the bolts some of which will be compared with the experimental data. This model is also aimed at explaining the interaction between the loaded holes in a double-bolt connection and predicting the load carried by each bolt.

3.2 MODELING APPROACH

Due to nonlinear effects, the ADINA (Automatic Dynamic Incremental Nonlinear Analysis) 7.3 finite element software was selected to model bolted connections in wood (ADINA R&D Inc. 1995). ADINA performs nonlinear incremental solutions with tolerances and minimum load increment size specified by the user. Its features include many complex aspects of the problem such as its flexibility in material modeling and its robust frictional contact algorithm.

Assuming a low ratio of the member thickness to bolt diameter ratio ($l/d<2$) results in negligible out of plane stresses. Hence two-dimensional eight-node plane stress elements were used to model the wood member. Taking advantage of the geometric symmetry about the axis of loading, one half of a connection loaded in tension parallel to grain was modeled using ADINA User Interface preprocessor (ADINA R&D Inc. 1997). A typical finite element mesh is shown in Fig. 3.1. Variation of the geometry and number of bolts resulted in slightly different meshes for each

configuration studied. Mesh refinement was necessary in the vicinity of the loaded hole boundary because of steep stress gradients.

One fourth of the bolt was modeled as rigid elements with a specified hole clearance due to its high stiffness compared to that of the wood plate (nearly 16 times larger). Nodes along the left edge are constrained to slide along the z-axis to enforce symmetry. A uniformly distributed load on the width of the plate was gradually applied at the lower end.

3.3 CONTACT MODELING

In order to model the geometric non-linearity caused by the increasing area of contact between the bolt and the wood member, the Lagrange Multipliers algorithm provided by ADINA was chosen. This algorithm enforces the compatibility of surface displacements at the contactor nodes and the Coulomb frictional conditions over the contact segments (Bathe and Chaudhary 1985). One half of the hole and the bolt were defined as two-dimensional contact surfaces.

To generate the equilibrium equations, an incremental procedure is followed where the contact conditions are imposed by adding the total potential of the contact forces to the usual variational indicator

$$\Pi^{(i)} = \Pi_t^{(i)} - \Sigma_K W_K^{(i)} \qquad (2.1)$$

where:

$\Pi^{(i)}$: resulting incremental potential for iteration (i)

$\Pi_t^{(i)}$: incremental total potential for iteration (i)

$\Sigma_K W_K^{(i)}$: total potential of the contact forces for iteration (i)

Non-linearities in the equilibrium equations are handled by a Full Newton iterative procedure. The convergence of the solution is based on energy and contact force criteria.

The basic geometric condition is that no material overlap can occur between the bodies in contact. During each iteration, the current geometry is used to determine and eliminate the overlap. As a consequence, contact forces are developed that act along the region of contact upon the target (being the bolt) and contactor (being the wood member), Fig. 3.2. An important distinction between a contactor surface and a target surface is that in the converged solution, the material overlap at the contactor nodes is zero, while the target nodes may overlap the contactor body.

To model friction between wood and the connector, the contact surface segment tractions are evaluated and the conditions of sticking and sliding nodes are checked. Two adjacent contactor nodes are in:

- sticking contact condition if $\mu T_n \geq T_T$
- sliding contact condition if $\mu T_n < T_T$

μ is the coefficient of friction, T_n is the normal traction and T_T is the tangential traction.

Although there may be variations in frictional characteristics over the contact surface between wood and the connectors, it is recommended that the variations are small enough to be neglected. A value of μ = 0.7 is found to be appropriate (Smith 1983) and is assumed to be constant over the contact surface.

3.4 CONSTITUTIVE MODELING

Because wood is a cellular and porous material, it can undertake permanent deformation under compression. Some uniaxial compressive tests undergoing large deformation have been performed for balsawood (Gibbson and Ashby 1986), aspen and maritime pine (Franois 1993), and spruce (Tan 1998). Figure 3.3 shows a typical stress-strain curve of spruce compressed parallel and perpendicular to grain. It can be seen that there is an initial phase with an approximately linear elastic response. Then compression in the axial direction shows some strain softening unlike compression perpendicular to grain and shear. This nonlinear permanent behavior may be described macroscopically within the framework of plasticity theory. Whereas in pure tension, wood behaves as a linear elastic brittle material.

When wood bolted connections are loaded parallel to grain, a high region of compression is observed beneath the bolt. To predict the post-elastic deformation caused by local wood crushing under the bolt, an orthotropic plasticity-based compressive material model is proposed. Wood is modeled as elasto-plastic orthotropic in bi-axial compression according to the Hill yield criterion, and linear elastic orthotropic

in tension with the maximum stresses taken as the failure criteria (see Fig. 3.4). Different strength values are considered for tension and compression along each material axis.

It is important to note that wood is a visco-elastic material, but usually the time dependency is ignored for short-term static loading. Furthermore, its mechanical properties are dependent on moisture content. A constant moisture-content of 12% will be assumed which corresponds to the dry experimental conditions (Chapter4).

3.4.1 Linear-Elastic Orthortopic Constitutive Behavior

Although wood microstructure is very complex, it is assumed to be homogeneous. Natural imperfections such as knots, taper, and distortions in the alignement of grain are ignored. If a sample is cut far enough from the centre of the tree so that curvature of the growth rings can be ignored, its properties may then be regarded as orthotropic. It has three orthogonal planes of material symmetry : longitudinal (L), radial (R), and tangential (T). The linear elastic orthotropic constitutive equations can be written in matrix form (Bodig and Jayne 1982):

$$\begin{Bmatrix} \varepsilon_{LL} \\ \varepsilon_{TT} \\ \varepsilon_{RR} \\ \gamma_{TR} \\ \gamma_{RL} \\ \gamma_{LT} \end{Bmatrix} = \begin{bmatrix} \frac{1}{E_L} & \frac{-\nu_{TL}}{E_T} & \frac{-\nu_{RL}}{E_R} & 0 & 0 & 0 \\ \frac{-\nu_{LT}}{E_L} & \frac{1}{E_T} & \frac{-\nu_{RT}}{E_R} & 0 & 0 & 0 \\ \frac{-\nu_{LR}}{E_L} & \frac{-\nu_{TR}}{E_T} & \frac{1}{E_R} & 0 & 0 & 0 \\ 0 & 0 & 0 & \frac{1}{G_{TR}} & 0 & 0 \\ 0 & 0 & 0 & 0 & \frac{1}{G_{RL}} & 0 \\ 0 & 0 & 0 & 0 & 0 & \frac{1}{G_{LT}} \end{bmatrix} \begin{Bmatrix} \sigma_L \\ \sigma_T \\ \sigma_R \\ \tau_{TR} \\ \tau_{RL} \\ \tau_{LT} \end{Bmatrix} \quad (3.2)$$

where,

E_L, E_T, E_R : Young's moduli in directions L, T, R

G_{LT}, G_{TR}, G_{RL}: Shear moduli for planes L-T, T-R, R-L

ν_{ij} : Poisson's ratio (i,j = L, T, R)

This assumption will be expanded to transverse isotropy, which assumes identical properties in the radial and tangential directions. This combined direction is referred to as perpendicular to grain ($\perp$) while the longitudinal is referred to as parallel to grain ($//$). The constitutive equations are reduced to:

$$\begin{Bmatrix} \varepsilon_1 \\ \varepsilon_2 \\ \gamma \end{Bmatrix} = \begin{bmatrix} \frac{1}{E_1} & \frac{-\nu_{21}}{E_2} & 0 \\ \frac{-\nu_{12}}{E_1} & \frac{1}{E_2} & 0 \\ 0 & 0 & \frac{1}{G_{12}} \end{bmatrix} \begin{Bmatrix} \sigma_1 \\ \sigma_2 \\ \tau \end{Bmatrix} \qquad (3.3)$$

where,

E_1, E_2 : Young's moduli in directions // and $\perp$ to grain, respectively

G_{12} : Shear modulus for plane 1-2

ν_{12} : Poisson's ratio

It is presumed that $\nu_{12} E_2 = \nu_{21} E_1$ (Bodig and Jayne 1982). All parameters are determined experimentally.

3.4.2. Elasto-Plastic Orthotropic Constitutive Behavior

3.4.2.1 Historical Background

The incremental plasticity is a macroscopic constitutive model that accounts for dissipative (irreversible) effects characterized by permanent strain accumulation. Hill was the first to conduct studies on anisotropic plasticity (Hill 1950). He postulated the form of the yield surface as an extension to Von-Mises criterion for isotropic materials. Only isotropic hardening was considered leading to a proportional change of the

orthotropic parameters during hardening. His work was later extended to account for nonproportional hardening (Whang 1969), differences in strengths for tension and compression (Shih and Lee 1978), other updated yield surfaces (Gotoh 1977) and softening behavior (Lourenço et al. 1997). Implementation of anisotropic plasticity in finite element modeling was achieved in 2-D and 3-D to analyze the behavior of multi-layered composite laminates (Dvorak and Bahei-El-Din 1982). The model is being incorporated in some finite element softwares with differing assumptions. However, they do not allow the user to define different yield or failure surfaces in tension and compression (ADINA R&D Inc. 1995).

3.4.2.2 Theory and Application to Wood

A theory of plasticity is a procedure by which a set of constitutive equations for a multiaxial stress state can be derived from uniaxial stress-strain test data. This is accomplished based on three basic properties: a yield criterion, a flow rule, and a hardening rule (Chen and Han 1988). In what follows, the general analytical formulation of the foregoing items will be presented with the application to wood in compression.

3.4.2.2.1 Yield Criterion

A generalization of the yield condition for plastically anisotropic materials is the general quadratic function f given by Shih and Lee (1978):

$$f = (\sigma_{ij}, \alpha_{ij}, A_{ijkl}, k) = 0 \tag{3.4}$$

where σ_{ij} is the second order stress tensor, A_{ijkl} (i,j,k,l = 1,2,3) denotes the fourth order tensor of anisotropic strength parameters describing the shape of the yield surface, α_{ij} describes the origin of the yield surface and k is a scalar parameter which stands for a reference yield stress.

In particular, a yield function that can capture orthotropy in the strength properties has been proposed by Hill (1950) as an extension of the Von Mises criterion for isotropic materials. As was demonstrated by Franl ois (1992), the limit state in compression for some species of wood can be approximated using this criterion. In plane stress and assuming transversely isotropic medium, the criterion for bi-axial compression can be expressed as:

$$f = \left(\frac{\sigma_1}{\sigma_{1c}}\right)^2 + \left(\frac{\sigma_2}{\sigma_{2c}}\right)^2 + \left(\frac{\tau}{S}\right)^2 - \frac{\sigma_1\sigma_2}{\sigma_{1c}^{\,2}} - 1 = 0 \tag{3.5}$$

where,

σ_1 : compressive stress // to grain

σ_{1c} : compressive strength // to grain

σ_2 : compressive stress $\perp$ to grain

σ_{2c} : compressive strength $\perp$to grain

τ : shear stress

S : shear strength

σ_{1c}, σ_{2c}, and S are material properties and determined experimentally.

f can alternatively be expressed in terms of the effective stress σ_e as follows if hardening is to be modeled:

$$f = \sigma_e - k(\chi) = 0 \tag{3.6}$$

where

$$\sigma_e = (A_{ij}\sigma_i\sigma_j)^{1/2} \tag{3.7}$$

and χ termed hardening parameter, and can be related to some measure of plastic deformation or plastic work.

A_{ij} is defined as:

$$A_{ij} = k^2 \begin{bmatrix} \frac{1}{\sigma_{1c^2}} & \frac{-1}{2\sigma_{1c^2}} & 0 \\ \frac{-1}{2\sigma_{1c^2}} & \frac{1}{\sigma_{1c^2}} & 0 \\ 0 & 0 & \frac{1}{S^2} \end{bmatrix} \tag{3.8}$$

3.4.2.2.2 Decomposition of the total strain increments

In the theory of plasticity, it is assumed that the total strain increment, $\{d\varepsilon\}$, consists of plastic components, $\{d\varepsilon^p\}$, and elastic components, $\{d\varepsilon^e\}$

$$\{d\varepsilon\} = \{d\varepsilon^p\} + \{d\varepsilon^e\} = \{d\varepsilon^p\} + [D^e]\{d\sigma\} \tag{3.9}$$

$[D^e]$ being the elastic compliance matrix, and can be expressed in terms of the material constants as:

$$[D^e] = \begin{bmatrix} \frac{1}{E_1} & \frac{-\nu_{21}}{E_2} & 0 \\ \frac{-\nu_{12}}{E_1} & \frac{1}{E_2} & 0 \\ 0 & 0 & \frac{1}{G_{12}} \end{bmatrix} \tag{3.10}$$

3.4.2.2.3 Flow rule

The flow rule determines the direction of plastic straining and is given as:

$$d\varepsilon^p = d\lambda \frac{\partial f}{\partial \sigma} = d\lambda\, a \tag{3.11}$$

$d\lambda$ being a plastic multiplier that determines the amount of plastic straining, $\frac{\partial f}{\partial \sigma} = a$ is termed the flow vector.

3.4.2.2.4 Hardening rule

An anisotropic hardening rule developed by Vaziri et al. (1993) will be adopted here. Such a theory allows for nonproportional change of the yield values and thus leads to a non-uniform expansion of the yield surface during plastic flow. Based on the notion of equivalent plastic work, the evolution of yield stresses is assumed to be governed by the following set of equations:

$$\begin{aligned} \sigma_{1c}^{\ 2} - \sigma_{1co}^{\ 2} &= \frac{E_{p1}}{H}(k^2 - k_o^{\ 2}) \\ \sigma_{2c}^{\ 2} - \sigma_{2co}^{\ 2} &= \frac{E_{p2}}{H}(k^2 - k_o^{\ 2}) \\ \tau^2 - \tau_o^{\ 2} &= \frac{G}{H}(k^2 - k_o^{\ 2}) \end{aligned} \qquad (3.12)$$

k_0 and k are the initial and updated effective yield stresses, respectively.

E_{p1}, E_{p2}, G_p are the plastic moduli defined by:

$$E_{p1} = \frac{E_1 E_{T1}}{E_1 - E_{T1}}$$
$$E_{p2} = \frac{E_2 E_{T2}}{E_2 - E_{T2}} \qquad (3.13)$$
$$G_p = \frac{G G_T}{G - G_T}$$

with E_{T1}, E_{T2}, and G_T being the tangent moduli of the stress-strain curves.

H' is the plastic modulus of the effective stress-effective strain diagram which can be identified with any one of the three basic stress-strain curves.

$$H' = \frac{d\sigma_e}{d\varepsilon_e} \qquad (3.14)$$

As mentioned earlier, wood undergoes softening in compression parallel to grain and hardening perpendicular to grain. Depending on the chosen value of H', perfect plasticity, slight hardening or softening can be modeled.

3.4.2.2.5 Incremental elasto-plastic constitutive equations

The consistency condition requires the state of stress to remain on the yield or loading surface during plastic flow and is expressed by:

$$df = 0 \qquad (3.15)$$

By substituting equation (3.5) in (3.15) and combining equation (3.9) and (3.11), the constitutive equations are given by

$$d\sigma_{ij} = C_{ij}^{ep}\, d\varepsilon_j \tag{3.16}$$

$$C_{ij}^{ep} = C_{ij}^{e} - \frac{C_{ik}^{e}\, a_k a_l C_{lj}^{e}}{(1 - \frac{1}{2k}\sigma_i \sigma_j \frac{\partial A_{ij}}{\partial k}) H' + a_m\, C_{mn}^{e}\, a_n} \tag{3.17}$$

C^e is the elastic stiffness matrix, and C^{ep} is termed the elasto-plastic stiffness matrix.

3.4.3. Finite Element Implementation

A Fortran program of the elasto-plastic compressive material model was written and inserted into the user-supplied material model of ADINA software. The algorithm proceeds as follows:

1. Read all quantities at the end of the previous increment (iteration) i^{th} step and the strains at the current increment $(i+1)^{th}$ step
2. The initial stress method developed earlier by Nayak and Zienkiewiz (1972) has been adopted as the computational process in the model. The computation of

stresses is done for all Gaussian sampling points. In what follows, the computation for only one Gaussian point will be considered. An elastic estimate of the stress increment is computed as :

$$d\sigma^e = C^e d\varepsilon \tag{3.18}$$

A trial stress state is then calculated

$$\sigma^t = \sigma^0 + d\sigma^e \tag{3.19}$$

3. Determine the loading state of the Gaussian point

- If the Gaussian point is under tension/tension or tension/compression, then it remains in an elastic state in *(i+1)*th step, and the final stress is $\sigma_f = \sigma^t$
- If the Gaussian point is under bi-axial compression state then evaluate $f(\sigma^t)$ (f being the yield function)
  - * If $f(\sigma^t) < 0$, the considered Gaussian point remains in an elastic state in *(i+1)*th step, and the final stress is $\sigma_f = \sigma^t$
  - * If $f(\sigma^t) > 0$, the Gaussian point enters into an elastic-plastic state in this load step, go to step 4.

4. Elasto-plastic stress computation (Figure 3.5)

There exists a scaling factor r such that

$$f(\{\sigma^0\} + r\{\Delta\sigma^e\}) = 0 \qquad 0 \le r < 1 \tag{3.20}$$

Equation (3.20) is nonlinear in the factor r. Developing this expression in a Taylor series gives

$$f(\{\sigma^0\} + r\{\Delta\sigma^e\}) = f(\{\sigma^0\}) + \left(\frac{\partial f}{\partial \sigma}\right)\Big|_m^T r\{\Delta\sigma^e\} + r^2\{\Delta\sigma^e\}^T \left(\frac{\partial^2 f}{\partial \sigma^2}\right)\Big|_m^T \{\Delta\sigma^e\} + \ldots \tag{3.21}$$

By neglecting higher order terms, equation (3.21) leads to an approximation in r as:

$$r = \frac{-f(\{\sigma^0\})}{\left(\frac{\partial f}{\partial \sigma}\right)\Big|_m^T \{\Delta\sigma^e\}} \tag{3.22}$$

5. An intermediate stress can then be found as

$$\sigma_i = (\{\sigma^0\} + r\{\Delta\sigma^e\}) + (1-r)C^{ep}\Delta\varepsilon \tag{3.23}$$

6. Yield stresses are updated by first updating the size of the yield surface k

$$k_f = k_0 + H'\Delta\bar{\varepsilon}^p \tag{3.24}$$

then using equations (3.12) and in turn the components of A_{ij} are updated.

7. In general σ_i will not lie on the updated yield surface and a correction step has to be made to meet the consistency condition

$$\delta\sigma = -a\frac{f(\sigma_i)}{a^T a} \tag{3.25}$$

The final stress is

$$\sigma_f = \sigma_i + \delta\sigma \tag{3.26}$$

8. Determine the plastic strain subincrements $\Delta\varepsilon_p$ using equation (3.11).
9. The final stresses are fed back into ADINA that solves for the strains in the (i+2) step.
10. Return to step 1.

3.5 COMPUTED RESULTS

The finite element program is run first with the elastic orthotropic material model everywhere in the wood member, then with the application of the elasto-plastic

orthotropic model in order to show the benefits of the proposed model over the elastic material model. The output of the program are strain values taken at specified nodal points for each load step using ADINA Use Interface postprocessor (ADINA R&D 1997). These correspond to strain gage values measured at stress concentrations. Another required output is the displacement of the wood member relative to the bolt and that corresponds to the global deformation of the connection. This can be compared to experimental data plots. Contact stresses and forces need to be determined in the contact surface. The values of the resultant contact forces in the direction of loading are calculated in order to determine the load carried by each bolt for double-bolt connections.

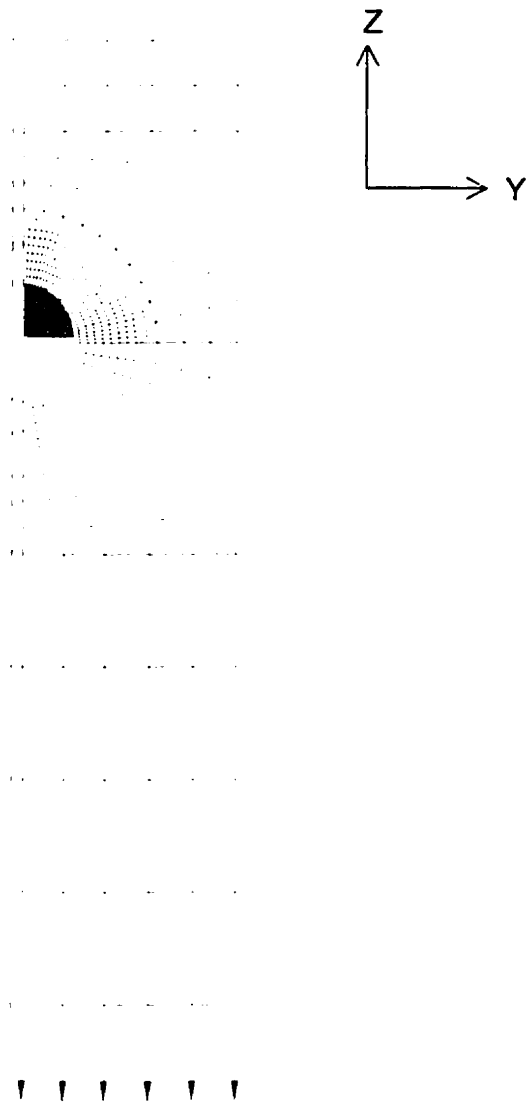

Figure 3. 1 Finite Element Mesh of a Single-Bolt Connection

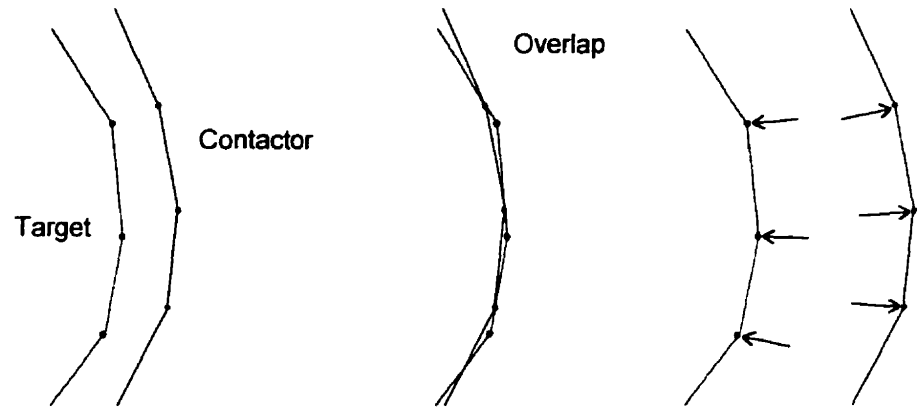

a) Condition prior to contact

b) Condition at contact

c) Contact nodal forces

Figure 3. 2 Contact Modeling

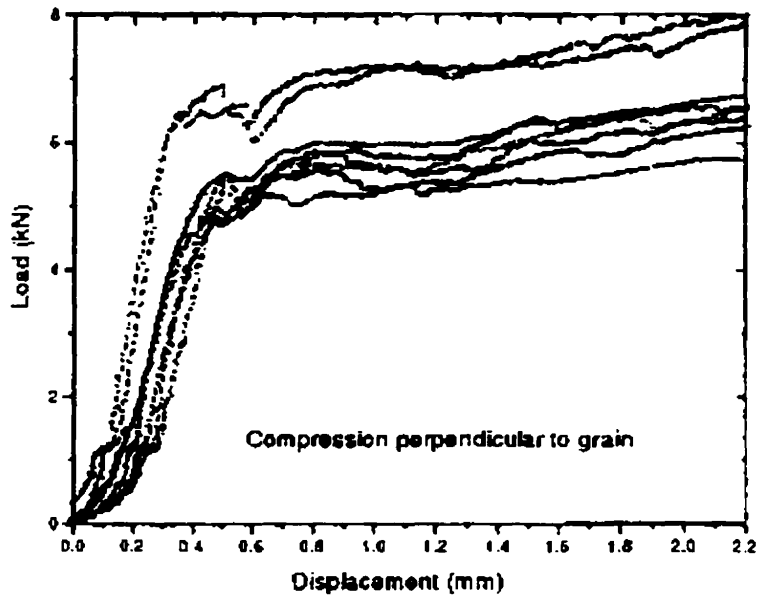

(a)

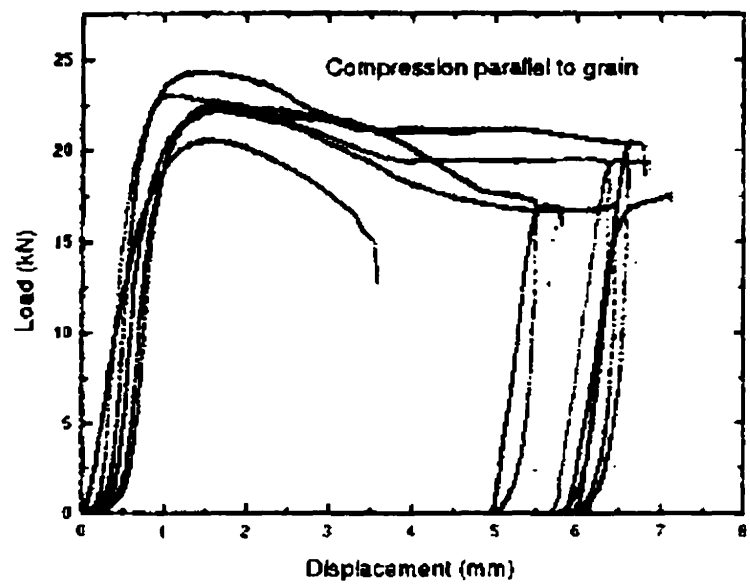

(b)

Figure 3. 3 Load-Displacement Curves of Spruce Compressed: (a) Parallel to Grain (b) Perpendicular to Grain (Tan 1997)

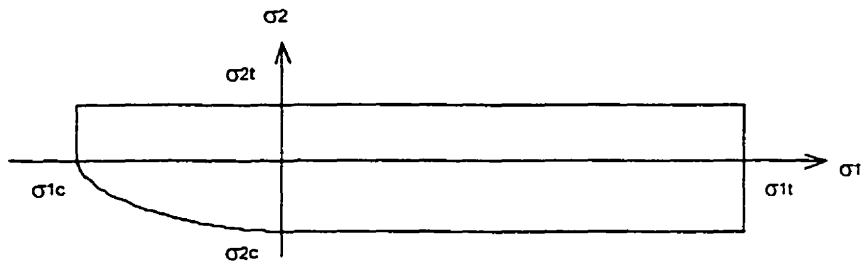

Figure 3. 4 Failure Envelope of Wood (1 = parallel to grain, 2 = perpendicular to grain)

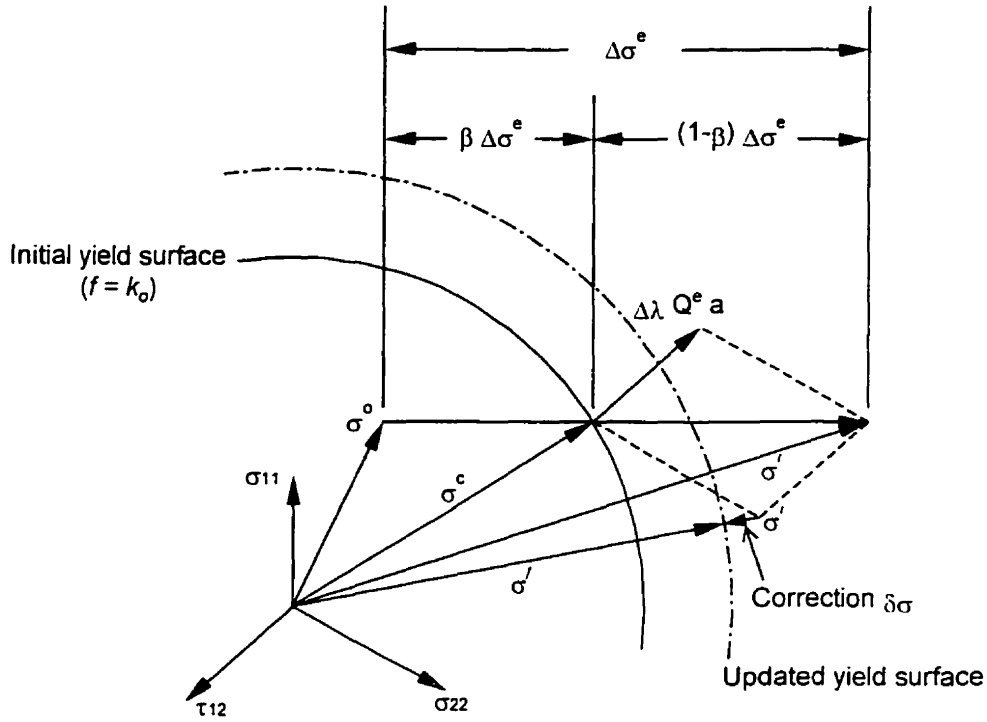

Figure 3. 5 Incremental Elasto-Plastic Stress Computation for an Initially Elastic Point

(Vaziri et al. 1992)

CHAPTER 4

EXPERIMENTAL PROCEDURE

4.1 MATERIAL CHARACTERIZATION

4.1.1 Introduction

The implementation of the numerical model of wood bolted connections requires the adequate characterization of some physical and mechanical properties of the material. Due to the complex microstructure of wood and the wide variability of its properties from one speicie to the other, it is necessary to conduct the appropriate tests on the same type of material which will be used in the connection experiments to verify numerical simulations. They must not only provide measurements of the moduli and stiffnesses but also strengths based on the transversely isotropic material assumptions, explained in Chapter 3. To accomplish this, standardized tests according to ASTM D143 (ASTM 1994) and non- standardized tests have been performed at the Structures laboratory of the Royal Military College of Canada in Kingston, Ontario (Mohammad 1997) to get measurements of the material properties in the longitudinal direction, i.e parallel to grain and in the radial direction, i.e perpendicular to grain. A critical review of

the characterization of wood material properties can be found in the report by Sawaya (1998).

4.1.2 Description of Tests

4.1.2.1 Material

The experiments involved testing specimens of one wood species designation and grade, 14t-EX grade Spruce Lodgepole Pine glued laminated timber (CSA 1994). Glulam is a very versatile and widely used material nowadays for load-carrying structures such as roof framing, bridges, towers, and marine construction. At the macroscopic level, this is a layered composite made of different layers of lumber. At the microscpic level, timber is a complex naturally occuring and renewable fibre-reinforced composite with a high strength to weight ratio. In fact, it is made of discontinuous hollow tubelike cells, also called tracheids, composed mainly of cellulose. Tracheids are nominally aligned parallel to the axis of the tree trunk and embedded in a continuous matrix of an amorphous, organic compound, called lignin (Bodig and Jayne 1982, Dinwoodie 1989).

4.1.2.2 Tension test parallel to grain

Ten specimens were tested in tension according to ASTM D143 (ASTM 1994). They were randomly selected from different billets, in such a manner that grains were parallel to the loading direction. A typical test specimen and test set up are shown in

Fig.4.1. Tests were carried out at a constant crosshead rate of 1.0 mm/minute. Load and deformation with a central gage length of 50 mm were recorded. From the load-deformation curves, the proportional limit stress, the ultimate stress, and the modulus of elasticity were calculated.

4.1.2.3 Tension test perpendicular to grain

The standard test for tension perpendicular to grain is not adequate nor sufficient to determine the desired properties. It can only provide a measurement of tensile strength perpendicular to grain, which is found to be very low due to the fact that stresses are not uniformly distributed over the specified cross section. To overcome this problem, a non-standardized test originally developed by Vasic et al. (1996) was carried-out. The test set-up and specimen geometry are shown on Fig.4.2. The specimen is glued to the steel blocks at both ends with toughened acrylic adhesive. This test, performed under deformation control, allows the measurement of ultimate stress and elastic modulus, as well as other fracture properties.

4.1.2.4 Compression test parallel to grain

Standard compressive tests according to ASTM D 143 (ASTM 1994) were performed on specimens of 50x50x200 mm as shown on Fig.4.3. Twenty specimens were sampled from five different boards. The top platen of the testing machine was equiped with a rotating semi-circular bearing plate to compensate for any slight irregularities of specimen dimensions. Loading was applied at a crosshead rate of 0.6

mm/minute. Deformation was recorded via one LVDT over a gage length of 140 mm. This compressive test gave measurements of proportional limit stress, ultimate stress, and modulus of elasticity.

4.1.2.5 Compression test perpendicular to grain

Ten prismatic specimens of 50x50x150 mm were tested according to ASTM D 143 (ASTM 1994). Spherical loading fixtures in compression were used together with a steel I-beam to apply a load at the radial surface over the central third of the surface area of the sample, Fig. 4.4. Loading was applied at a crosshead rate of 0.3 mm/minute and deformation recorded using two LVDT's at each end. By assuming an elastic behavior up to 2.5 mm deformation, the modulus of elasticity was calculated along with the ultimate stress.

4.1.2.6 Shear test parallel to grain

A standardized test to measure the shear modulus does not exist. A vibration test suggested earlier by Chui (1991) was undertaken on five beams of 76x76x1000 mm to estimate the shear modulus. The specimen is suspended on two soft springs located at the nodal points for the fundamental mode of vibration and excited by a hammer. The response is recorded using an accelerometer, Fig. 4.5. The force and response signals were analyzed by a FFT (Fast Fourier Transform) spectrum analyzer. The data for the first two natural frequencies (w1 and w2) were in conjunction with simultaneous Timoshenko beam vibration equations to estimate G and E parallel to grain.

A second test was carried out according to ASTM standards to find the shear strength (ASTM 1994). It consists of the notched specimen loaded under compression in a shear box as shown in Fig. 4.6. The ultimate shear stress is simply calculated as the ultimate load P divided by the sheared area.

4.1.3 Test results and material properties used in numerical modeling

Tables 4.1 and 4.2 provide a summary of the test results and nominal material properties which are used as input for the elastic orthotropic material model. Some of the standard testing methods are not adequate for experimental characterization of wood properties perpendicular to grain and for shear. These tests are modified to get more reliable results. There is variability in the values found due to the complex wood microstructure. It should be noted that no tests have been undertaken to obtain Poisson's ratios. A value of 0.3 which is taken from literature is assumed (Bodig and Jayne 1982). As for material constants characterizing the plastic behavior of timber in bi-axial compression, slight hardening/softening observed on the compressive stress-strain curves on Figure 3.4 (Tan 1998) is modeled with the values presented on table 4.3. Material strengths in compression for both directions and in shear are taken as the initial yield stresses.

4.2 CONNECTION TESTS

4.2.1 Introduction

To validate the numerical predictions, a series of tensile tests on glued-laminated timber connections with relatively low ratio of member thickness-to-bolt diameter was performed in the Structures Laboratory of the Royal Military College of Canada (Mohammad 1997). The standard tests according to ASTM D 1761 (ASTM 1988) consist of double shear connections which counteract out of plane deformation. However since the present tests are intended to give local and global measurements of deformation of the wood center member, the testing arrangement is modified and is described below. Different configurations for one- and two-bolt timber connections were tested which gave insight into the interaction between the geometry and the behavior and failure mode of the connection.

4.2.2 Materials

The experiments involved testing specimens of one specie, 14t-EX grade Spruce Lodgepole Pine glued laminated timber (CSA 1994). One of the main advantages of glulam is the ease of manufacturing large structural members from standard commercial sizes of lumber. All specimens were cut from longer billets (3.5, 5.5, and 10 m) and kept

in a conditioning chamber to reach approximately 12% equilibrium moisture content (EMC). The average specific gravity was about 0.40. Knots were avoided in the joint area as much as possible.

Steel bolts used to connect the timber specimens were ¾ inch Grade 2 bolts (Lamson and Sessions, undated). These are low carbon steel bolts with a minimum tensile strength of 510 MPa and yield strength of 390 MPa. SAE Grade 2 bolts are used because it is reportedly common practice in Canada to use these and because ASTM A307 bolts (ASTM 1994) are not readily available.

4.2.3 One-Bolt Connection Tests

The test set-up of a single bolted connection is shown in Fig 4.7. It consists of supporting blocks with holes drilled to accommodate ¾ inch (19 mm) bolts. These blocks are attached at the bottom to a rigid steel plate and are placed apart with a gap equal to the specimen thickness plus two millimeters. Specimens were loaded in static tension using two steel plates and dowels. Short-term loading was applied using a universal testing machine at a constant cross head movement of 0.9 mm/minute to cause failure within 10-15 minutes.

Each specimen was individually marked and drilled with a drilling bit size that ensured a hole radial clearance of 1 mm. This conforms with design specifications (CSA 1994). The nuts were turned finger tight. Five single-bolt configurations were tested.

Specific specimen configurations have been selected to induce different types of failure. Parameter combinations were: end distance, e, of 3d and 5d at an edge distance, w, of 1d, and e of 3d, 5d, and 7d at w = 2d (d being the diameter of the bolt). The thickness is constant for all configurations and taken to be equal to 17 mm to ensure failure in the main member before any plastic bending occurs in the bolts. Table 4.4 details the schedule of single bolt connection tests.

To obtain measurements of longitudinal or transverse strains in critical locations near stress concentrations, electrical resistance strain gages were mounted on the front face of the wood members at 0 or 90 degrees to the loading direction (Fig 4.8). In this regard, strain gage #1 records compressive longitudinal strain five millimeters away from the hole. It is in a region of high bi-axial compression due to the contact between the bolt and the hole. The applied tensile load causes a constant stress in the gross section which becomes a tensile stress concentration in the net section adjacent to the bolt hole. For this reason, strain gage #2 is placed adjacent to the hole at a distance of three millimeters to measure tensile strain parallel to grain. The compression contact zone acts like a wedge that tends to open the end of the connection, thus causing high stresses perpendicular to grain. That is where strain gage #3 records tensile strains perpendicular to grain two millimeters from the end of the wood member. The compression zone also causes a high shear stress concentration. Measurements of shear strains were made possible using delta strain rosettes mounted close to the hole at 10 degrees from the horizontal. This latter measurement was made on six replicates of only one single-bolt configuration (W2E5) with e = 5d and w = 2d.

Global load-deformation curves were also obtained. Two LVDT's were employed to measure the movement of the timber member relative to the bolt (one LVDT on each side of the specimen). The failure loads and the failure patterns were also recorded for each tested specimen.

4.2.4 Two-Bolt Connection Tests

A similar test set-up is used for double-bolted connections with two bolts in a row and is depicted on Fig 4.9. In order to prevent failure at the loading end, the top loading end was reinforced.

Four double-bolt configurations were tested to represent combinations of end distances,e, and spacings, s, (e = 3d or 5d, and s = 3d or 5d). The thickness is constant for all configurations and taken to be equal to 17 mm. Table 4.5 gives the details of the geometries tested and the number of replicates. It should be noted though that parameter combinations were chosen to aid verification of the FEM model and may not represent values commonly used.

Figure 4.10 shows the location of strain gages on a double-bolt timber specimen. Strain gages #1 and #2 measure longitudinal compressive strains on the upper and lower holes, respectively, while strain gages #3 and #4 measure longitudinal tensile strains adjacent to the upper and lower hole, respectively. Strain gage #5 is installed at the end to measure transverse strain perpendicular to grain. Two gages were also

installed on the upper part of each bolt in an attempt to measure the load fractions carried by each bolt. Four LVDTs were mounted on each side of the wood member to measure the relative movement at the level of each bolt. For all tests undertaken, failure loads and failure modes are noted.

4.2.5 Experimental Results and Observations

Electrical signals and deformation from the instrumentation were recorded at regular time intervals with the corresponding loads. The results are discussed in Chapter 5 in comparison with numerical findings. As was expected there was a lot of variability in the results, which can be attributed to the variability of wood properties and joint fabrication tolerances. With the two-bolt connection configurations, it was observed that one of the bolts may transmit almost no load during a major portion of the test. This is due in part to the procedure followed to mark and drill the holes that can cause it to be off location with regard to spacing, line (double bolt) or relative to the line of the applied load.

Generally, failure occurred in the main wood member due to crushing (bearing) of the wood, shear, net tension, splitting or combination of these modes. A summary of the failure loads and modes for each series can be found in Tables 4.6 and 4.7. A wide variability is observed in the failure loads especially with configurations having a short end distance (e = 3d). The series of specimens with a one-bolt connection and having a

Fig.4.11. By increasing the end distance, bearing of wood beneath the bolt becomes more important. For the series with two-bolt connections, plug shear out failure in the end distance or the spacing between the bolts was again the predominant failure mode as can be seen on Fig.4.12. Splitting was observed in the configurations having longer end distance.

Table 4. 1 Material Elastic Parameters

Elastic constant	Type of test	Number of specimen	Average (MPa)	COV (%)
$E_{c//}$	ASTM D 143	20	9158.8	23.2
$E_{t//}$	ASTM D 143	10	14335	14
$E_{c\perp}$	ASTM D 143	10	325	19
$E_{t\perp}$	Vasic et al. (1996)	10	538	11
G	Chui (1991)	5	756	10

Table 4. 2 Material Strengths

Material strength	Type of test	Number of specimen	Average (MPa)	COV (%)
$\sigma_{c//}$	ASTM D 143	20	43.8	5
$\sigma_{t//}$	ASTM D 143	10	102.50	17
$\sigma_{c\perp}$	ASTM D 143	10	7.70	4
$\sigma_{t\perp}$	Vasic et al (1996)	10	6.20	19
S	ASTM D143	11	9.10	19

Table 4. 3 Material Plastic Parameters

Plastic constant	Perfect plasticity	Hardening	Softening
H'	0	+0.05	-0.05
E_{p1}	0	+125.0 MPa	-125.0 MPa
E_{p2}	0	+1.0 MPa	-1.0 MPa
G_p	0	+60.0 MPa	-60.0 MPa
Y_0	43.8 MPa	43.8 MPa	43.8 MPa
Z_0	7.7 MPa	7.7 MPa	7.7 MPa
S_0	9.10 MPa	9.10 MPa	9.10 MPa

Table 4. 4 Geometry of the Tested Configurations for Single-Bolted Connections

Configuration	w/d	e/d	Number of replicates
W1E3	1	3	7
W1E5	1	5	7
W2E3	2	3	3
W2E5	2	5	3(7)
W2E7	2	7	3

Table 4. 5 Geometry of the Tested Configurations for Double-Bolted Connections

Configuration	w/d	s/d	e/d	Number of replicates
S3E3	2	3	3	6
S3E5	2	3	5	6
S5E3	2	5	3	6
S5E5	2	5	5	6

Table 4. 6 Experimental Failure Loads and Modes for One-Bolt Timber Connection

(NT: Net Tension; SH: Shear; SP: Splitting; B: Bearing of Wood)

Configuration	Number of replicates	Average Failure load	COV (%)	Failure modes
W1E3	7	5.33	31.5	**NT**,SP,SH
W1E5	7	9.3	17	**NT**,SP,SH
W2E3	7	6.96	32.7	**SH**,SP
W2E5	10	9.8	15	**SH**,SP
W2E7	3	9.9	4.8	**B**

Table 4. 7 Experimental Failure Loads and Modes for Two-Bolt Timber Connections

Configuration	Number of replicates	Average Failure load (kN)	COV (%)	Failure modes
S3E3	6	12.78	42.2	**SH**
S3E5	6	15.37	22.4	**SH**,SP
S5E3	6	15.05	28.1	**SH**
S5E5	6	16.14	28.2	**SH**,SP

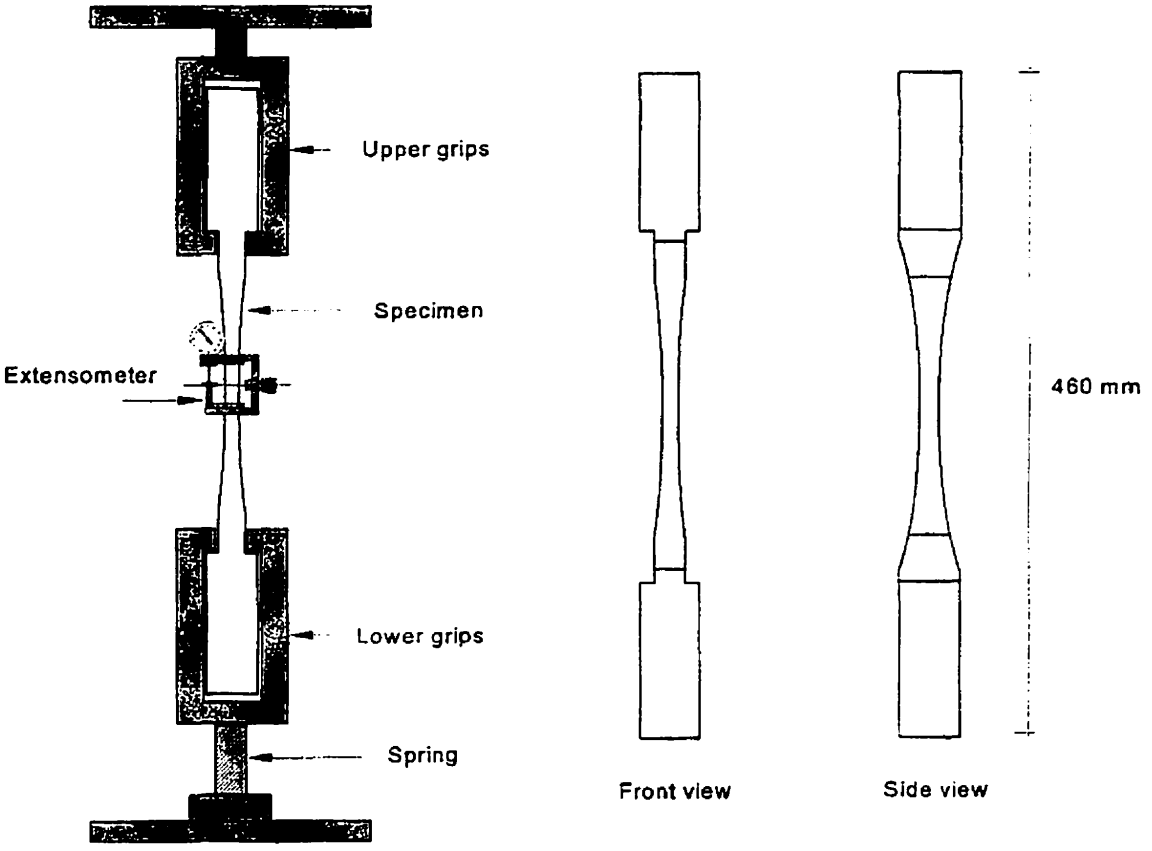

Figure 4. 1 Specimen and Test Setup for Tension Parallel to Grain (ASTM D 143)

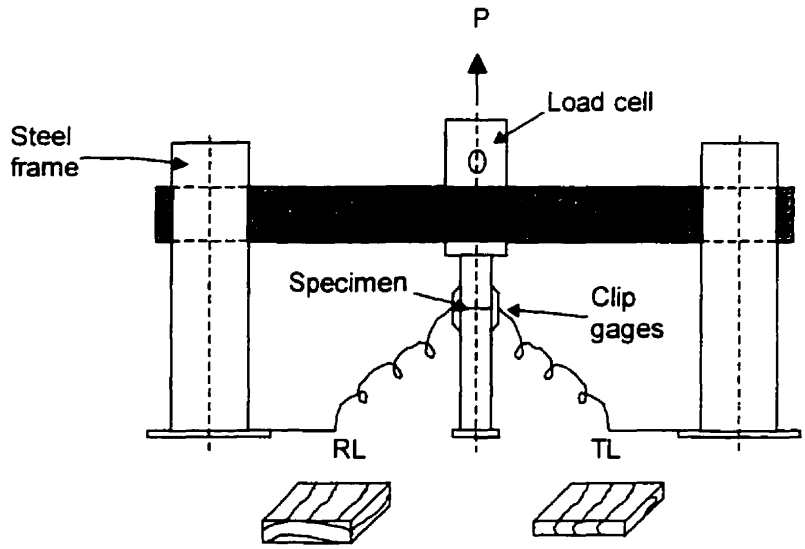

Figure 4. 2 Specimens and Test Setup for Tension Perpendicular to Grain (Vasic et al. 1996)

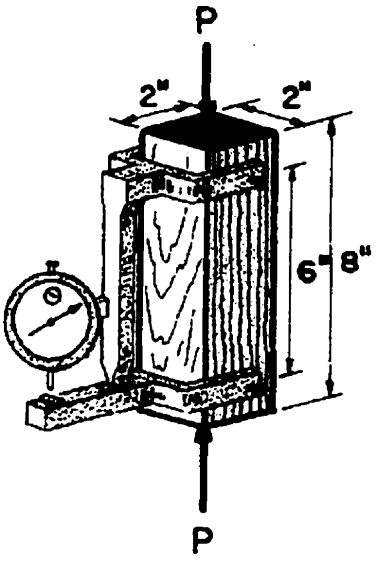

Figure 4. 3 Specimen and Test Setup for Compression Parallel to Grain

(ASTM D 143) (Bodig and Jayne 1982)

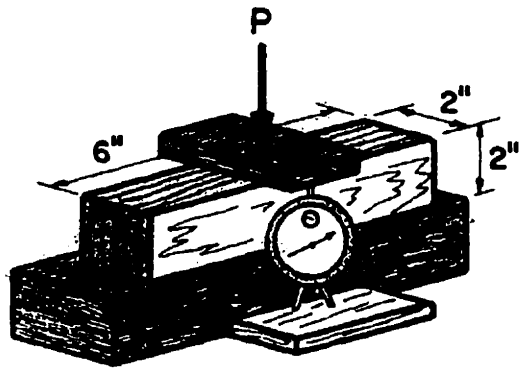

Figure 4. 4 Test Setup for Compression Perpendicular to Grain

(Bodig and Jayne 1982)

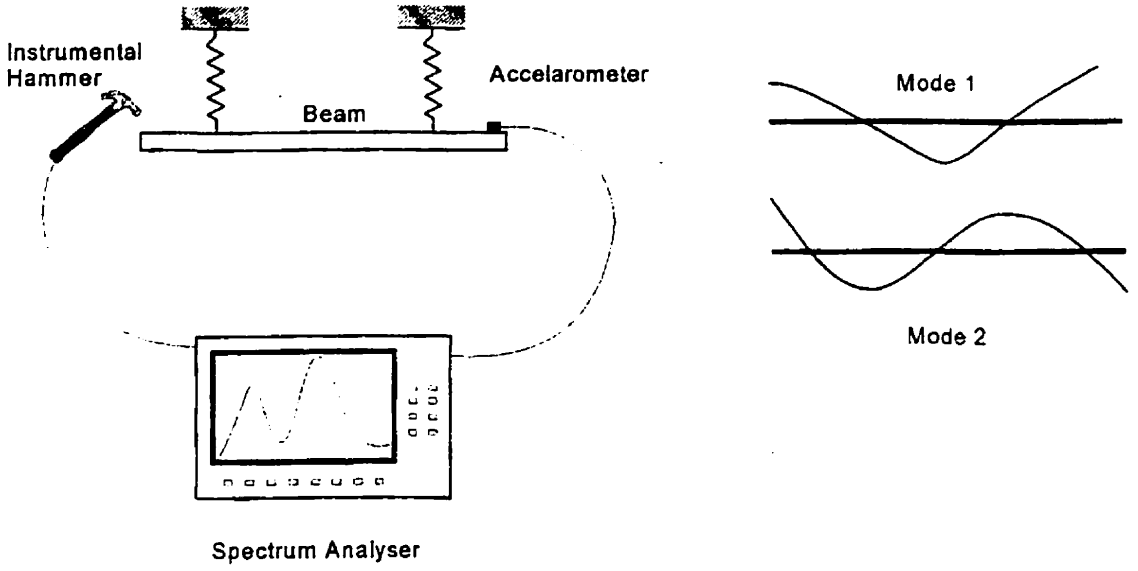

Figure 4. 5 Test Arrangement and Mode Shapes for the Vibration Test (Chui, 1991)

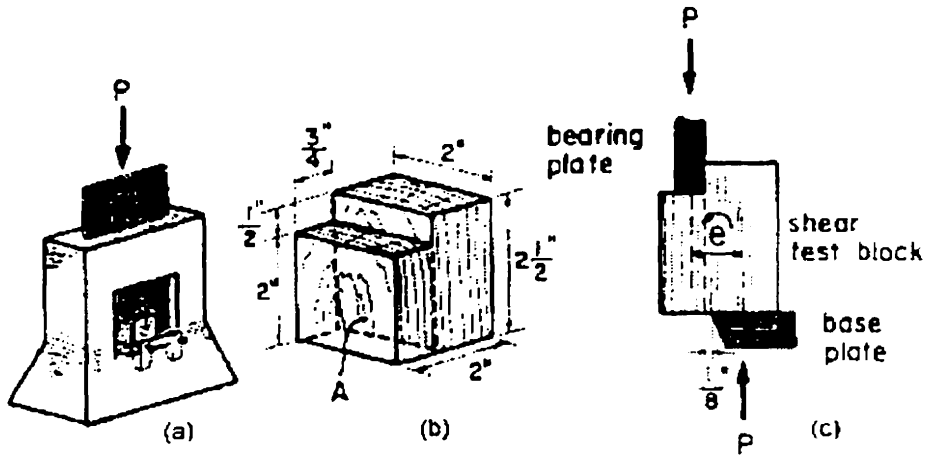

Figure 4. 6 Shear Test Parallel to Grain (ASTM D 143), (a) Test Setup, (b) Specimen Dimensions and Shape, (c) Loading Conditions (Bodig and Jayne 1982)

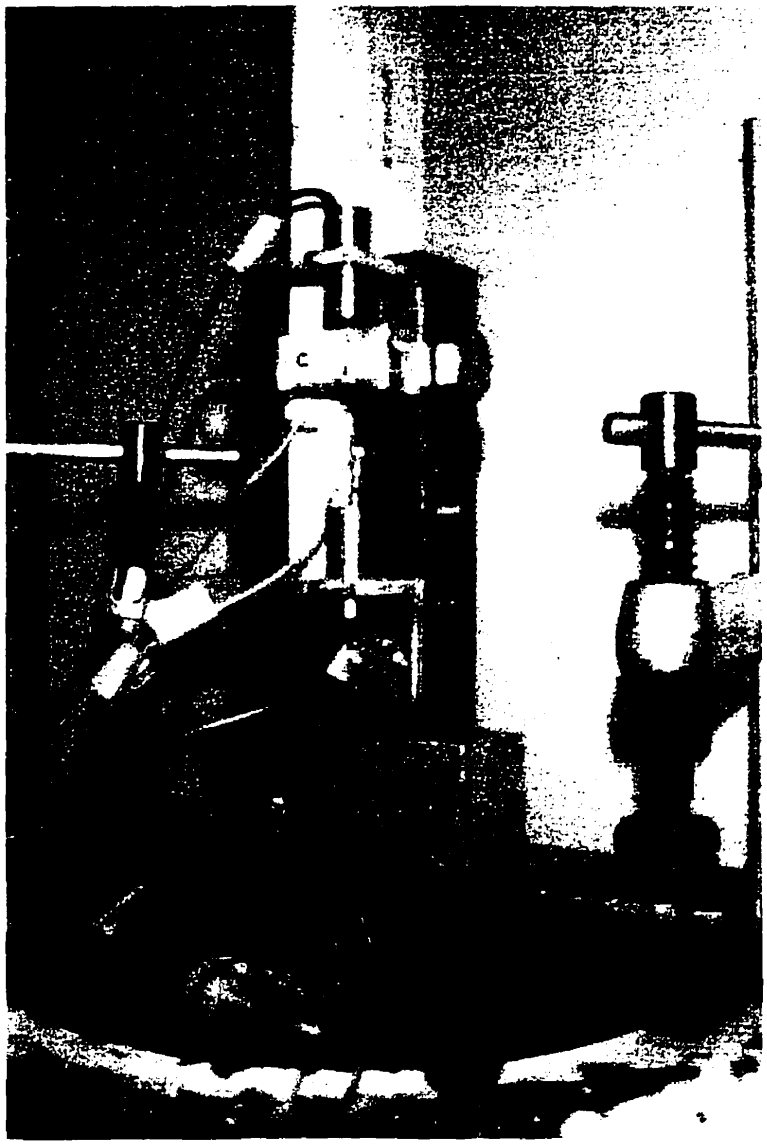

Figure 4. 7 Test Setup for One-Bolt Connection

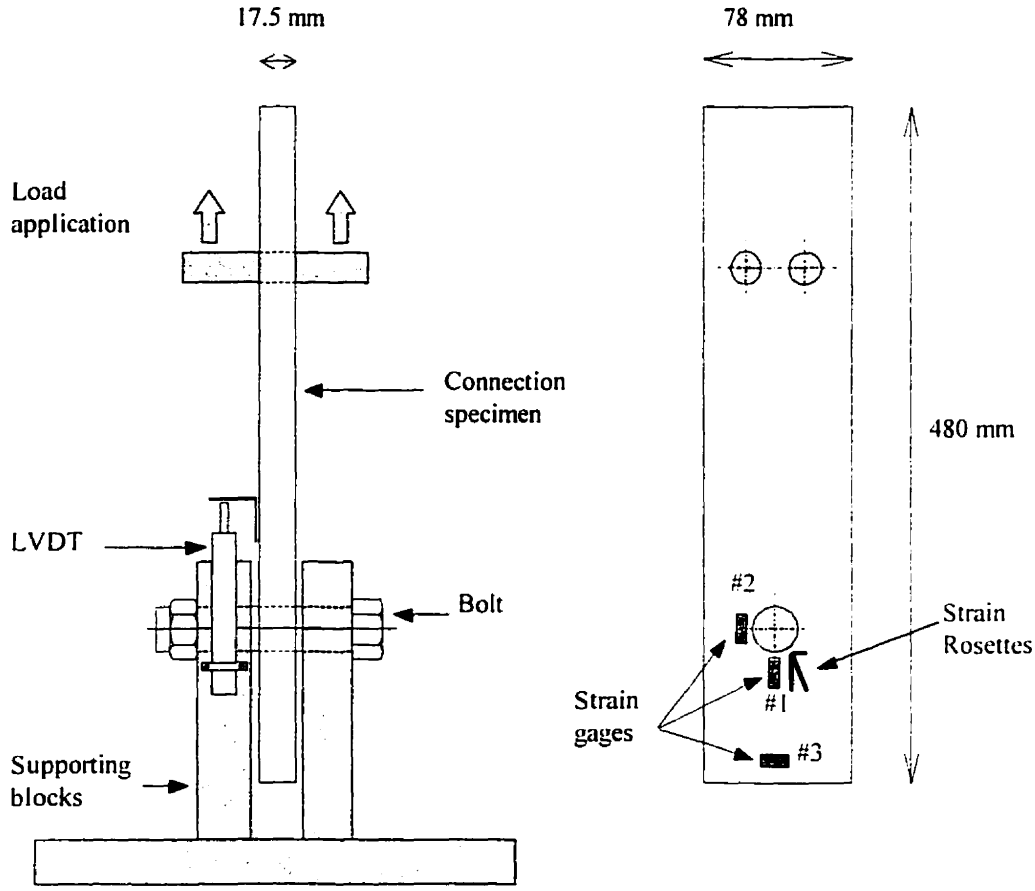

Figure 4. 8 Location of Strain Gages on a One-Bolt Connection Specimen

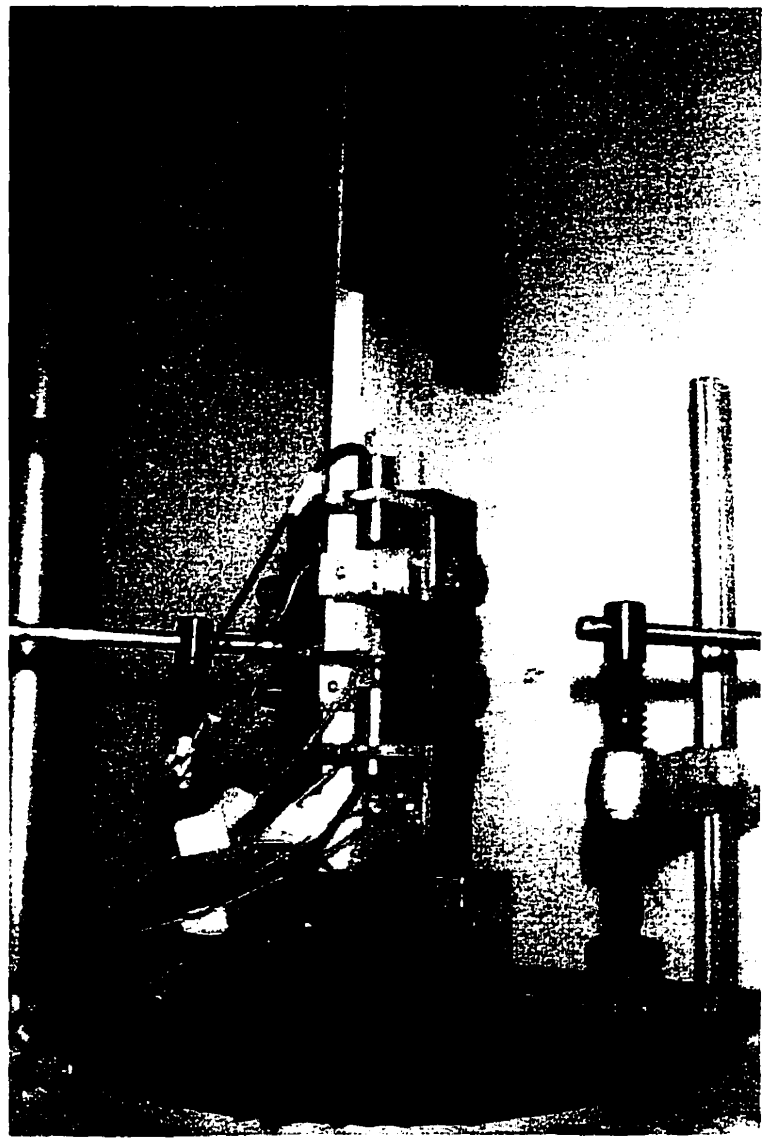

Figure 4. 9 Test Set-up for Two-Bolt Connection

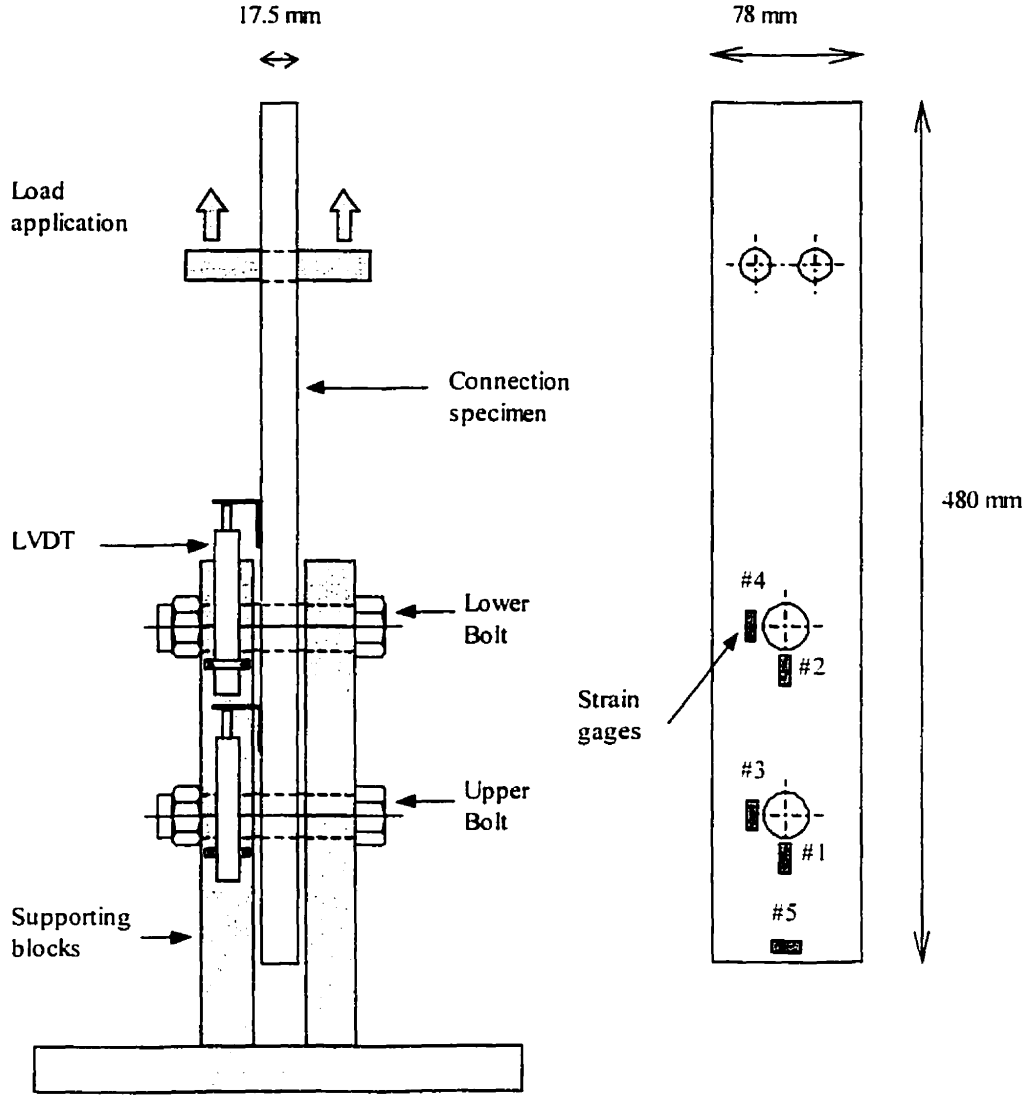

Figure 4. 10 Location of Strain Gages on a Two-Bolt Connection Specimen

Figure 4. 11 One-Bolt Connection Failed Specimen

Figure 4. 12 Two-Bolt Connection Failed Specimen

CHAPTER 5

RESULTS AND DISCUSSION

5.1 INTRODUCTION

A two-dimensional finite element model of wood bolted connections has been described, which appears to capture the nonlinear material and geometric effects of the problem. The experimental results of the material characterization tests are used as input data for the program. An extensive experimental program was then presented in which local and global deformations of one- and two-bolt timber connections were recorded. To completely fulfill the objectives of this thesis, it remains to check the ability of the proposed model to replicate the experimental behavior and to demonstrate the adequacy of the compressive material model to trace the inelastic deformation of the connections. In this chapter, these aspects are addressed first by conducting numerical simulations on pinned joints in wood and perforated fiber-reinforced composite tension strip for which solutions are available from literature. Thereafter, the model is applied to the problem of single- and double-bolted timber connections under short-term static loading and the generated numerical results are compared to experimental data.

5.2 VERIFICATION OF THE FINITE ELEMENT MODEL

5.2.1 Pin-loaded wood plate

In order to assess the accuracy of the finite element model with the elastic orthotropic material model, numerical results are generated to be compared to earlier experimental measurements of strains in a pinned-loaded wood plate (Wilkinson 1981). The sitka Spruce plates are 0.25 in thick with a 0.5 in diameter hole loaded by close-fitting steel pins parallel to grain (Fig 5.1). Plates with different e/d and w/d ratios were tested. Strains were measured using strain gages and Moiré fringes. Stresses were then computed based on linear elastic orthotropic theory.

The finite element mesh is similar to the one described in chapter 3. The material properties are given in table 5.1. Linear elastic orthotropy is assumed everywhere in the wood plate. Frictional contact between the pin and the wood plate was modeled with a coefficient of friction of 0.7 as suggested in the reported study.

The agreement found between the present finite element results and Wilkinson's experimental measurements of compressive stresses parallel to grain along the end line (Fig. 5.2) provides evidence of the adequacy of the linear elastic analysis away from stress concentrations. Measurements of strains near the hole were made possible with Moiré fringes. Figures 5.3 (a, b, and c) show a comparison between numerical and experimental compressive longitudinal stresses obtained using Moiré fringes. It is worth

noting that these measurements were taken at low load levels. Indeed the experimental failure load of these geometries was about 1600 lbs/in. The measurements at higher loads were not as accurate. It can be seen that predicted numerical stresses generated in the bolt-hole contact zone are higher than the recorded values. Also, the difference between the experiment and the analysis increases as the loading is increased. This is due to limitations of the elastic orthotropic material model that ignores inelastic deformation of wood beneath the pin.

5.2.2 Effect of friction

To study the effect of friction on the behavior of the wood joint, the model is run with frictionless contact using the same geometry described above. A comparison of two stress distributions on the hole boundary with a friction coefficient of 0.7 and ignoring friction (Fig. 5.4) shows that friction decreases the maximum compressive stresses parallel to grain beneath the bolt (Fig. 5.4a), and results in a more uniform bearing pressure distribution. Moreover, friction develops an extended region of compression perpendicular to grain (Fig 5.4b), and decreases shear stresses in the contact region (Fig. 5.4c). Overall, friction softens locally the behavior of the connection. This contrasts with past numerical findings by Wilkinson and his co-workers (Wilkinson 1981, Rahman et al. 1985) but is consistent with experimental findings by Rodd (1981). Therefore it is important to consider friction if local failure is to be modeled.

5.2.3 Perforated composite tension strip

The elasto-plastic material model is tested for an example of a perforated tension strip made of unidirectional Boron/Aluminum (U/D B/Al) metal matrix composite material. An experimental study of its elasto-plastic response was reported by Rizzi et el. (1987). The experiments involved loading the specimen as shown in Figure 5.5 with fibers oriented at 90° to the load. Many strain gages were mounted on the front and rear faces of the specimen.

The material properties used in the developed program are presented in table 5.2. For this particular problem, the Hill yield criterion is applied in tension and compression. The finite element mesh is less refined than the one described in chapter 3. Moreover, no contact modeling was needed.

Incipience of yield was found to occur adjacent to the hole at a remote stress of 4 ksi. Figure 5.6 shows representative illustrations of the development of plastic zones at increasing remote stresses of 6, 9.43, and 10.7 ksi, respectively. These plots are comparable to earlier numerical studies conducted by Vaziri et al. (1992). At the maximum remote stress of 10.7 ksi, the plastic zone appears to have progressed completely adjacent to the hole and across the specimen. The distribution of transverse tensile strains along the edge line is depicted in figure 5.7 for all load steps considered in the reported study. Agreement is found between Rizzi's recordings of strains and the present numerical predictions of elasto-plastic strains. These results confirm the accuracy of the elasto-plastic material model.

The elasto-plastic compressive material model can now be applied with confidence to the problem of bolted connections in wood. This proposed material model seeks improvement over the linear elastic orthotropic model in the predictions of local and global deformation of the connections. Its effect on the load transfer for double-bolted connections is also studied.

5.3 POST ELASTIC DEFORMATION OF ONE-BOLT CONNECTION

5.3.1 Connections with edge distance w = d (W1E3, W1E5)

The variation of strains with the applied load for strain gages #1, 2, and 3 are shown on figures 5.8 (a, b, and c) for the configuration W1E3 and figures 5.9 (a, b, and c) for the configuration W1E5. Numerically predicted strains are compared with strain gage readings recorded for seven replicates of each configuration. A plot of the numerical strains obtained using the elasto-plastic compressive material model is also included if the values are different than those obtained using the linear elastic orthotropic material model. The same scale for the axes of strains (up to 0.01) has been chosen for comparative assessement of the relative magnitudes of strains in different directions.

In general, the trends exhibited by the FEM results are consistent with the experiment. The nonlinear behavior of compressive longitudinal strains observed at

gage #1 for both configurations (fig. 5.8a and fig. 5.9a) is initially caused by the increased contact between the bolt and the hole. The predicted strains with the linear elastic material model fall in the lower range of the recorded curves and become softer as the load is increased. Better predictions are obtained with the elasto-plastic material model that seems to capture the stiffening behavior of the strains. This becomes more evident in the configuration with longer end distance, i.e W1E5. At a load approaching the experimental average failure load of about 9 kN, the numerical strains soften since the nodal point enters the plastic state. Lower experimental and numerical compressive strains are found for this latter configuration than for W1E3.

Tensile strains adjacent to the bolt-hole at gage #2 (fig. 5.8b and fig. 5.9b) are proportional to the applied load. The linear elastic orthotropic material model predicts very close values for both configurations that are in the average range of the experimental curves. Transverse tensile strains at the end of the connection depicted at strain gage location #3 are also proportional, in most cases, to the applied load (Fig. 5.8c and Fig. 5.9c). The agreement between the linear elastic numerical solutions and the experimental results appears fair. The elasto-plastic material model did not affect stresses and strains at these particular locations, and the same values were predicted. It is of interest to note that much higher strains perpendicular to grain are found with the configuration having shorter end distance, i.e W1E3.

Load versus displacement curves displayed on Fig. 5.10 for the configuration W1E3 and Fig. 5.11 for W1E5 represent the average of two curves recorded on each side of the wood member. Both curves were almost identical in most cases. Some of

the experimental curves are shifted to the right at the origin by removing the "uptake" region typically found due to small misalignements and roughness of the contact surface that are not modeled numerically. Numerically predicted load versus deformation curves with both material models are also plotted for comparison. As expected, they are slightly stiffer than the experiment. By modeling wood as elasto-plastic orthotropic, the curve becomes nonlinear as can be clearly seen from Fig. 5.11 for W1E5 having longer end distance, which agrees with the experimental curves. This is a notable improvement over the linear elastic orthotropic material model, usually assumed in the modeling of bolted connections.

To gain further insight into the extent of compression in the contact zone, numerical stresses on the hole boundary are plotted on Fig. 5.12 and Fig. 5.13 for this group of configurations at their respective average experimental failure loads (5.33 kN for W1E3, and 9.3 kN for W1E5). Compressive stresses parallel and perpendicular to grain substantially exceed the associated strengths with the linear elastic material model (average compressive strengths being $\sigma_{//}$ = 43 MPa and $\sigma_{\perp}$ = 8 MPa), as opposed to the post-elastic material model which increases the contact angle by 30% for W1E3 and 68% for the W1E5 configuration. This angle is found by noting the value on the curves at which the state of stress changes from compression to tension in both directions for each configuration considered. A region of high tension perpendicular to grain is being developed in both configurations.

Stress contour plots with both material models further prove the adequacy of the proposed material model to predict the post-elastic behavior of single-bolted

connections. Again, these contours are generated at the average experimental failure load for W1E3 (Fig.5.14) and W1E5 (Fig. 5.15). The contact compression zone is found to increase significantly for the W1E5 configuration causing a higher tension zone perpendicular to grain right after the end of contact between the bolt and the hole. This is also causing the region of high shear to shift on the hole boundary. Net tension caused by high tensile stresses parallel to grain and adjacent to the hole is one possible failure mode. Shear-out due to combined shear and tensile stresses perpendicular to grain on the boundary after the contact zone is an other possible failure mode. In fact these are the predominant failure modes noted in the experiments.

5.3.2 Connections with longer edge distance w = 2d

This group of connections entails the following set of configurations with increasing end distances: W2E3, W2E5, and W2E7. Using a longer edge distance results in a higher compressive zone in the contact area, but a lower tensile zone adjacent to the hole in the direction of loading. Tension perpendicular to grain at the end of the wood member becomes more critical for this group of connections. These observations can be inferred by comparing the strains at the same gage location for configurations from both groups having the same end distance, thus taking for example W1E3 vs W2E3, and W1E5 vs W2E5.

Similar trends in strain behavior as a function of load are observed, i.e. nonlinear in compression parallel to grain, and linear in tension parallel and perpendicular to grain. Although only three replicates have been tested, we can say that predicted numerical compressive strains with the linear elastic model are in general softer than the experimental strains (Fig. 5.16a, Fig. 5.17a, Fig. 5.18a). It is worth noting that recording strains as a function of load for the configuration W2E5 had to be stopped at low load values. The remaining seven replicates of this configuration were instrumented with strain rosettes. The model with the elasto-plastic orthotropic material improves the predictions of compressive strains particularly with connections having longer end distance which show stiffening of strains (W2E7). Numerical tensile strains agree with the tests (Fig. 5.16b, Fig. 5.17b, Fig. 5.18b). Like with the first group of connections, transverse strains decrease as the end distance is increased (Fig. 5.16c, Fig. 5.17c, Fig. 5.18c).

It is important to note that all of the previous plots near strain concentrations were along the line of symmetry where shear is negligeable with respect to the chosen axes. The point of the rosette location is however under a bi-axial state of compression and shear. Strains were recorded seven millimeters away from the hole and at 10 degrees from the horizontal at 0 deg. (ε_0), 45 deg. (ε_{45}), and 90 deg. (ε_{90}). Shear strains, ε_{shear} can then be calculated as :

$$\varepsilon_{shear} = 2\varepsilon_{45} - \varepsilon_{90} - \varepsilon_0 \qquad (5.1)$$

The components of strains for the rosettes are plotted on Fig. 5.19, along with FEM predictions. Numerical compressive strains parallel and perpendicular to grain fall within the experimental recorded curves (Fig. 5.19a, b). With the linear elastic orthotropic model, predicted shear strains fall below the experimental values (Fig. 5.19c). With the elasto-plastic orthotropic model, shear strain values are over-predicted at the beginning of loading. At the onset of plasticity (P= 5 kN), strains start decreasing. Even though the trend is not similar to the experimental curves, which are very variable, softening of shear is accomplished with the proposed material model.

The plots of the overall load versus deformation of connections W2E5 and W2E7 (Fig. 5.20 and Fig. 5.21, respectively), demonstrate once more the predictive capability of the proposed model to trace the inelastic deformation of the load-slip behavior. No bending of the bolt was observed at the end of the test although it might have been deformed slightly. To determine the effect of the bolt deformation on the load-slip curve, the bolt was modeled as a steel beam for the connection having an end distance of 7d. With the new 3-D model, it is found that deformation is only 5% higher than the one found using a 2-D model. Furthermore the inelastic deformation is solely caused by the post-elastic deformation of wood beneath the bolt. The constant increase in displacements without further increase in load beyond the maximum load is caused by cracking failure of the wood member and is not modeled numerically.

The predicted curves are once more stiffer than the experimental curves. This can be attributed, in large part, to the roughness of the hole surface which leads to a

'soft layer' that the model ignores. In other words, the effective hole is rather larger than the actual drill diameter. To study the effect of oversizing the hole diameter on the behavior of the connection, numerical results for the W2E5 configuration are generated with a diametral clearance of 2.5 mm. Initially, for the locations studied, oversizing the hole does not appear to have any effect on the predicted local strains. A softer behavior is predicted at high load levels for compressive strains at gage location #1 (Fig. 5.22a). On the other hand, the load slip curves are softened as the clearance is increased (Fig. 5.22b).

Figure 5.23 shows the difference in the contact angles on the hole-boundary as a function of load between both analyses made for W2E5 configuration. The contact angles are approximated by multiplying the number of contact segments found numerically in each load step by 1.5 degrees since one quarter of the hole is divided into thirty elements. The contact between the bolt and the hole increases nonlinearly with the load. A difference of almost 42 % is observed at maximum load. This is accompanied by an increase in the bi-axial compression zone and a shifting of a high shear-stressed zone along the boundary as can be inferred from comparing the contour plots of this configuration using the elastic orthotropic model and the elasto-plastic orthotropic model (Fig. 5.24 a and b). An increase in tensile stresses perpendicular to grain right after the contact zone can also be observed. Combined shear and tension perpendicular to grain can cause cracking of planes parallel to the fibers along the sides of the contact zone. This corresponds to the shear-out predominant failure observed in the experiments.

The spreading of plastic zones and contours of the non-dimensional effective stress σ_e/k for the same configuration W2E5 are depicted in Figure 5.25 for three different load levels: 4, 7, and 10 kN respectively. Incipience of plastic deformation was found to occur right beneath the bolt at a low load of approximately 2 kN. As the loading increases, the plastic zone extends in depth towards the end member in the direction of loading and in large along the hole-boundary. The characteristic shape and growth of the plastic zone at the maximum load, about 10 kN, can be associated with the compressed "column" of material which fails in bearing parallel to grain.

5.4 Post Elastic Deformation of Double-Bolted Connections

5.4.1 Connections with spacing s = 3d (S3E3, S3E5)

5.4.1.1 Load distribution

One of the problems encountered in multi-bolted connections employing stocky bolts is that the load is not equally shared among the bolts. There is an interaction of the stress fields around the bolts that is not fully understood or determined and that depends on configuration parameters such as the number of bolts, the spacing between the bolts, the end and edge distances. The unequal load sharing observed for the double-bolted timber connections tested was verified numerically by calculating the value of the resultant contact forces in the direction of loading on each contactor or

target surface for each load step. It was not always possible to verify this experimentally by the recorded strains on each loaded bolt.

Figure 5.26 shows the variation of the load fractions in each bolt as a function of the total load applied for the S3E3 configuration. A higher portion of the load is carried by the lowest bolt. This was also supported by the experiments for which strain readings on the bolts indicated that the lower bolt carried approximately 55% of the load. This is very close to what is predicted numerically using both material models for up to a load of 5 kN. Then the difference between load fractions increases with the linear elastic material model, while it remains almost constant with the elasto-plastic material model. This means that with the proposed model the load gets redistributed over the bolts. This disparity in load sharing causes a difference in the contact area of about 20% at the average experimental failure load (Fig. 5.27). The increase in contact angle is nonlinear with the applied load with both analyses. A higher contact area is found with the proposed model on both bolts.

By increasing the end distance and keeping the spacing relatively small, the load becomes almost equally shared between the bolts for the S3E5 configuration. This can be concluded from Fig. 5.28. Both analyses give very close predictions in load proportioning, but there is still a difference in the contact area, which is found to be much larger using the elasto-plastic material model (Fig. 5.29).

5.4.1.2 Stress and strain distribution

It was mentioned in the experimental results and observations that due to imperfections in the experiments, one of the bolts may transmit almost no load during a major portion of joint loading. Even though six replicates have been tested for this group of configurations, the bolts start to load the wood member at the same time in only two tests for the S3E3 configuration and three tests for the S3E5 configuration. The strain readings for these tests as a function of load are shown on Figures 5.30 and 5.31 for five locations near stress concentrations of the upper and lower holes. The readings for all replicates were included for tensile strains parallel and perpendicular to grain.

Better numerical predictions of compressive strains parallel to grain for the upper and lower bolts were obtained with the elasto-plastic material model when compared to experimental strain recordings (Figs. 5.30a, b for the S3E3 configuration and Figs. 5.31a, b for the S3E5 configuration). In the first configuration studied, the compressive strains obtained with the elasto-plastic model depart from the elastic numerical strains at an earlier load in the lower bolt (about 3 kN) because this bolt carries a higher portion of the total load. Whereas for the latter configuration, and since the load carried by each bolt is almost equal, both gage locations enter the plastic stress state simultaneously at a load of about 6 kN.

Tensile numerical strains parallel to grain and adjacent to the lower bolt are higher than those predicted adjacent to the upper bolt. Agreement is found between the tests and FEM model for both configurations (Fig. 5.30c, d and Fig. 5.31c, d). Higher

tensile strains perpendicular to grain are predicted for the first configuration S3E3 having a shorter end distance (Fig. 5.30e compared with Fig. 5.31e). Like with the single bolted connections, the elasto-plastic material model does not give different values for tensile strains in the specified locations. Furthermore, the nonlinear relationship between compressive strains and load and the linear relationship between tensile strains and load is still verified experimentally and numerically for each individual bolt-hole interaction.

Regarding the global deformation of double-bolted connections, it is not possible to compare the numerically predicted load versus displacement curves with the experimental curves because the number of tests is not representative of the variation of these curves. For this reason, the curves depicted on Fig. 5.32 are the ones found numerically using both the elastic and elasto-plastic analysis for the S3E3 configuration. We should note however that non-linearity starts at the same level of loading as in the experiment, that is 12 kN.

The interaction of stress fields between the two bolts is illustrated on the stress contour plots for S3E3 on Fig. 5.33 and S3E5 on Fig. 5.34 using the elasto-plastic material model. Shear failure can be triggered by excessive shear stress between the bolts and tension perpendicular to grain on the lower bolt.

5.4.2 Connections with longer spacing s = 5d (S5E3, S5E5)

5.4.2.1 Load distribution

By increasing the spacing between the loaded holes in the wood member, the difference in load sharing increases. With the shorter end distance, both numerical analyses predict a load distribution of about 60% for the lower bolt and 40% for the upper bolt for the S5E3 configuration at a load of 4 kN (Fig. 5.35). It is the largest difference amongst all the configurations tested. Then this difference increases with the applied load with the linear elastic material model, while it decreases with the elasto-plastic material model and drops to 55% for the lower bolt and 45% for the upper bolt at the average experimental failure load. Once bearing starts beneath the lower bolt, more load gets absorbed by the upper bolt. The contact area on the lower bolt is greater for this particular configuration and reaches almost 70 degrees on the hole boundary at maximum load (Fig. 5.36).

Increasing the end distance does not seem to have much effect on load sharing or contact as with the first group of connections. This can be inferred from comparing Fig. 5.35 and Fig. 5.37 for load fractions, and Fig. 5.36 with Fig. 5.38 for bolt-hole contact. Table 5.3 summarizes the variation of load sharing with spacing and end distance for the four double-bolted connections studied. The values are obtained at the average experimental failure loads for each configuration. The disparity in load fractions decreases if the spacing is decreased or the end distance is increased. It is interesting

to note that the same load fraction (55% for the lower bolt and 45% for the upper bolt) is reached at the maximum load for S3E3, S5E3, and S5E5. A summary of the variation of the maximum contact angle with spacing and end distance is shown in table 5.4. The same effect as on load sharing is found.

An estimate of the connection strength can be found by taking the inverse of the maximum load proportion. For the S5E3 configuration for example, the elasto-plastic model gives an destimate of 1/0.55=1.8 x the strength of a single bolted connection. This value is bounded by the EYM prediction, being 2, and the linear elastic prediction, being 1/0.65=1.5 and which is judged to be conservative. Therefore, the proposed model gives a better estimate of the connection strength with multiple bolts than the EYM or the linear elastic model.

5.4.2.2 Stress and strain distribution

By comparing the local strain distributions parallel to grain in the contact area using both types of analyses for both configurations (Figs. 5.39a, b and Figs. 5.40a, b), it is interesting to note that stiffening of the strains with the elasto-plastic material model occurs mainly in the lower bolt. That is a direct consequence of this bolt carrying a higher portion of the joint load. Closer agreement is obtained with the experiment. Predicted strain values at gage #1 for the upper bolt don't change significantly using the elasto-plastic analysis, and show agreement with experimental values.

With this second group of double-bolted connections, higher tensile strains are obtained in strain gage #4 than for the first group (Fig. 5.39d and Fig. 5.40d) while lower

values are found for gage #3 (Fig. 5.39c and Fig. 5.40c). As was expected, tension perpendicular to grain is higher in the S5E3 configuration (Fig. 5.39e compared with Fig. 5.40e).

The general stress distribution is further illustrated on contour plots using the proposed material model (Fig. 5.41 and Fig. 5.42). Higher contact zones are found beneath the lower bolt, for which stresses are deemed more critical. There does not seem to be much interaction between the loaded bolts as for the first group of connections. But the same shear-out mode of failure, resulting from shear and tension perpendicular to grain on the lower bolt, can be noted.

5.5 CONCLUSIONS

The proposed compressive material model has improved the predictions of the local wood behavior surrounding the bolts for the different single- and double-bolted connections studied. This was concluded from comparing predicted strains using both material models with strain gage readings at stress concentrations. It is found that inelastic deformation starts at low load levels beneath the bolt. As loading progresses, a larger contact area between the wood member and the bolt is developed. Failure is believed to be caused by combined shear stresses and tensile stresses perpendicular to grain along failure planes that lie either side of the compressed contact zone. This is consistent with the predominant shear-out failure mode observed in the experiments and reported in the literature.

Though the general failure is brittle, the load-slip curves of the single bolted connections with end distances of 5d and 7d show some ductility. These curves are of primary concern to engineers designing bolted connections since they are an indication of global deformation. The post-elastic deformation is caused by localized wood bearing. Unlike the linear elastic material model, the elasto-plastic model is capable of tracing this nonlinear deformation of the connections.

In the double-bolted connection configurations, the bolts start to load unequally at the beginning of the test. Then as bearing is developed beneath the bolt carrying the highest load fraction, the load gets redistributed over both fasteners and tends to be evenly shared at the end of the test. This confirms what is observed in the experiments. In this respect, and unlike the elastic model, the elasto-plastic compressive material model reflects the real behavior of double-bolted connections. A better estimate of the connection strength is also obtained when compared with the elastic material model or the EYM.

Table 5. 1 Input Material Properties for the Pin-Loaded Plate of Sitka-Spruce (Wilkinson 1981)

Elastic constant	**Input value (Psi)**
E_1	2.4×10^6
E_2	1.2×10^5
G	1.4×10^5
υ_{21}	0.5

Table 5. 2 Input Material Properties for the Perforated Tension Strip of U/D B/Al (Vaziri et al. 1992)

Elastic constant	**Input value (Psi)**
E_1	29.4×10^6
E_2	19.1×10^6
G	7.49×10^6
υ_{21}	0.169
Plastic constant	
E_{T1}	29.4×10^6
E_{T2}	4.0×10^6
G_T	0.22×10^6
σ_{10}	204×10^3
σ_{20}	13×10^3
S_0	6.5×10^3

Table 5. 3 Load Fractions on a Double-Bolted Connection at Average Experimental Failure Load

		s/d=3		**s/d=5**	
		Elastic analysis	*Elasto-plastic*	*Elastic analysis*	*Elasto-plastic*
e/d=3	*Upper*	42%	45%	35%	45%
	Lower	58%	55%	65%	55%
e/d=5	*Upper*	48%	48%	40%	46%
	Lower	52%	52%	60%	54%

Table 5. 4 Contact Angles for a Double-Bolted Connection at Average Experimental Failure Load

		s/d=3		**s/d=5**	
		Elastic analysis	*Elasto-plastic*	*Elastic Analysis*	*Elasto-plastic*
e/d=3	*Upper*	33°	48°	40°	40°
	Lower	42°	63°	45°	69°
e/d=5	*Upper*	36°	54°	38°	57°
	Lower	42°	69°	45°	69°

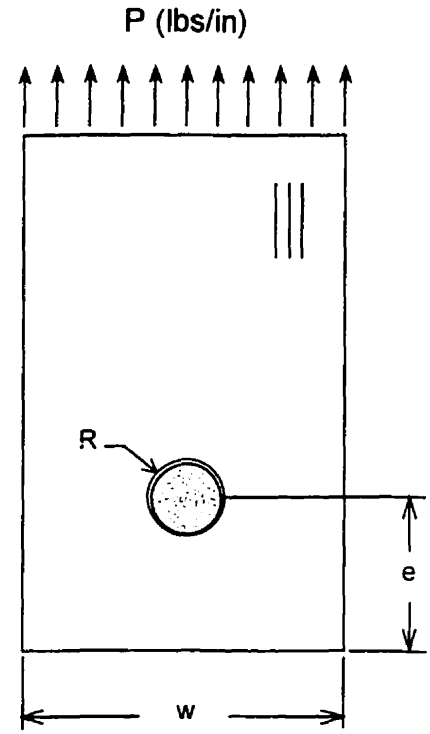

Figure 5. 1 Schematic of a Pin Loaded Wood Plate (Wilkinson 1981).

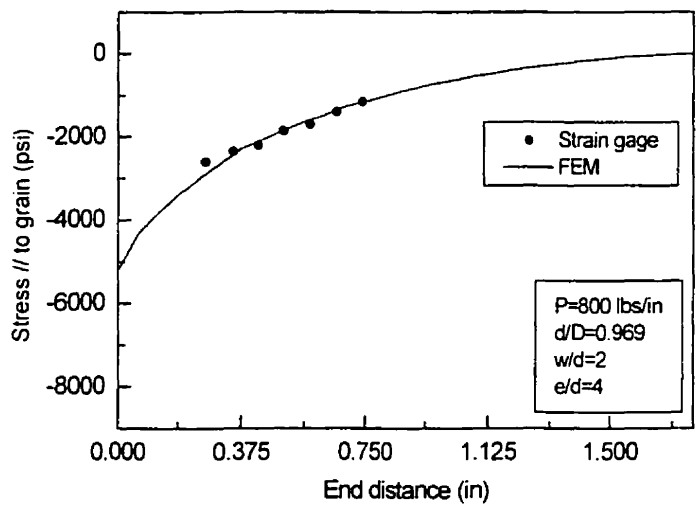

Figure 5. 2 Comparison between numerical and experimental compressive stresses along the end line using strain gages (Wilkinson 1981)

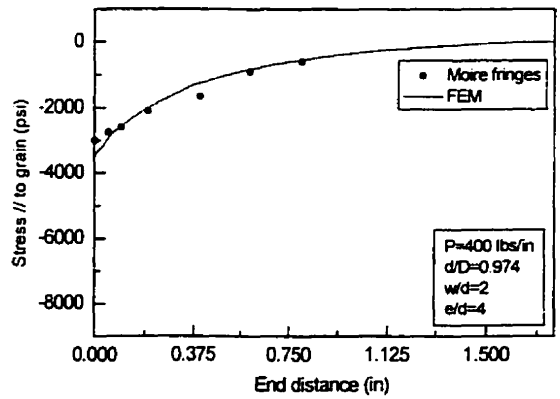

(a)

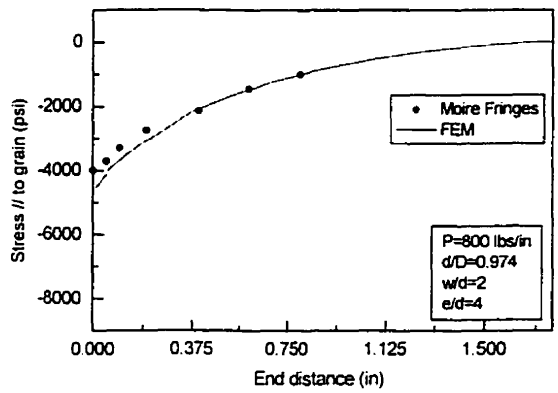

(b)

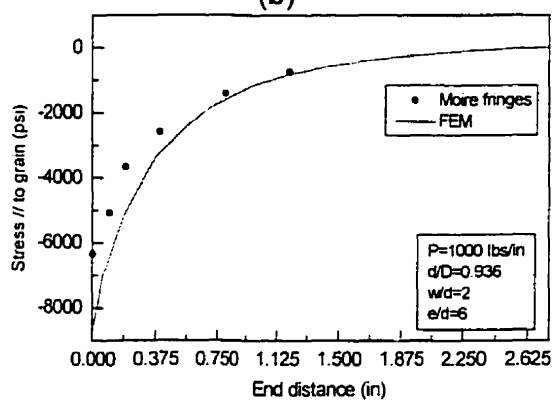

(c)

Figure 5. 3 Comparison between numerical and experimental compressive stresses along the end line using Moiré fringes (Wilkinson 1981)

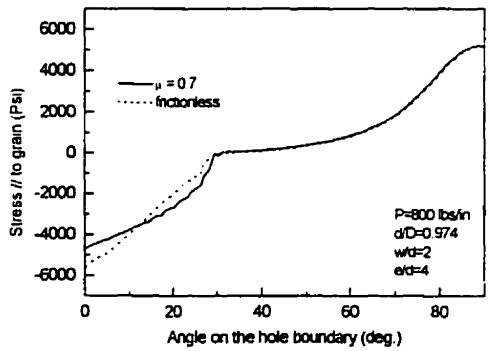

(a)

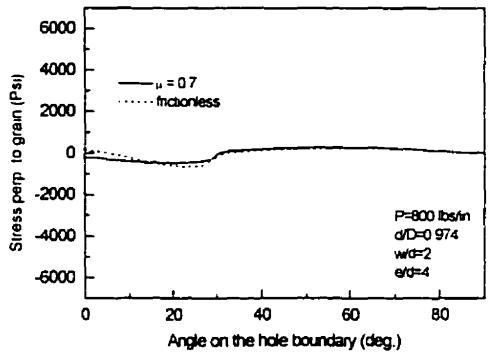

(b)

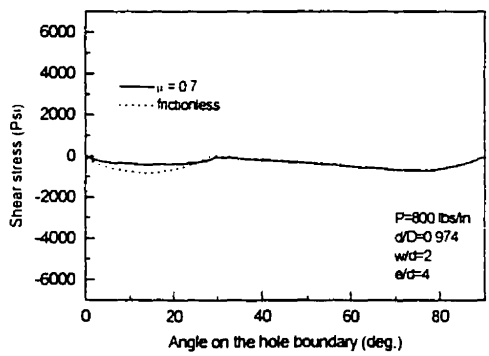

(c)

Figure 5. 4 Effect of friction on stress distribution along the hole boundary:

a) σ_z, b) σ_y, c) τ_{yz}

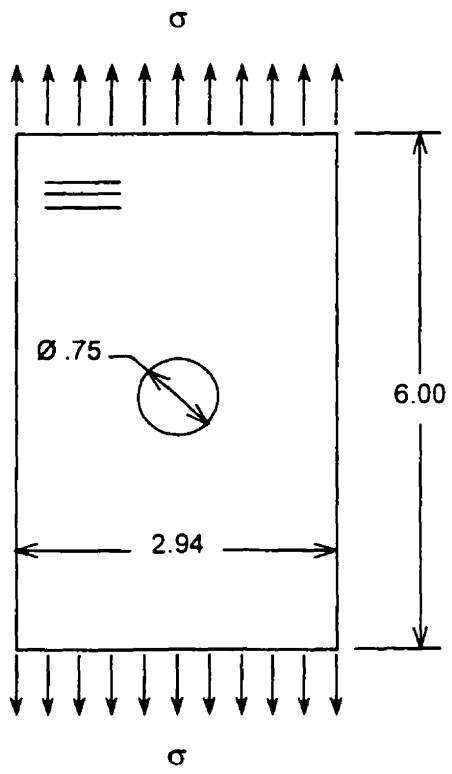

Figure 5. 5 Geometry of a Perforated 90° U/D B/Al Test Specimen (Rizzi et al. 1987).

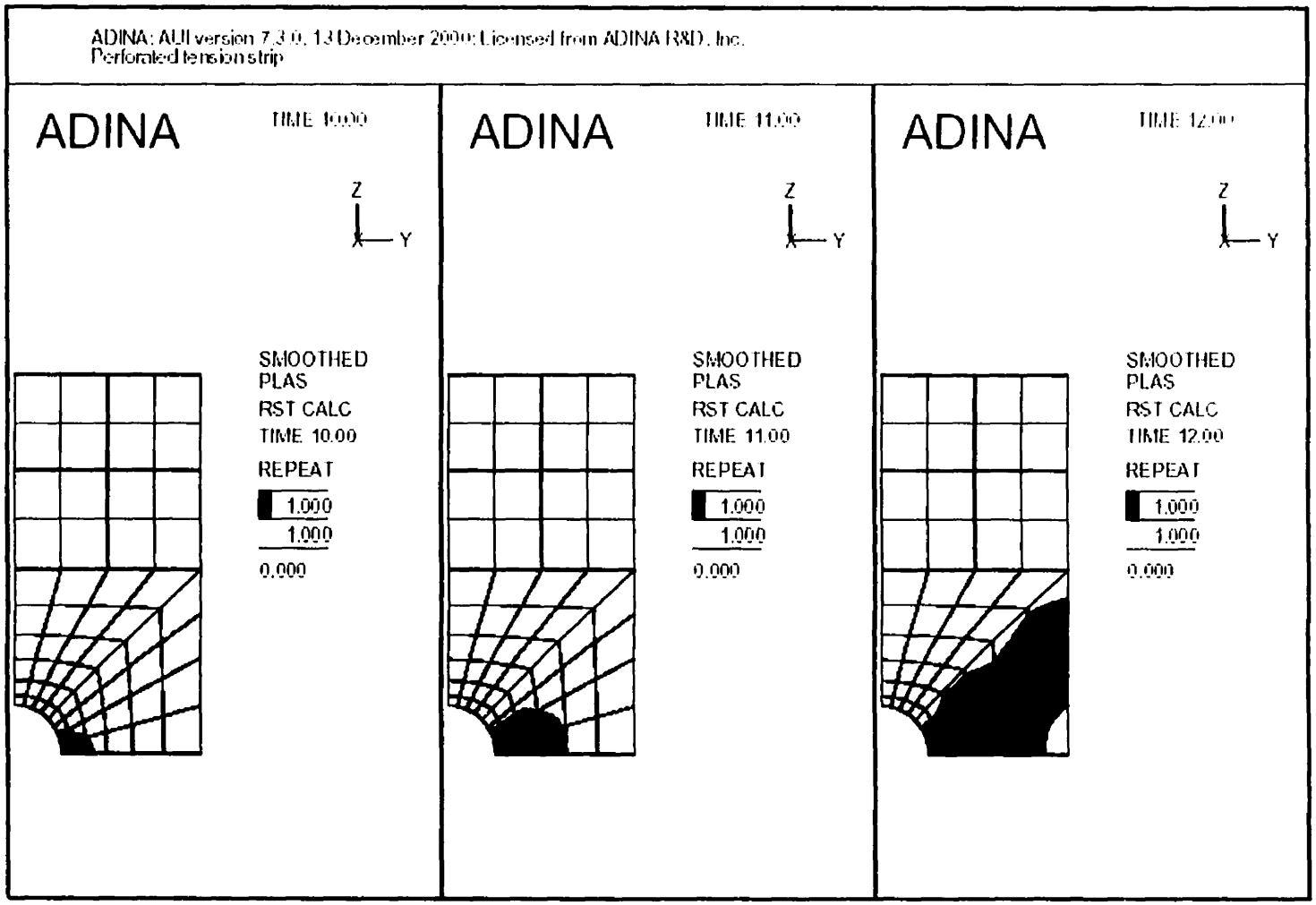

Figure 5. 6 Spread of Plasticity in a Perforated Tension Strip of U/D B/Al

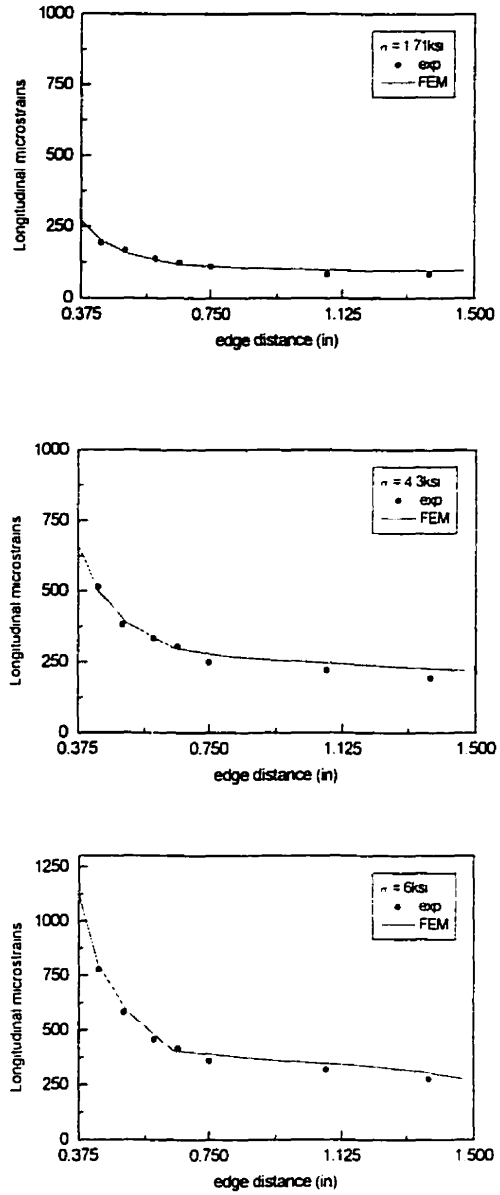

Figure 5. 7 Comparison between numerical and experimental transverse strains along the net section of a perforated 90° layer of U/D B/Al (Rizzi et al. 1987).

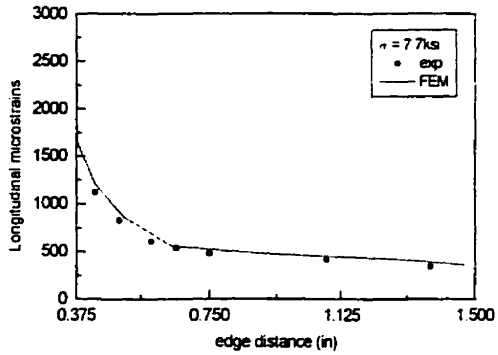

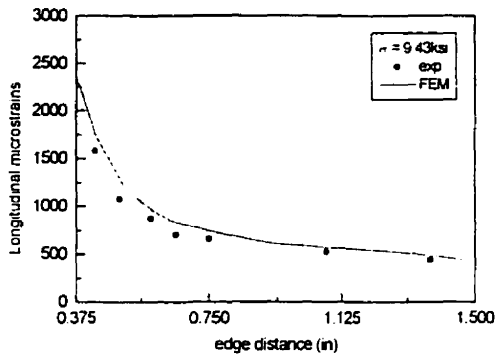

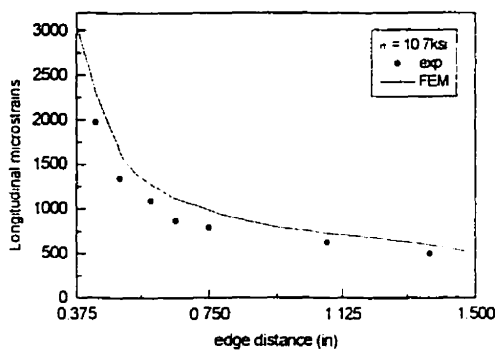

Figure 5.7 Continued.

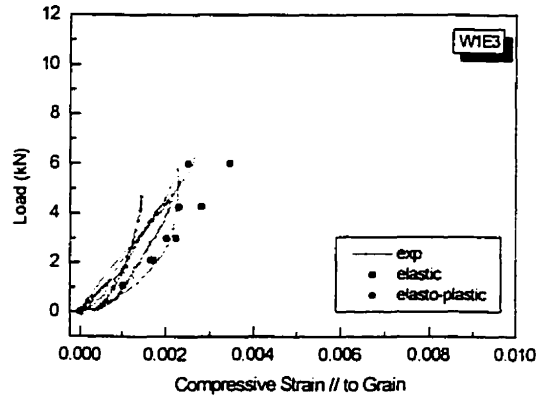

(a)

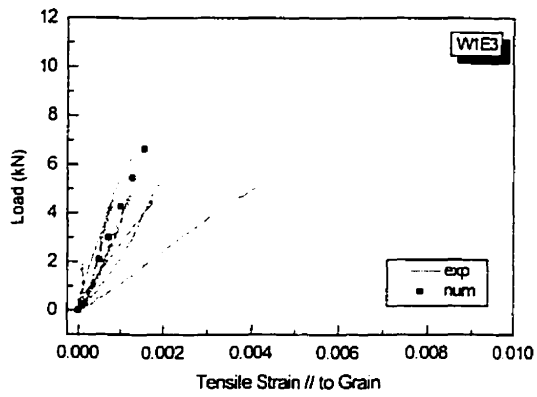

(b)

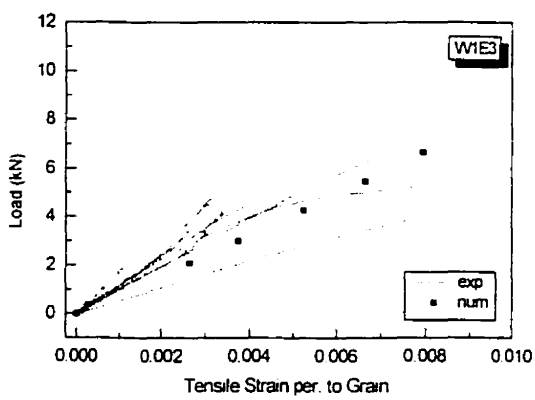

(c)

Figure 5. 8 Comparison between Numerical and Experimental Strains for W1E3

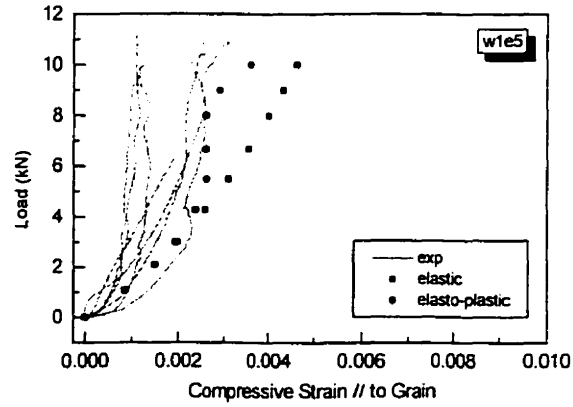

(a)

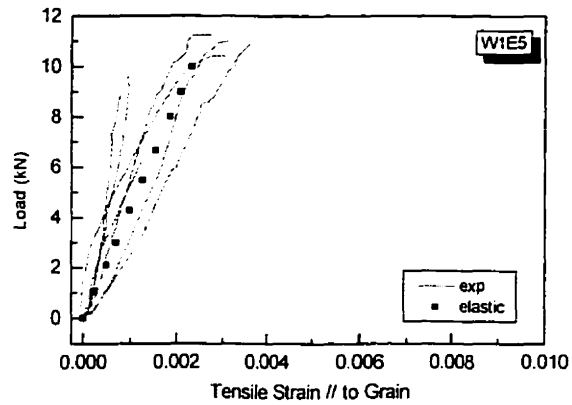

(b)

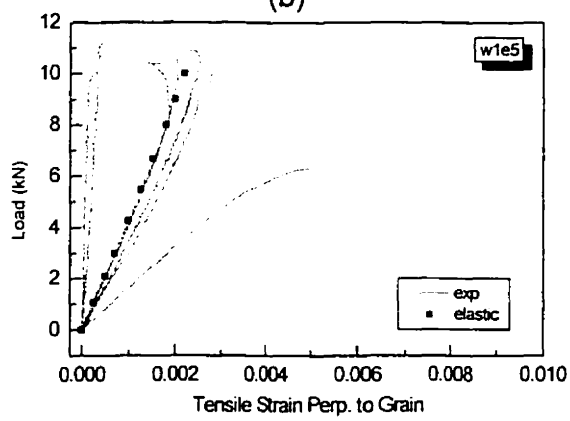

(c)

Figure 5. 9 Comparison between Numerical and Experimental Strains for W1E5

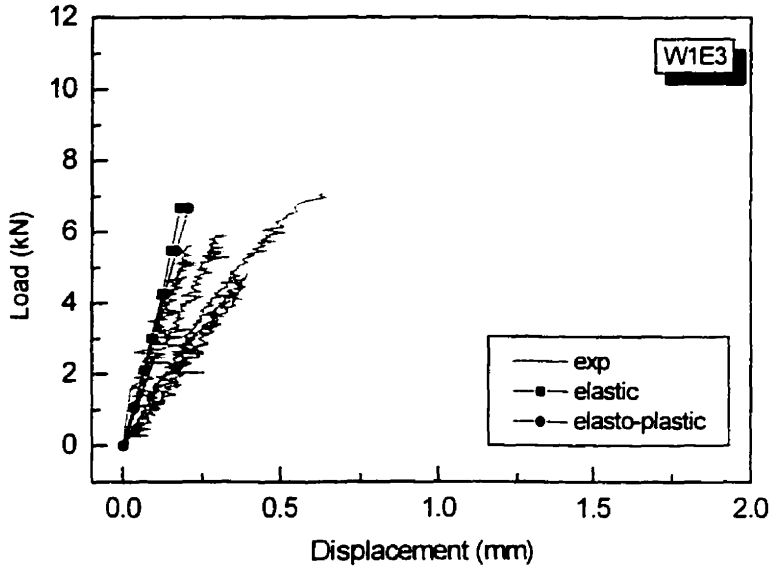

Figure 5. 10 Comparison between Numerical and Experimental Load vs. Deformation Curves for W1E3

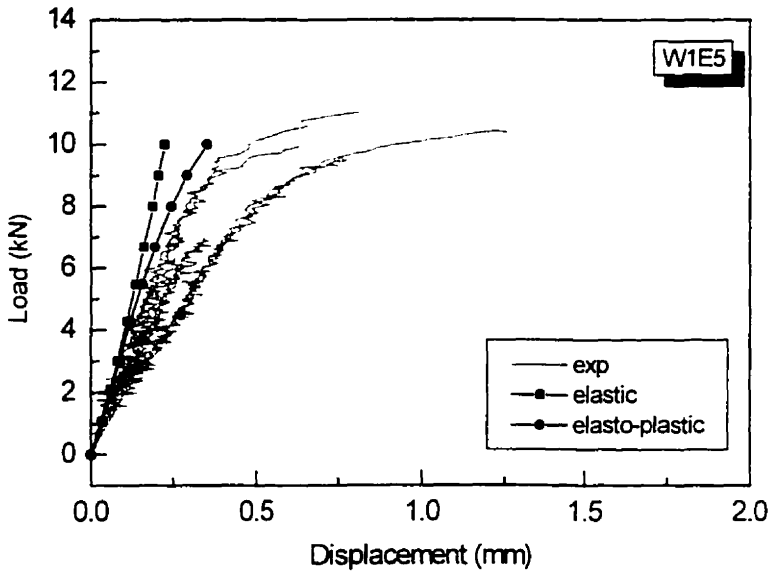

Figure 5. 11 Comparison between Numerical and Experimental Load vs. Deformation Curves for W1E5

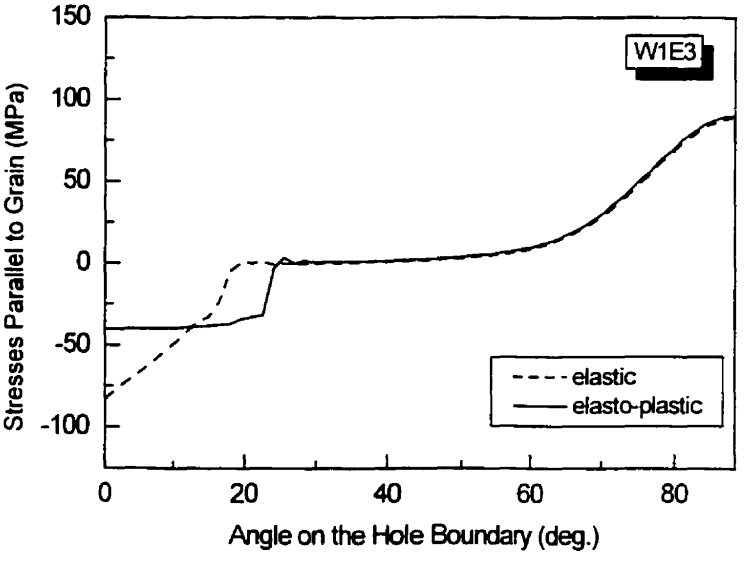

(a)

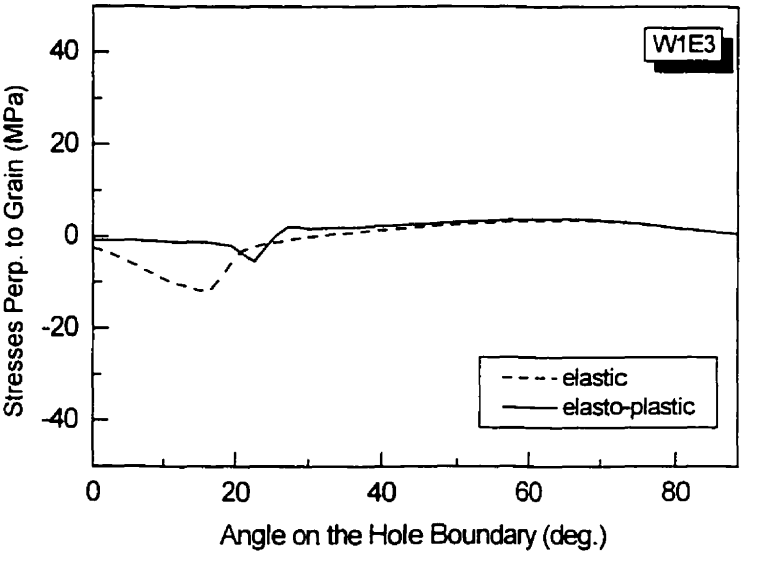

(b)

Figure 5. 12 Predicted Stress Distribution along the Hole Boundary for W1E3: a) Parallel to Grain, b) Perpendicular to Grain.

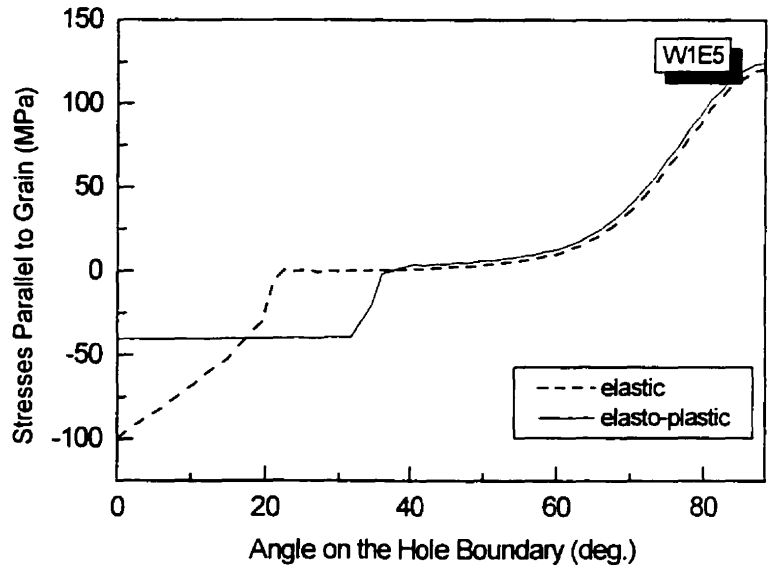

(a)

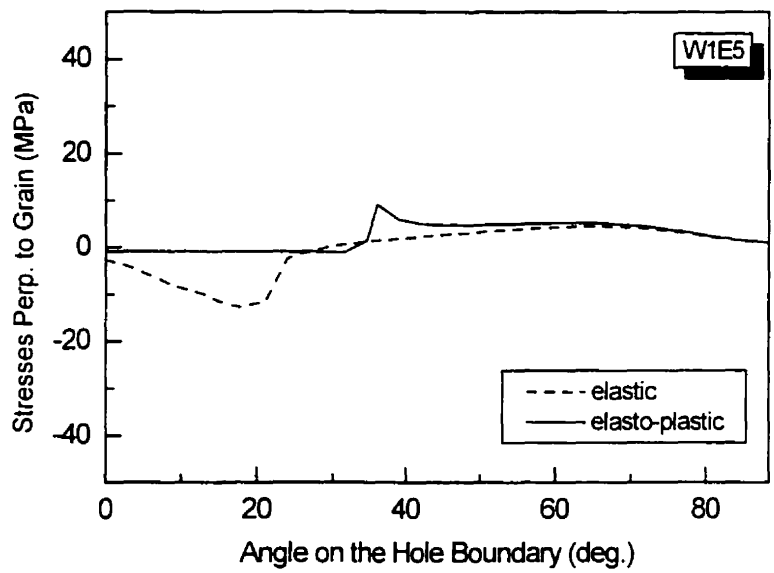

(b)

Figure 5. 13 Predicted Stress Distribution along the Hole Boundary for W1E5: a) Parallel to Grain, b) Perpendicular to Grain.

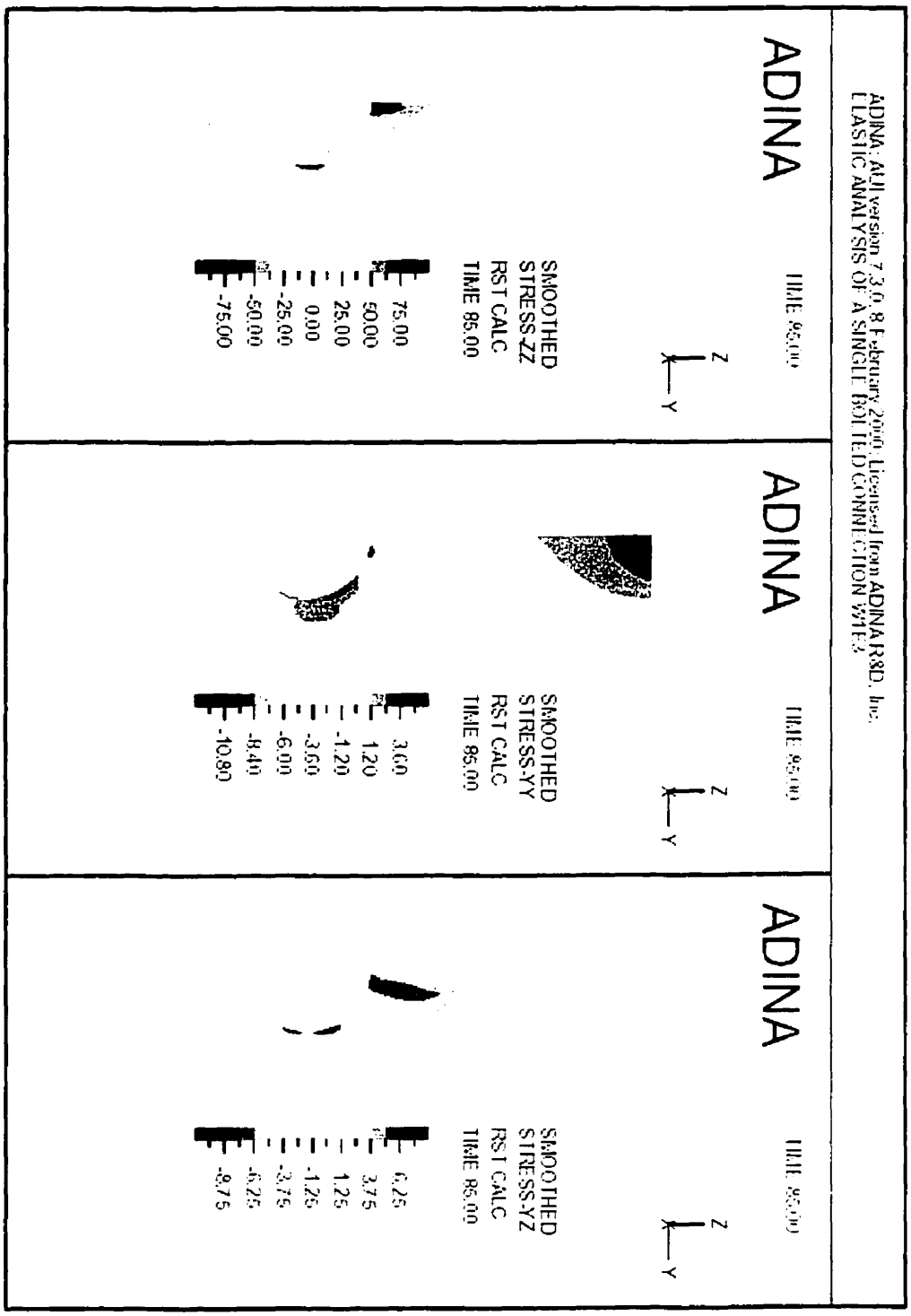

Figure 5. 14a Elastic stress distribution in a one-bolt connection W1E3

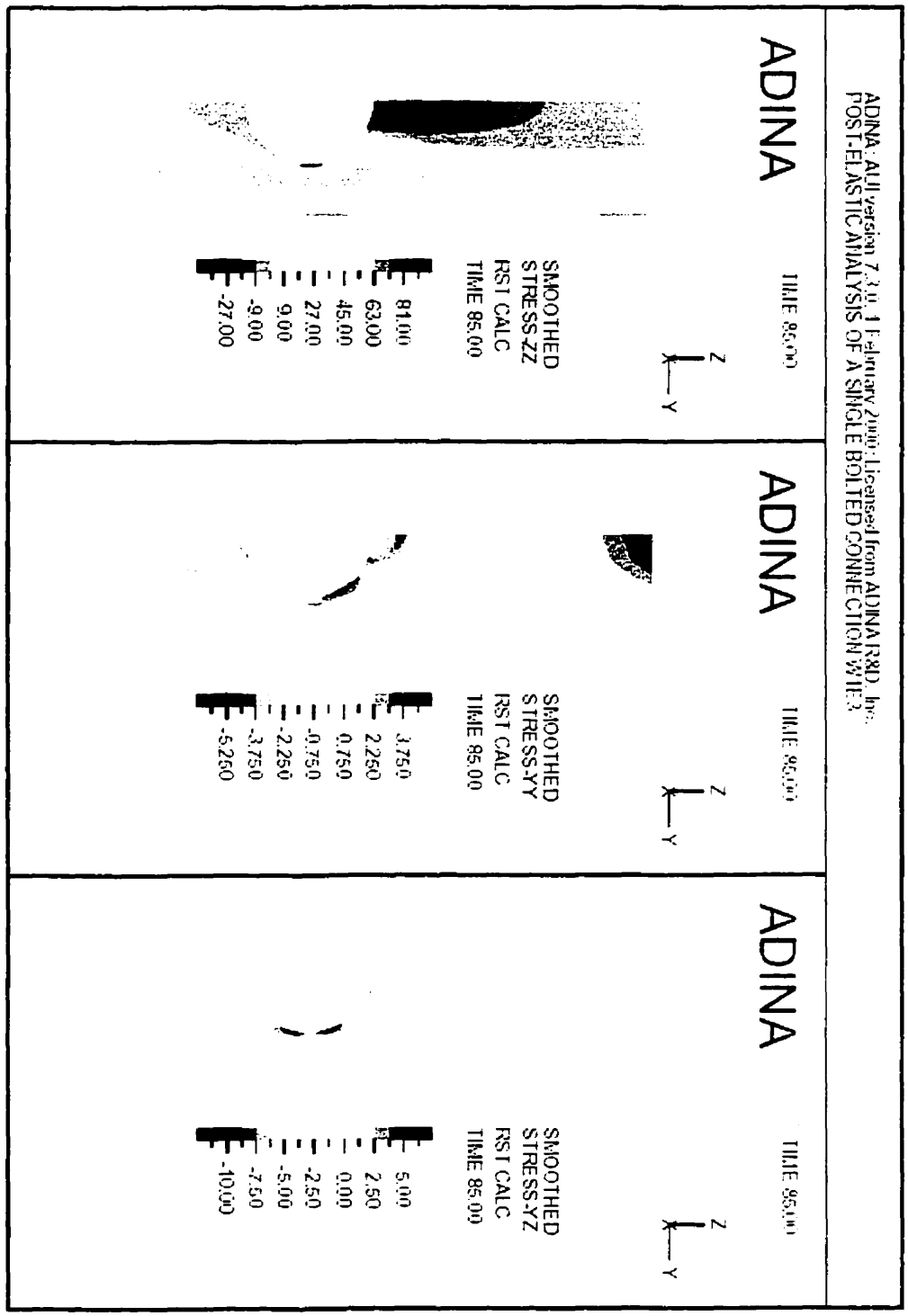

Figure 5. 14b Elasto-plastic stress distribution in a one-bolt connection W1E3

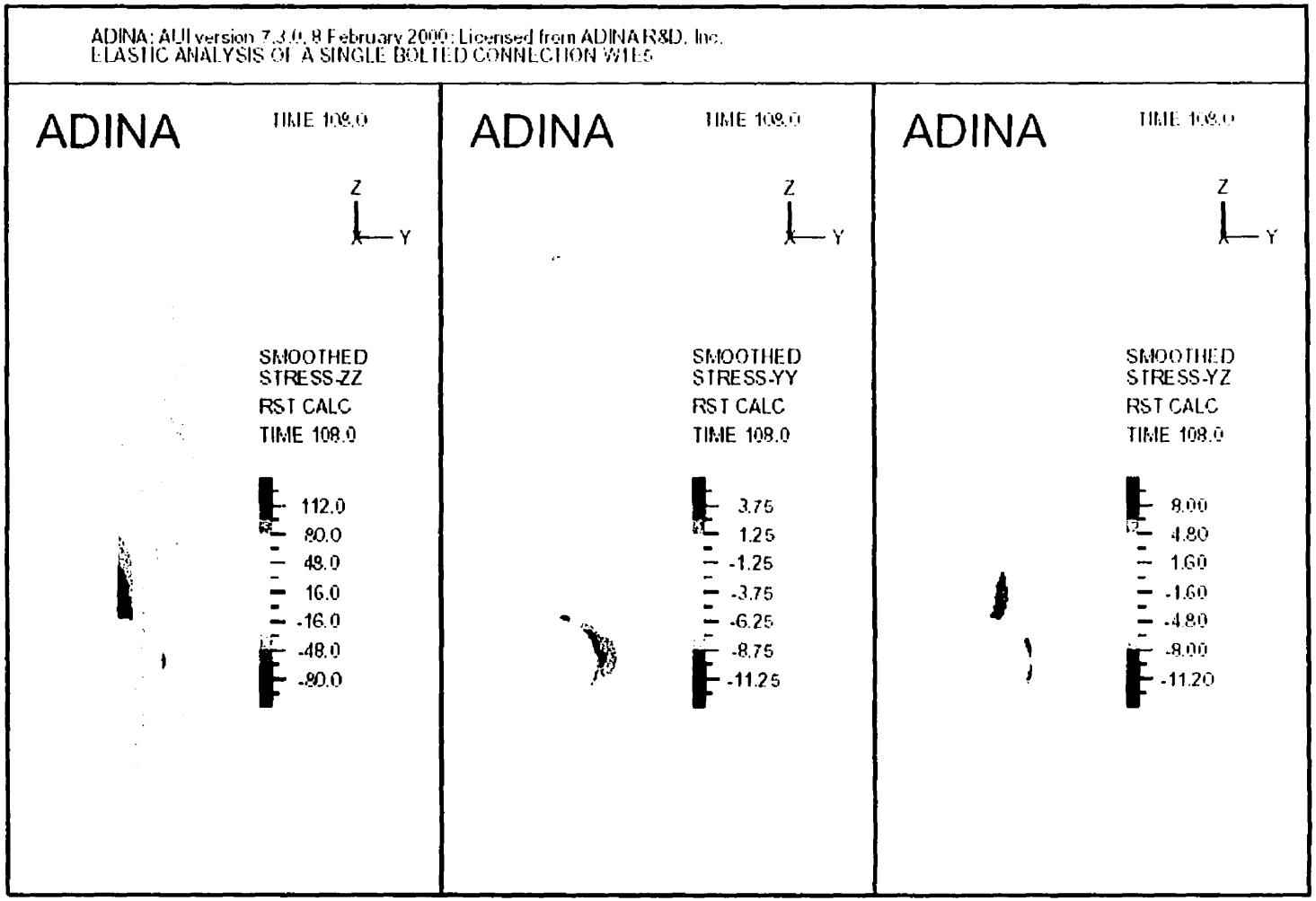

Figure 5. 15a Elastic stress distribution in a one-bolt connection W1E5

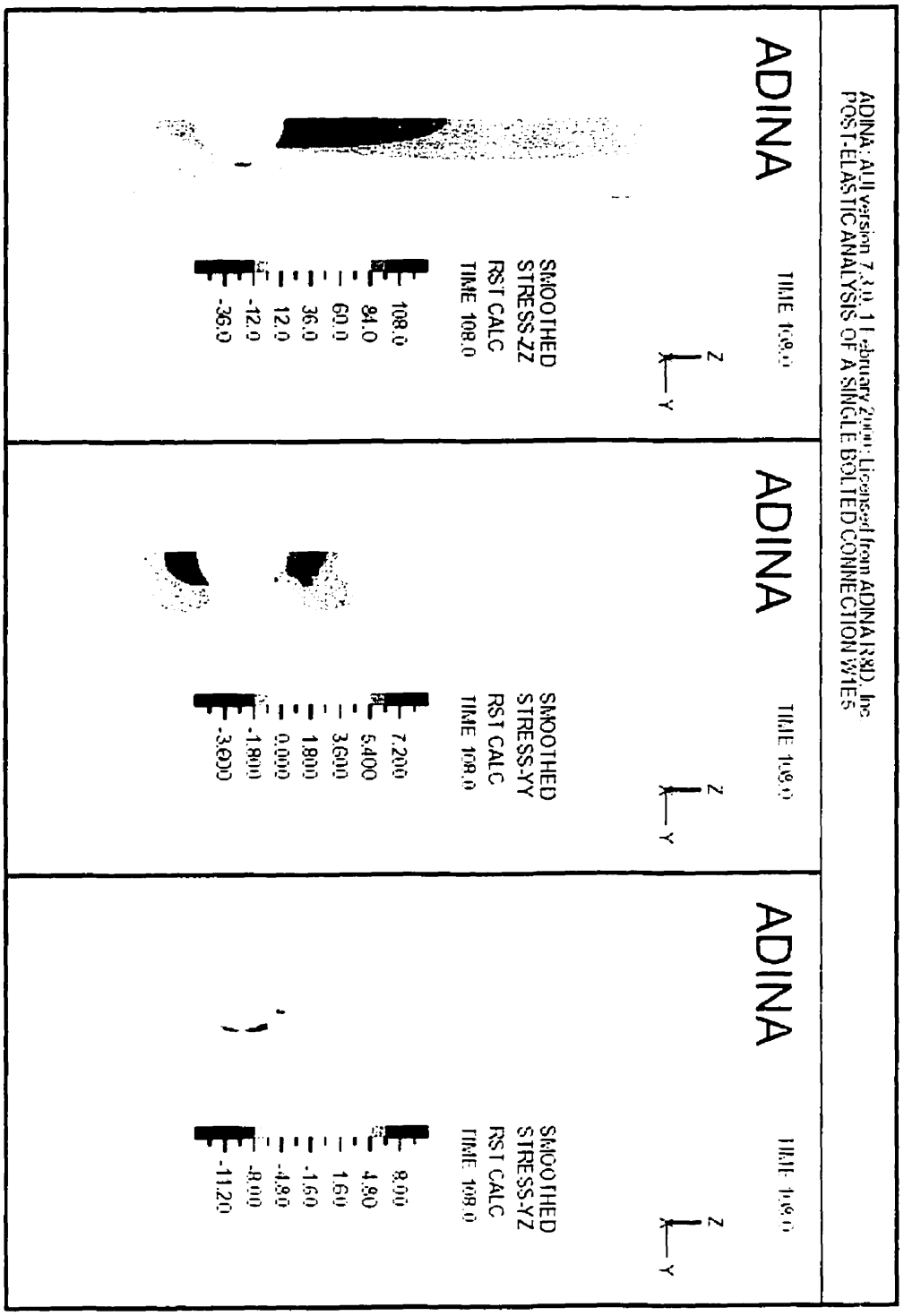

Figure 5. 15b Elasto-plastic stress distribution in a one-bolt connection W1E5

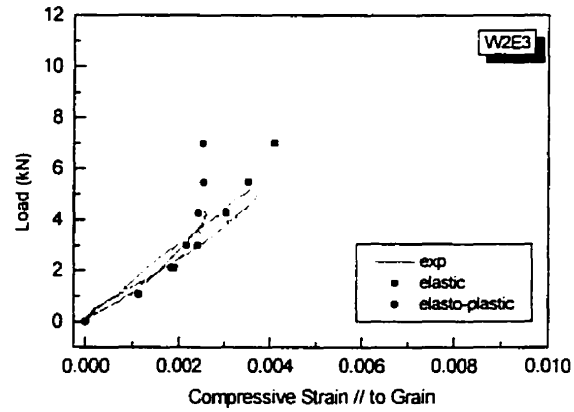

(a)

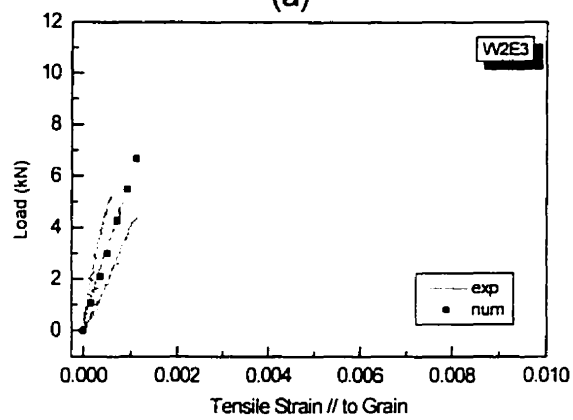

(b)

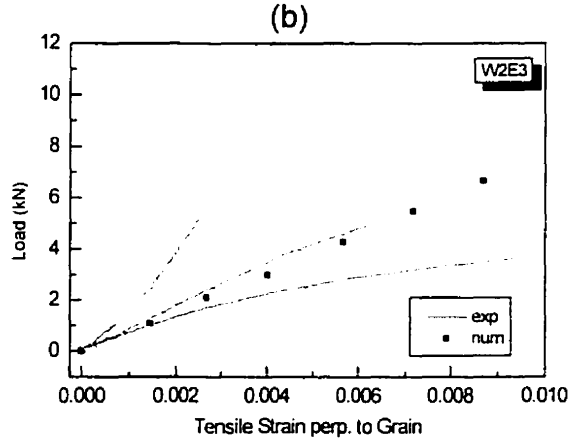

(c)

Figure 5. 16 Comparison between Numerical and Experimental Strains for W2E3

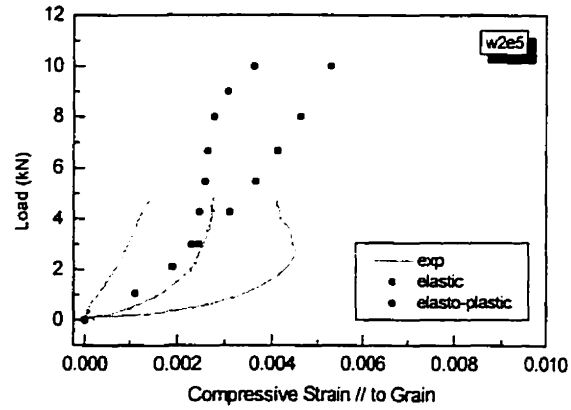

(a)

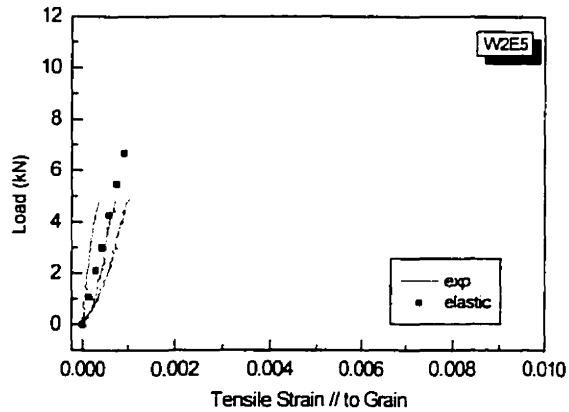

(b)

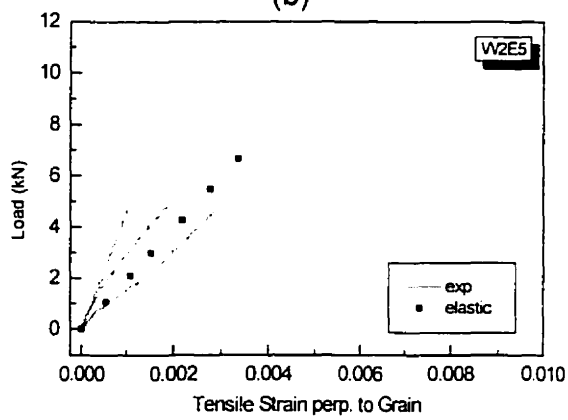

(c)

Figure 5. 17 Comparison between Numerical and Experimental Strains for W2E5

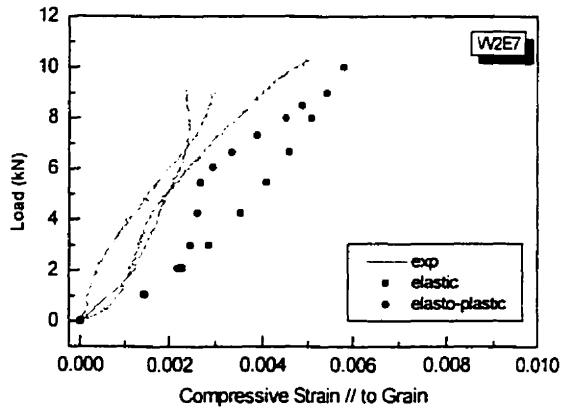

(a)

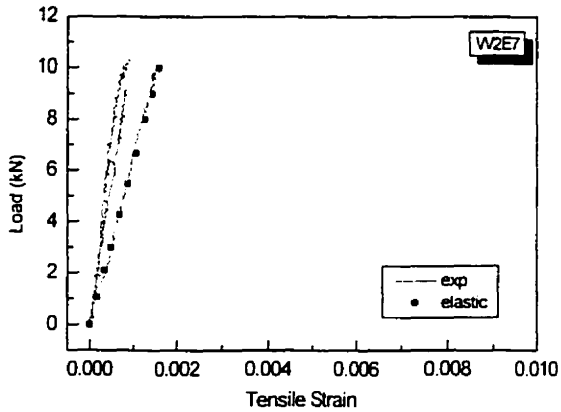

(b)

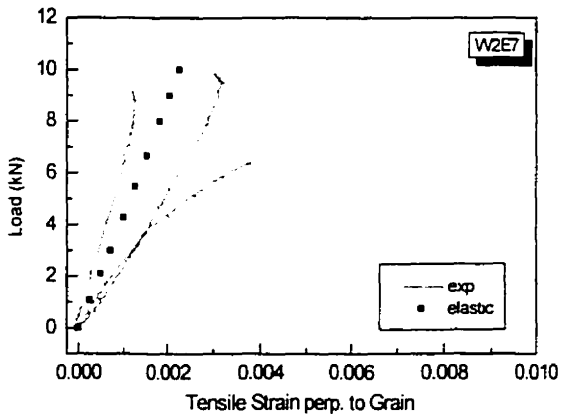

(c)

Figure 5. 18 Comparison between Numerical and Experimental Strains for W2E7

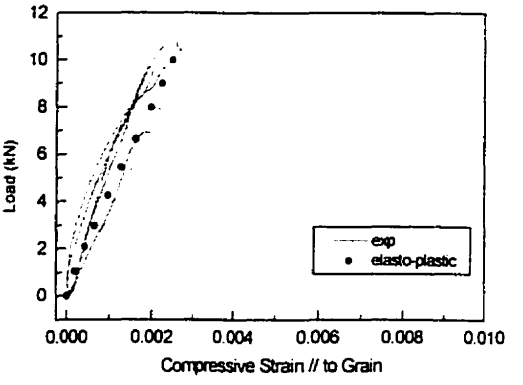

(a)

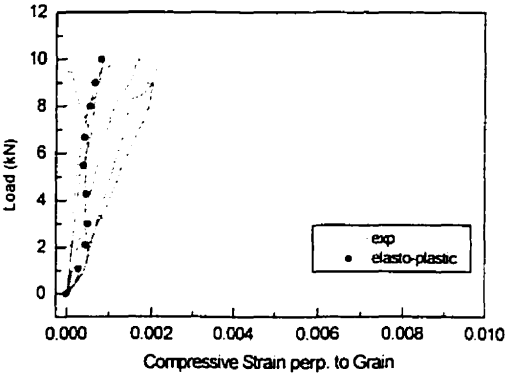

(b)

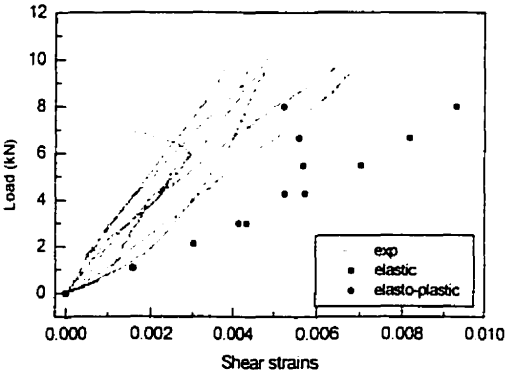

(c)

Figure 5. 19 Comparison between Numerical and Experimental Strains using Strain Rosettes for W2E5

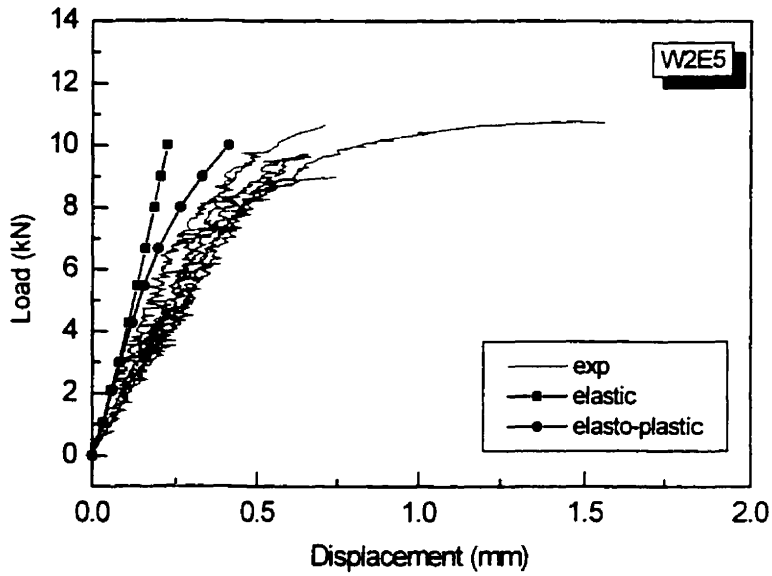

Figure 5. 20 Comparison between Numerical and Experimental Load vs. Deformation Curves for W2E5

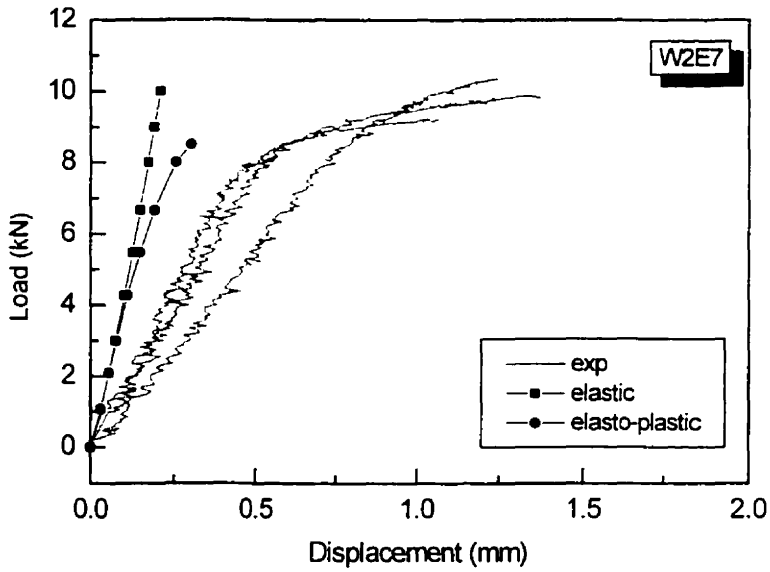

Figure 5. 21 Comparison between Numerical and Experimental Load vs. Deformation Curves for W2E7

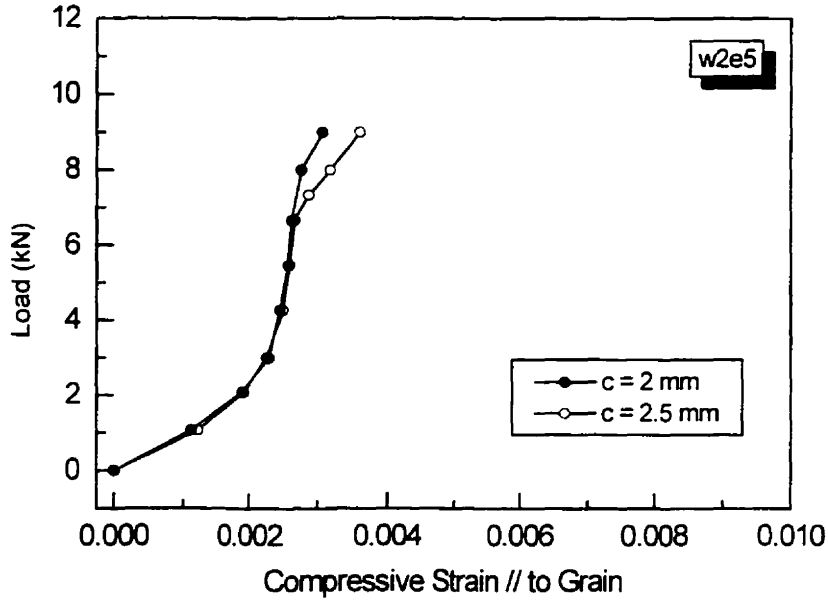

Figure 5. 22a Effect of Oversizing the Hole on Compressive Strains at Gage Location # 1 for W2E5

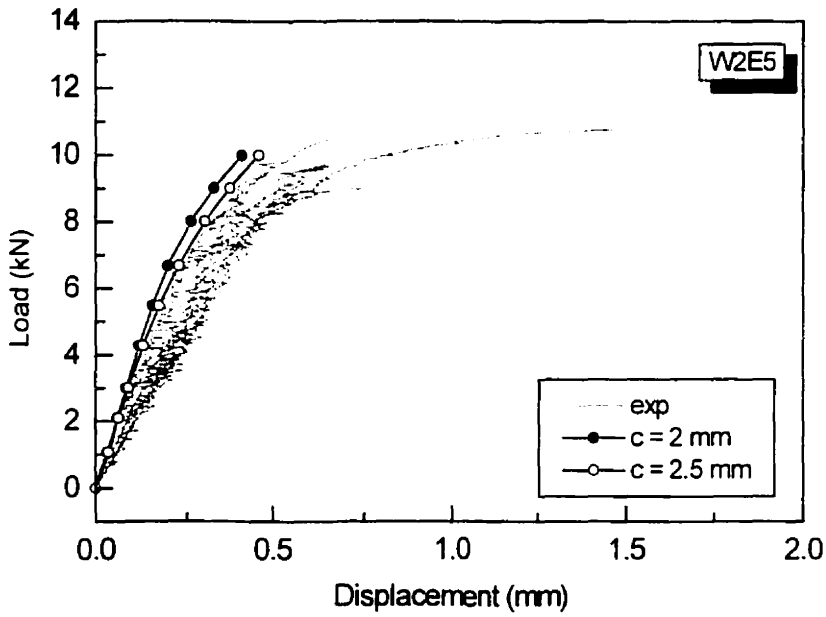

Figure 5.22b Effect of Oversizing the Hole on Load vs. Displacement Curve for W2E5

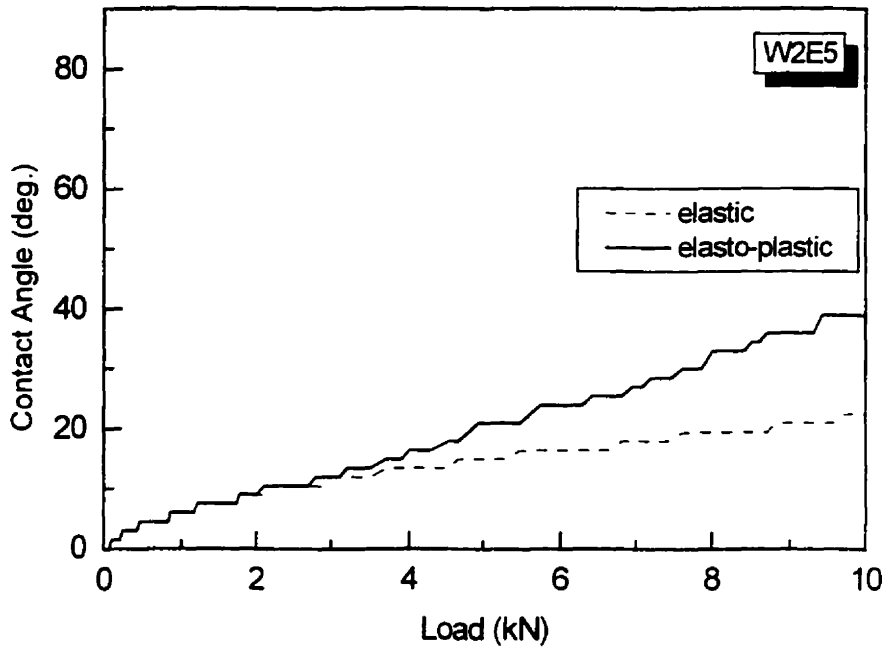

Figure 5. 23 Contact Angle as a Function of Load on the Hole Boundary

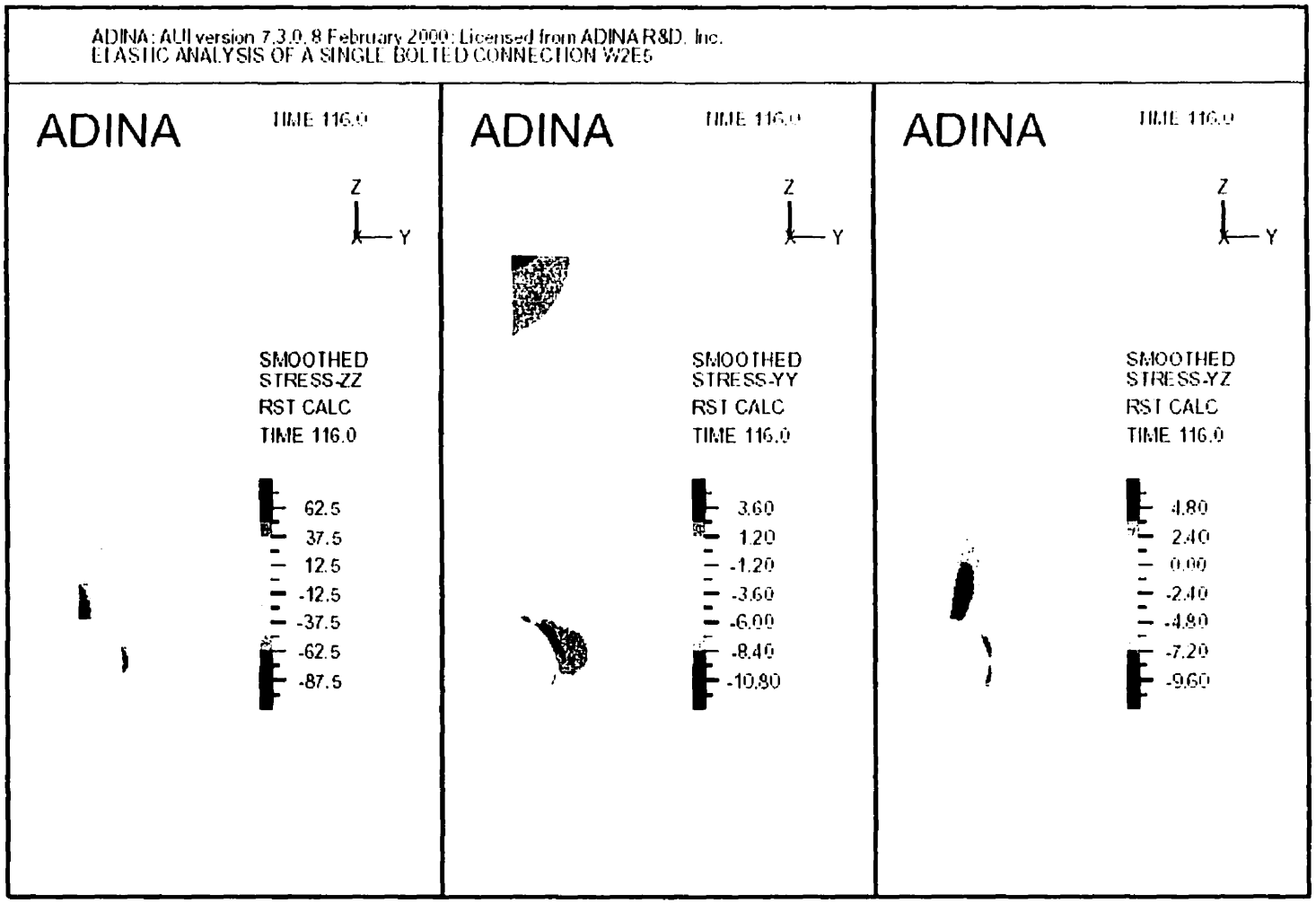

Figure 5. 24a Elastic stress distribution in a one-bolt connection W2E5

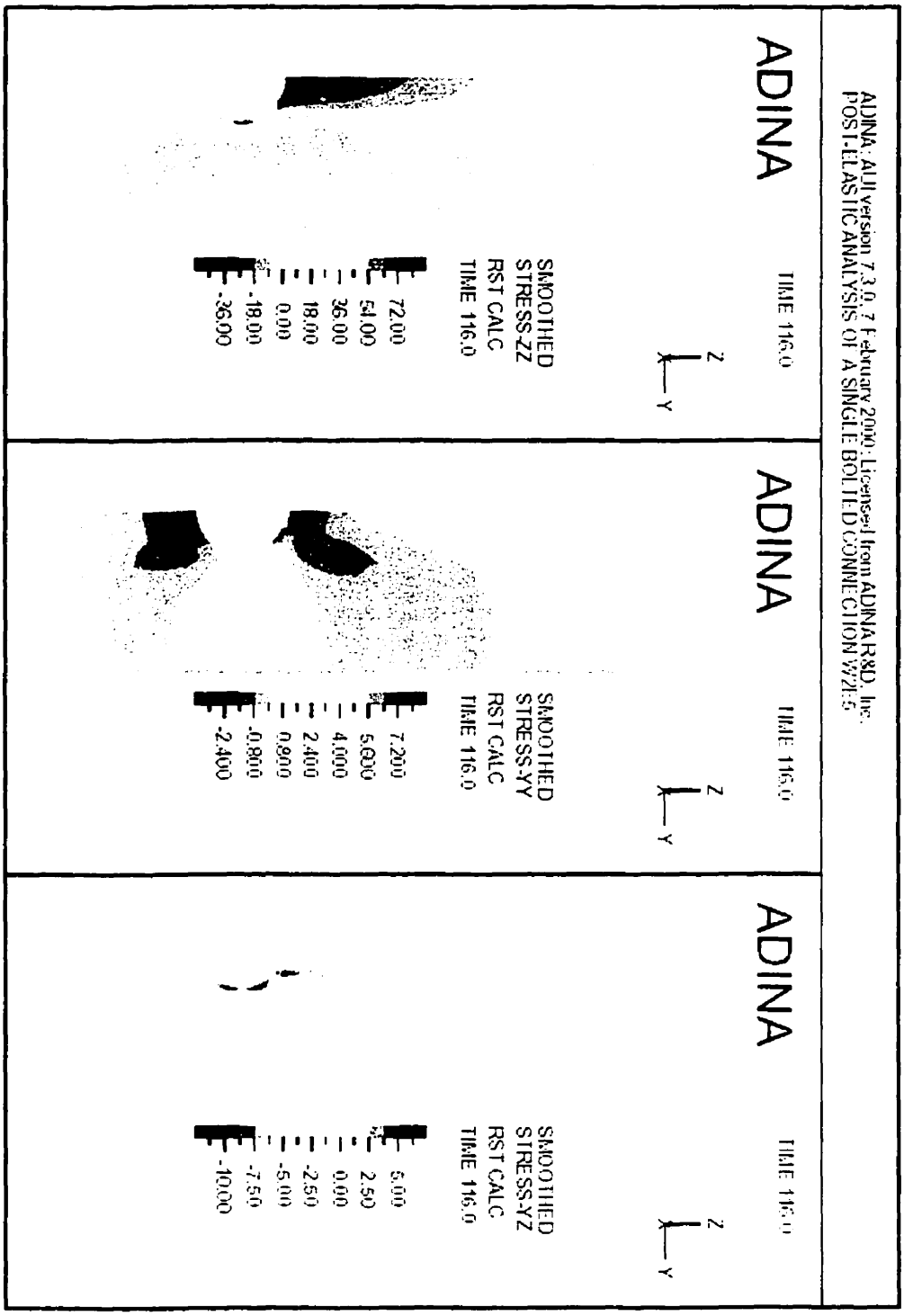

Figure 5.24b Elasto-plastic stress distribution in a one-bolt connection W2E5

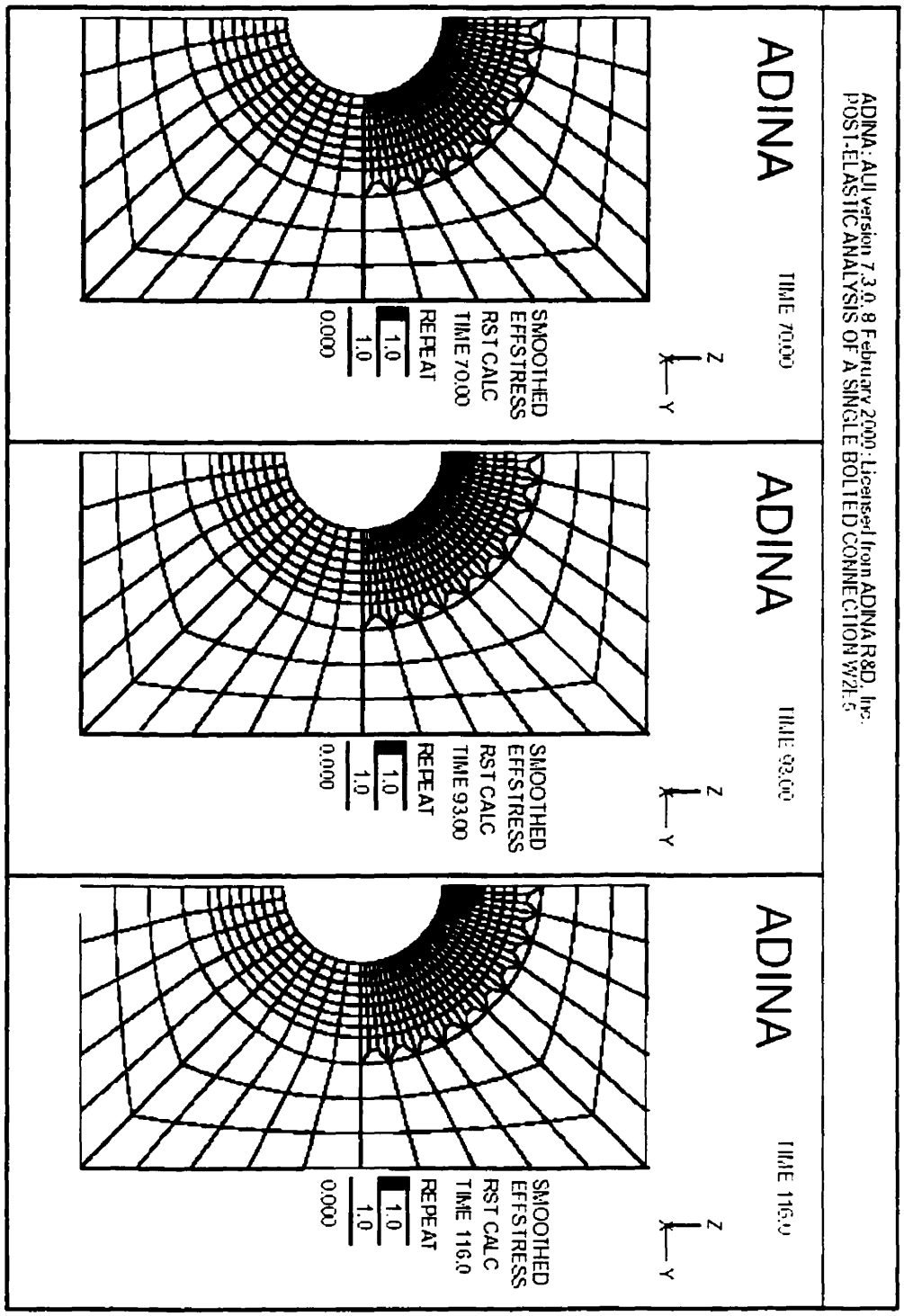

Figure 5. 25 pread of plasticity in a one-bolt connection W2E5

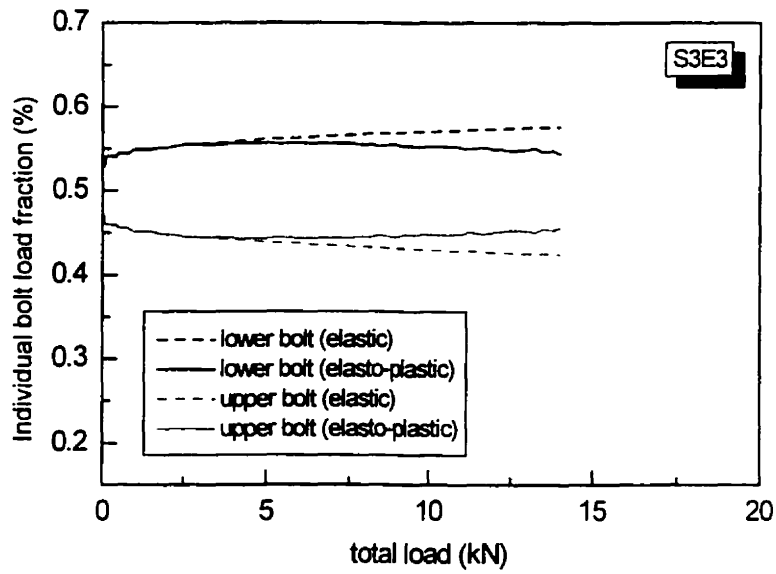

Figure 5. 26 Load Sharing among Two Bolts in a Row for S3E3

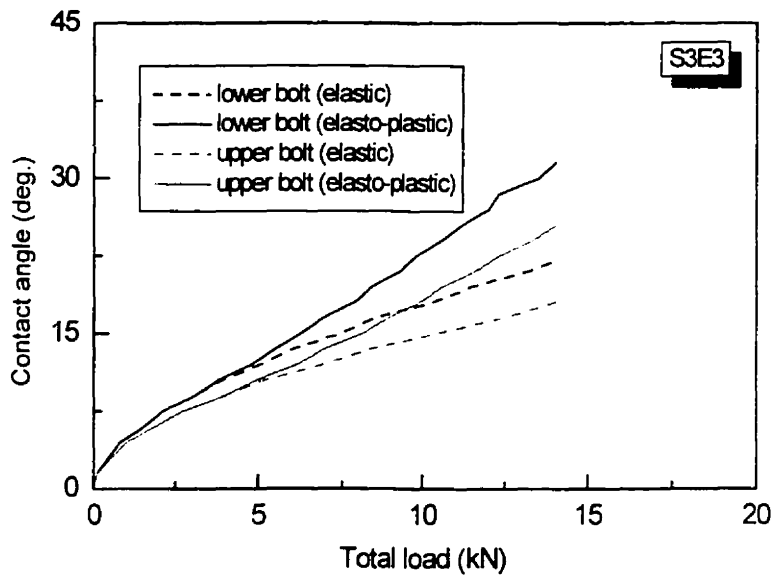

Figure 5. 27 Contact Angles as a Function of Load on Each Bolt for S3E3

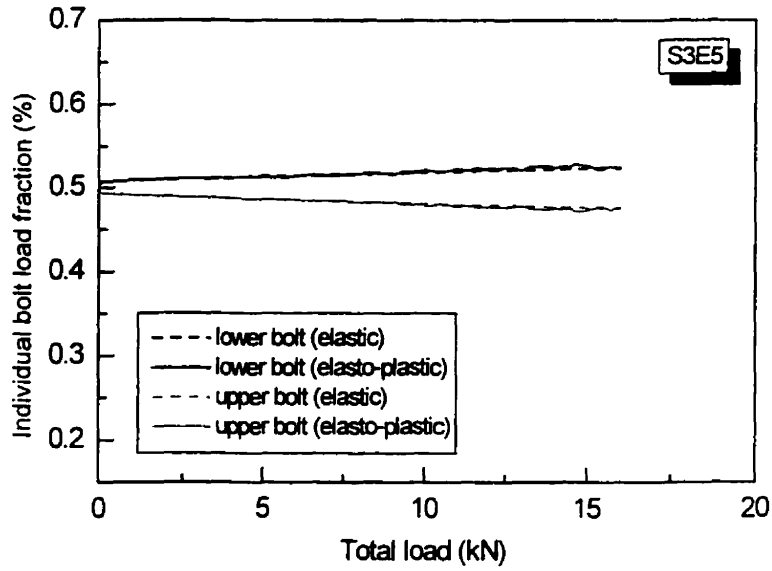

Figure 5. 28 Load Sharing among Two Bolts in a Row for S3E5

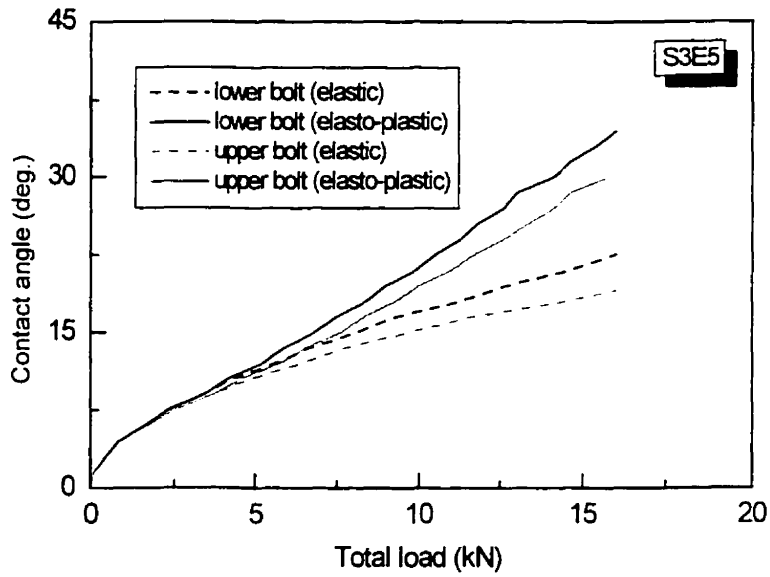

Figure 5. 29 Contact Angles as a Function of Load on Each Bolt for S3E5

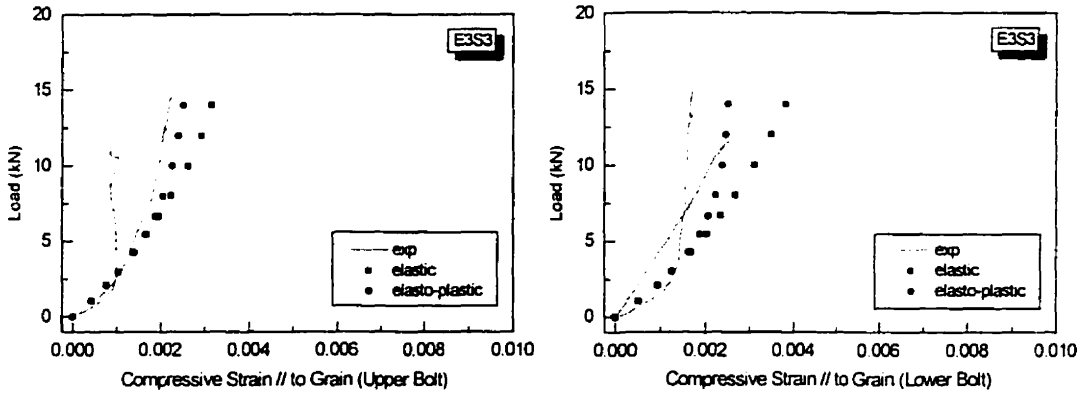

(a)

(b)

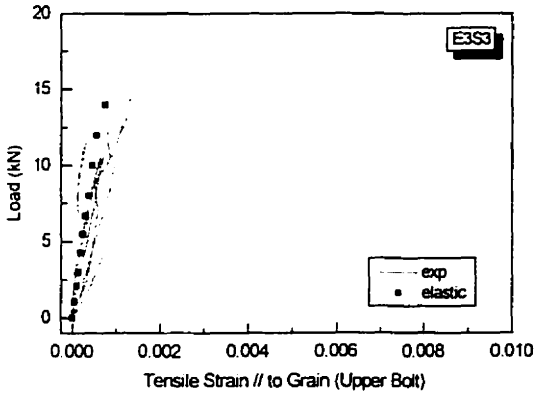

(c)

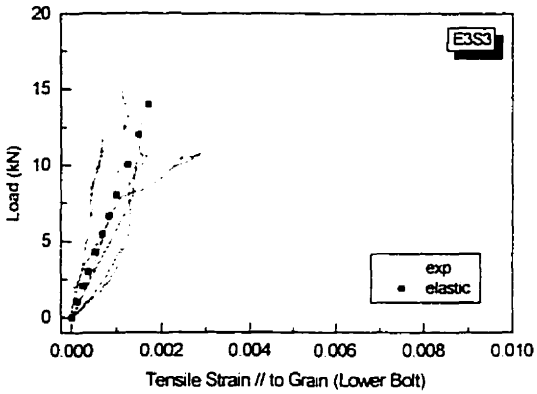

(d)

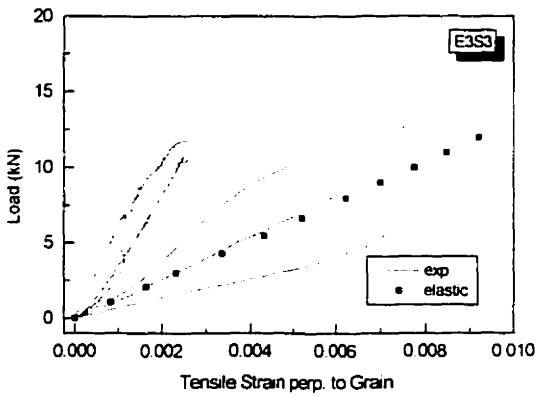

(e)

Figure 5. 30 Comparison between Numerical and Experimental Strains for S3E3

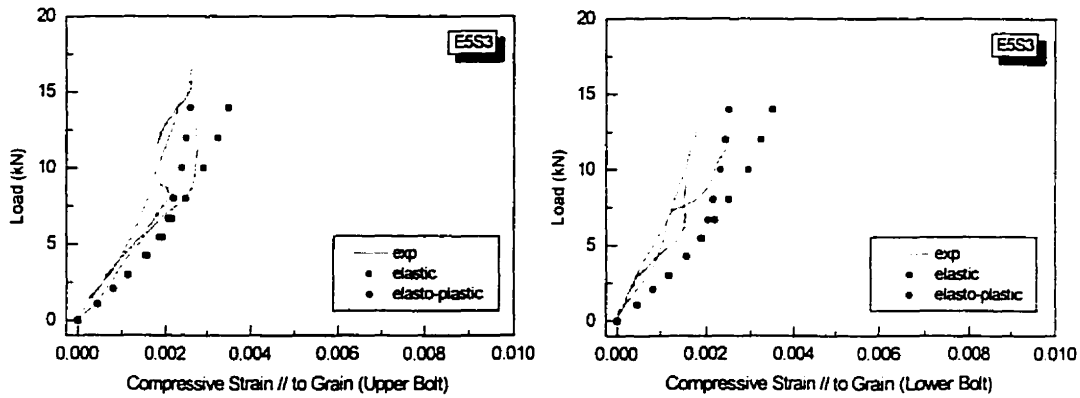

(a)

(b)

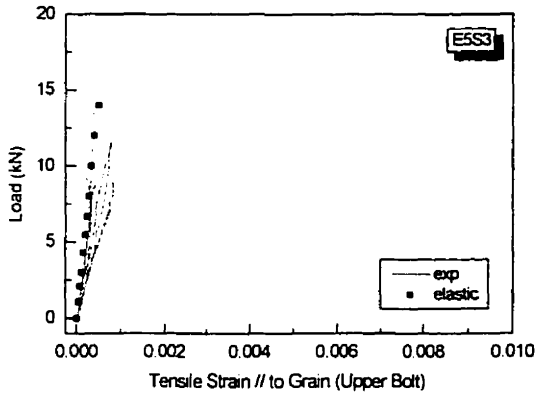

(c)

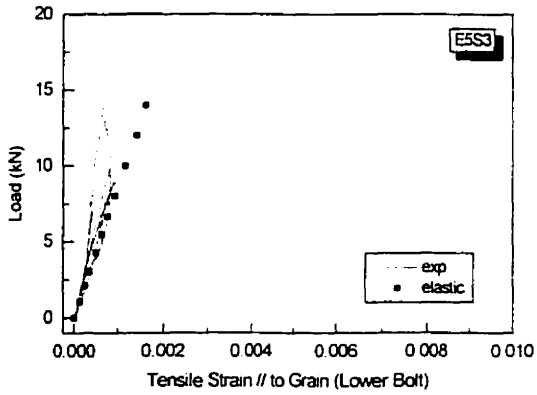

(d)

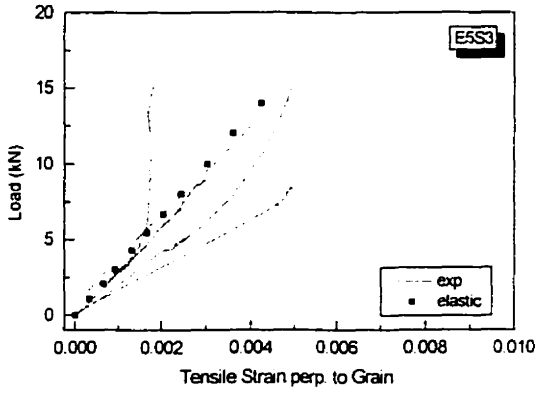

(e)

Figure 5. 31 Comparison between Numerical and Experimental Strains for S3E5

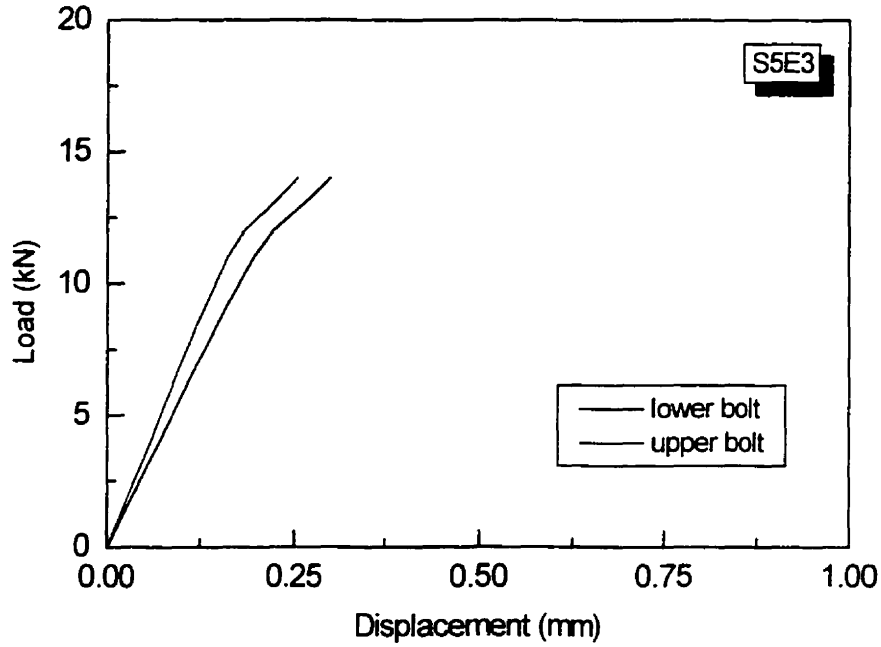

Figure 5. 32 Predicted Load vs. Deformation Curves for the Double-Bolted Connection S5E3

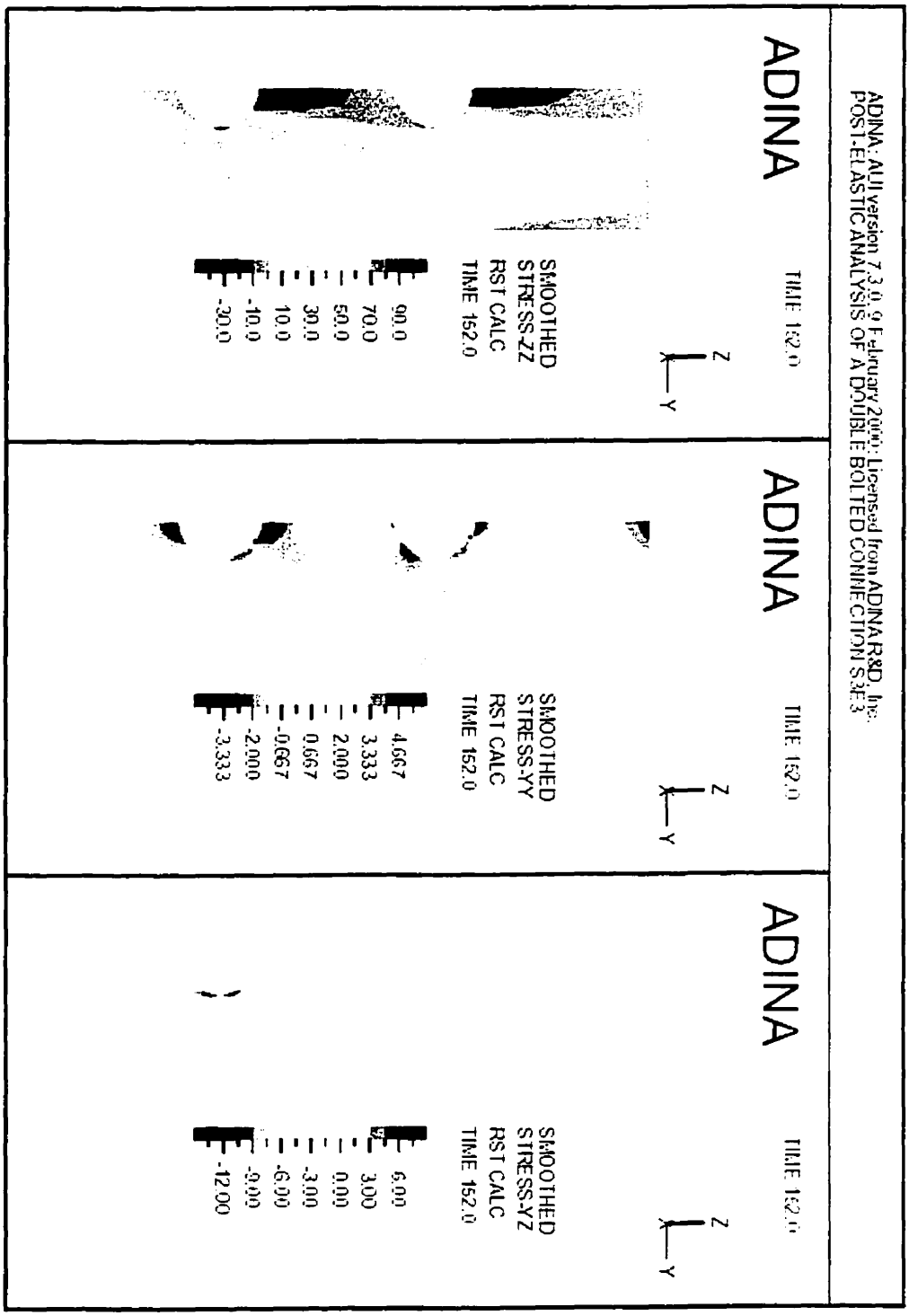

Figure 5. 33 Elasto-plastic stress distribution in a two-bolt connection S3E3

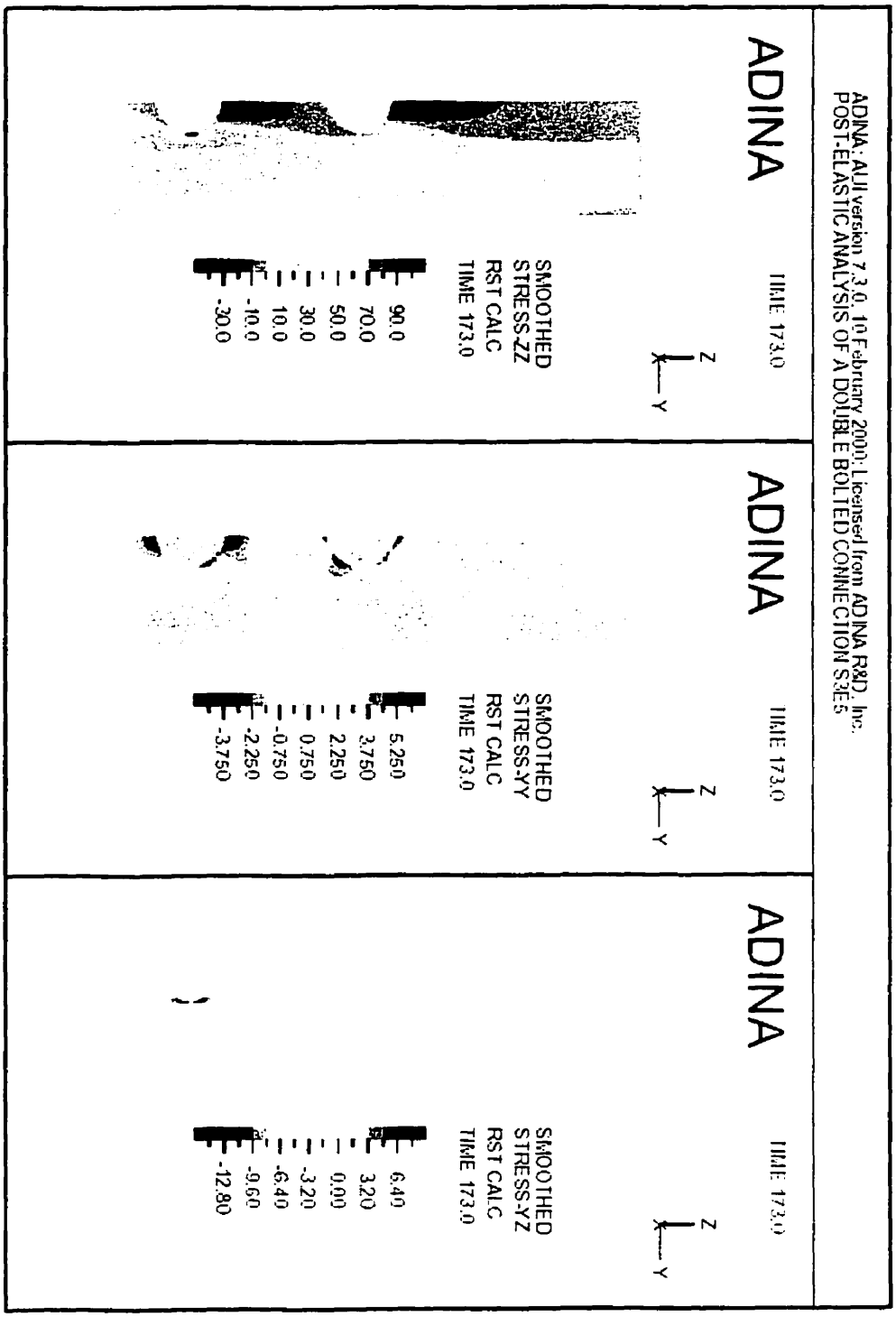

Figure 5. 34 Elasto-plastic stress distribution in a two-bolt connection S3E5

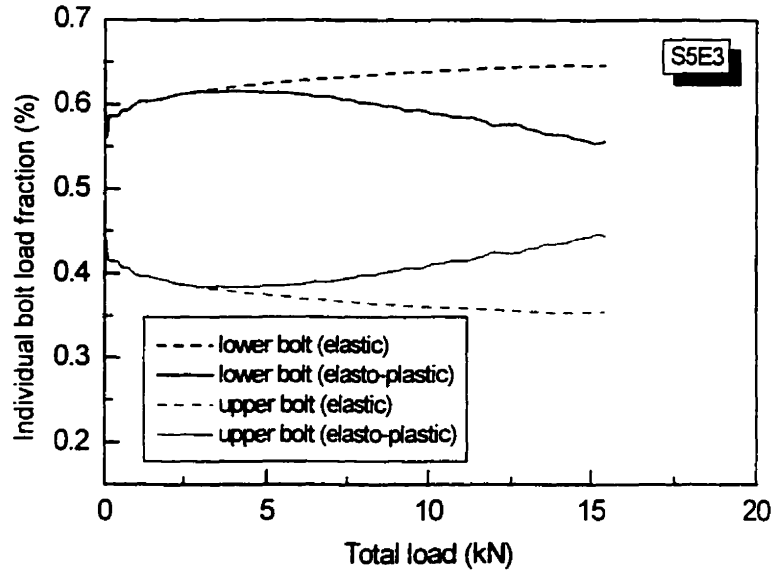

Figure 5. 35 Load Sharing among Two Bolts in a Row for S5E3

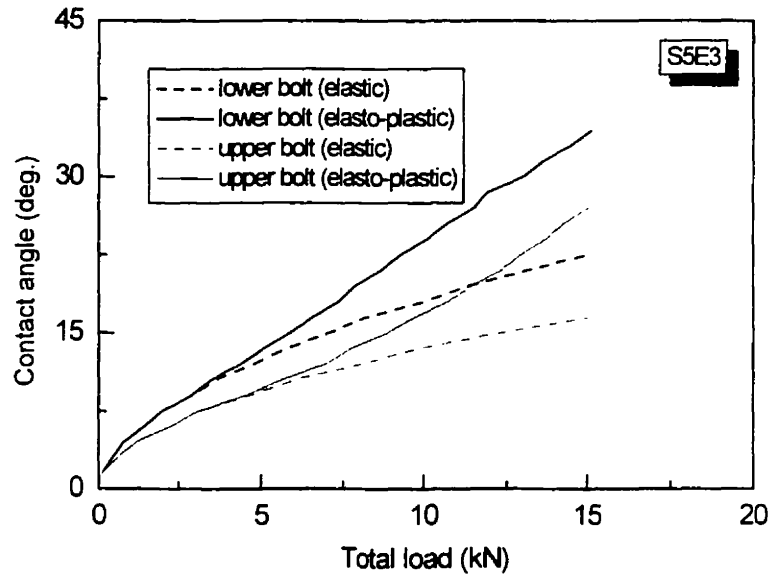

Figure 5. 36 Contact Angles as a Function of Load on Each Bolt for S5E3

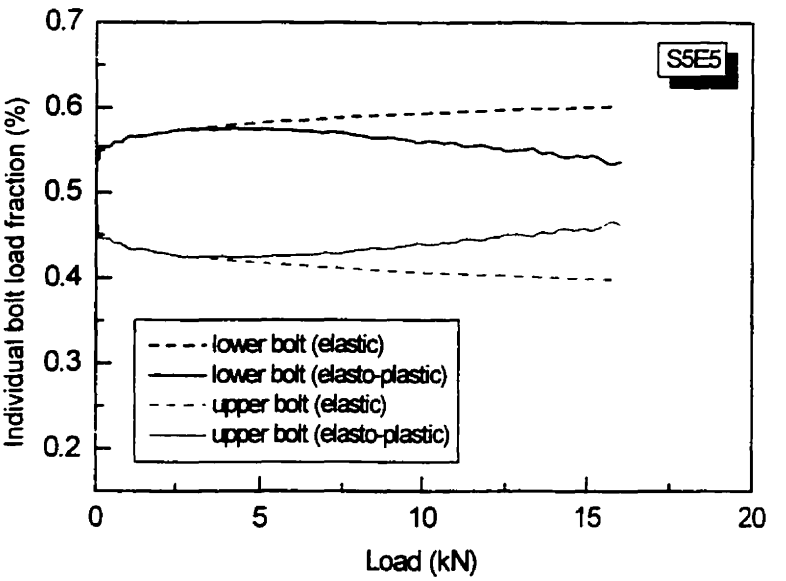

Figure 5. 37 Load Sharing among Two Bolts in a Row for S5E5

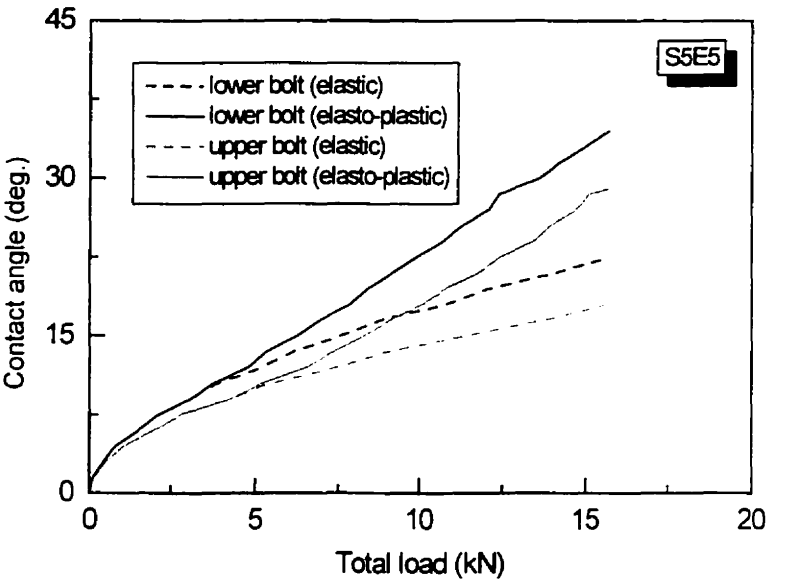

Figure 5. 38 Contact Angles as a Function of Load on Each Bolt for S5E5

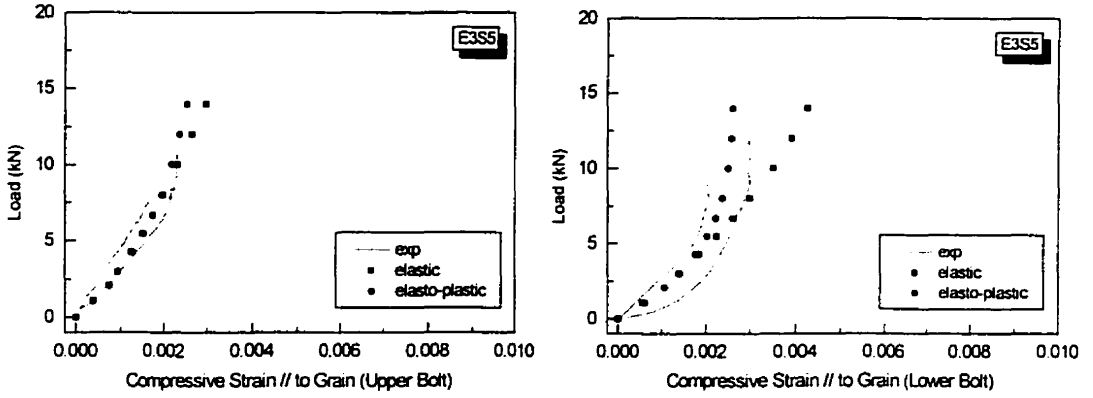

(a)

(b)

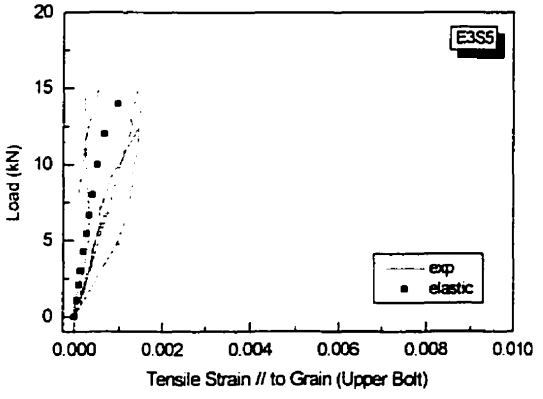

(c)

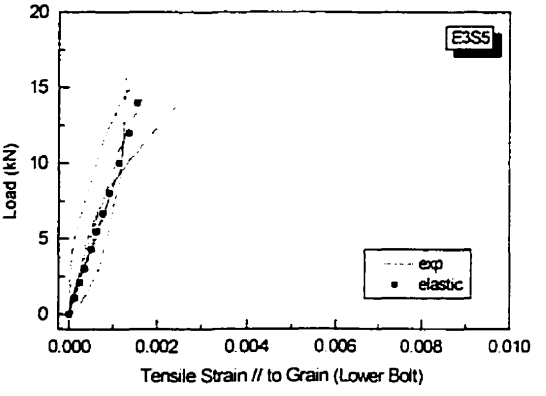

(d)

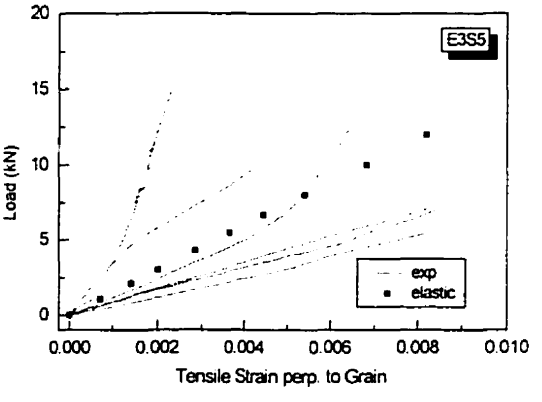

(e)

Figure 5. 39 Comparison between Numerical and Experimental Strains for S5E3

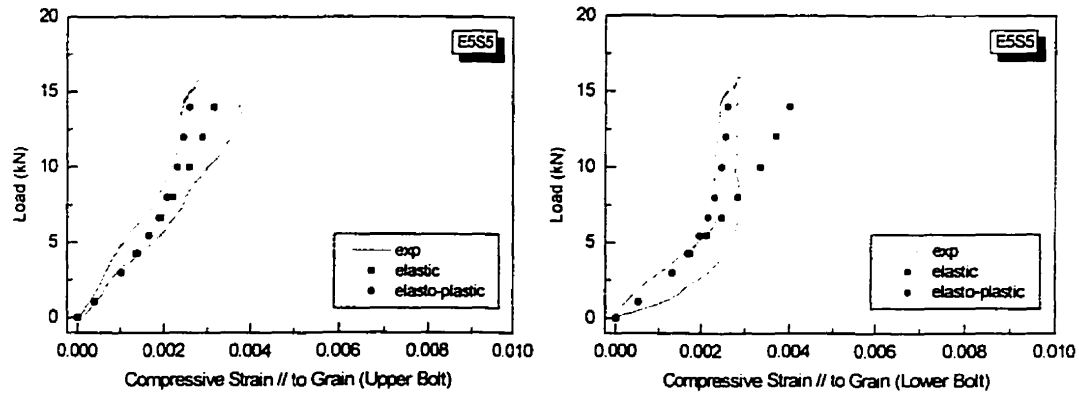

(a)

(b)

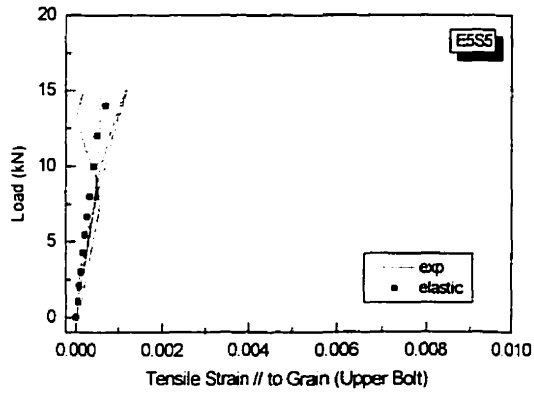

(c)

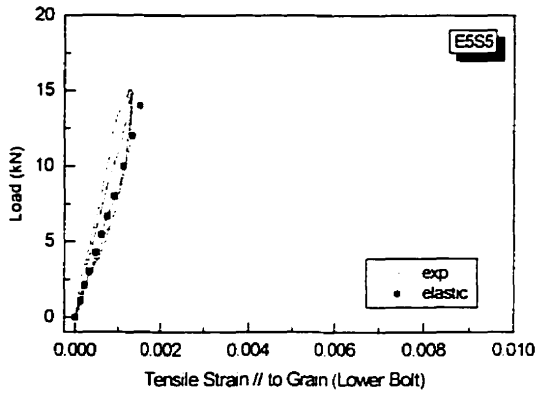

(d)

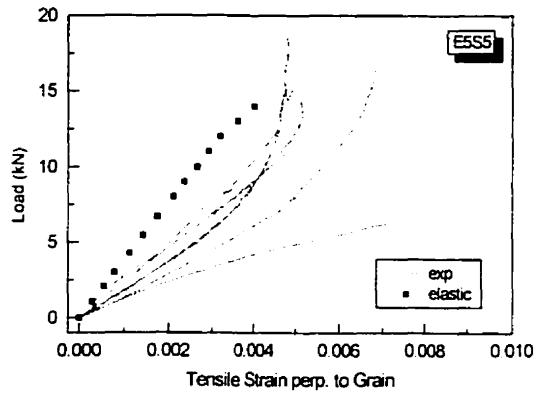

(e)

Figure 5. 40 Comparison between Numerical and Experimental Strains for S5E5

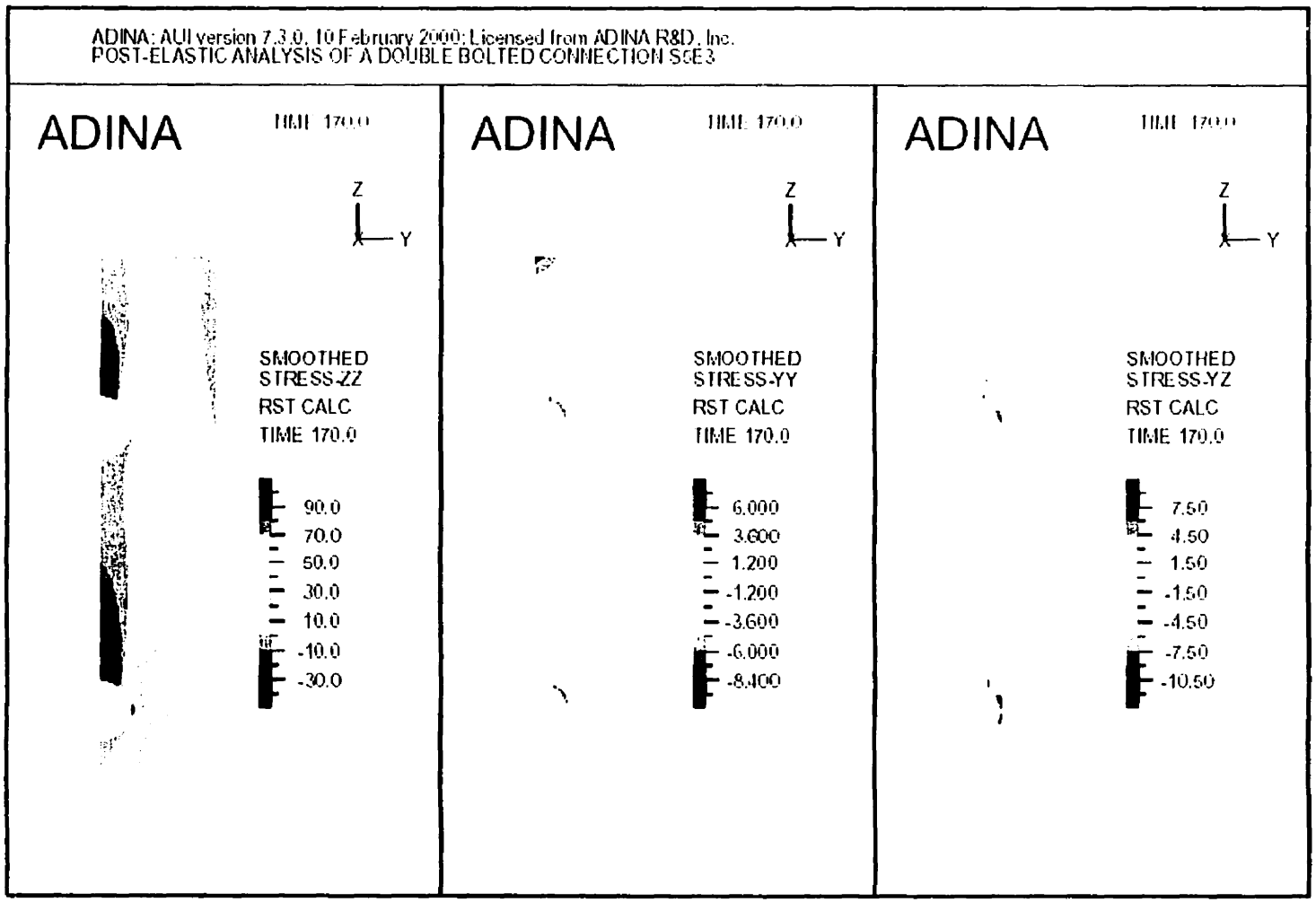

Figure 5. 41 Elasto-plastic stress distribution in a two-bolt connection S5E3

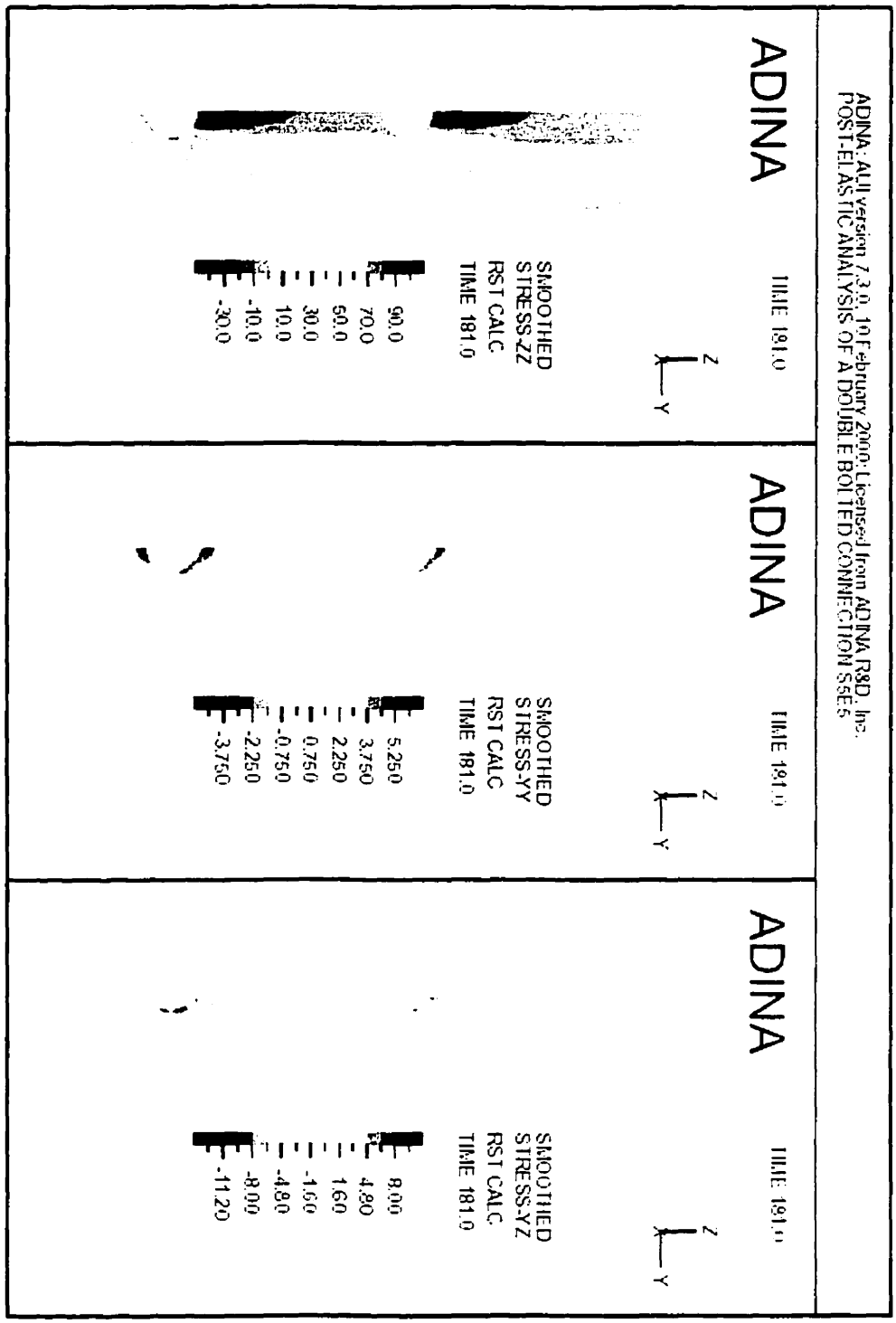

Figure 5. 42 Elasto-plastic stress distribution in a two-bolt connection S5E5

CHAPTER 6

CONCLUSION

6.1 SUMMARY

The use of glulam timber in many structural applications often involves the use of bolted connections. To date, there is no well-established design rule for predicting the brittle failure of such mechanical joints with relatively low member thickness to bolt diameter ratio. The fully plastic behavior model (so-called European Yield Model) is a reliable means of predicting the ductile failure capacity of connections using slender bolts. However, understanding the behavior of bolted connections in timber using stocky bolts (larger diameter bolts) is a matter of predicting stress concentrations that strongly influence the deformation and ultimately define the brittle failure mechanism. In the present study, the post-elastic behavior of one- and two-bolt timber connections is analyzed where stocky bolts load glued-laminated timber parallel to grain.

A two-dimensional finite element model is developed using ADINA software for single- and double-bolt connections under monotonic loading. The increased sliding contact between the bolts and the center member is modeled using the Lagrange

Multipliers algorithm. The compatibility of surface displacements is enforced at the contactor surface, being the wood member. The Coulomb frictional conditions are imposed over the contact segments with a coefficient of friction of 0.7. Contact causes a high bi-axial compressive exceeding the elastic regime in a zone(s) beneath the bolt(s). A plasticity-based compressive material response is proposed to model wood as elasto-plastic orthotropic according to the Hill yield criterion in regions of bi-axial compression. Linear elastic orthotropic material response is applied otherwise. The model is implemented in the finite element code to carry out the analysis of bolted connections. The required input material properties including strengths and stiffnesses in different directions are obtained from tests on clear glulam specimens. A series of tensile tests on glulam timber connections under short-term static loading undertaken at the Structure Laboratory of the Royal Military College of Canada in Kingston is used to validate numerical simulations of local and global deformations. To achieve this, strain gages, strain rosettes and LVDT's are mounted on a wood center member with varied end distance, edge distance and spacing between the bolts for single- and double-bolt connections to obtain measurements of strains and displacement.

The performance of the program with the elastic orthotropic material model and the effectiveness of the elasto-plastic orthotropic model are first verified with experimental data from literature. Thereafter, numerical simulations using the finite element model of the connection with the proposed elasto-plastic compressive material model are compared with experimental measurements of global deformation of connections and strains near stress concentrations. The reasonable agreement

between numerical predictions and experimental results illustrate the model's capability to trace the inelastic deformations locally and globally. Bearing of the material immediately adjacent to the contact points is causing nonlinear global deformation of the connection. This post-elastic behavior is more pronounced as the end distance is increased. Contour plots of stress distributions have revealed that excessive shear stresses and tensile stresses perpendicular to grain are developed along the sides of the contact zone. These are believed to cause the predominant brittle failure mode of the joints as observed in experiments, especially with members having larger edge distance. For two-bolt joint, numerical predictions of load proportions are a function of load even at low load levels. Redistribution of the load results from the inelastic deformation of wood. Forces are still unevenly shared as the load approaches the ultimate capacity. The disparity of load fractions decreases if the spacing is decreased or the end distance is increased. The load-carrying capacity of a double-bolt connection can be estimated by multiplying the capacity of a single-bolt connection by the inverse of the highest load fraction carried by either bolt. Better predictions are obtained with the proposed elasto-plastic material model than with the EYM or the linear elastic model.

6.2 CONCLUDING REMARKS

This study is a step further in understanding the behavior of bolted connections in timber failing in a brittle fashion. Numerical and experimental investigations conducted point to the fact that the behavior of single- and double-bolted connections with

relatively low member thickness-to-bolt diameter ratio is governed by inelastic deformation of wood beneath the bolt at low load levels. With the proposed constitutive elasto-plastic compressive material model, the nonlinear finite element model of the connection could replicate local and global experimental deformations with reasonable accuracy. The predicted failure mode caused by shear and tension perpendicular to grain along the sides of a frictional contact zone is consistent with experimental observations. Furthermore, the unequal load sharing among the bolts for a double-bolt connection was verified. The estimated joint capacity is bounded by the EYM and the linear elastic model. To this end, the established model provides a reliable basis for further detailed brittle failure modeling and more complete three-dimensional models of timber bolted connections.

6.3 FURTHER AREAS OF RESEARCH

The following recommendations should be considered in order to extend and improve the present study:

- The finite element model can be applied to connections in other species of wood or other orthotropic materials, such as some classes of advanced man-made composite materials for which bearing is an issue.
- The finite element model can be extended to include other arrangements of multiple bolts in a series or in a row, to determine the load carried by each bolt and estimate the joint strength.

- Modeling the brittle failure of bolted connections to predict the single joint capacity can be achieved by applying an average stress criterion of combined shear and tension perpendicular to grain.
- The present finite element model is developed for a bolted connection in 2-D and 3-D, thus it can be applied to members using nails or slender bolts and exhibiting brittle failures because of sub-optimum spacing between the fasteners.
- Modeling the behavior of the connection under other types of loading, such as compressive loading, cyclic loading and loading perpendicular to grain.
- Due to the wide variability of the material properties, a stochastic model is to be sought to determine the ultimate capacity of the connection.

ORIGINALITY AND CONTRIBUTION TO KNOWLEDGE

The present research contains the following contributions to knowledge:

- A plasticity-based compressive constitutive material model is developed to predict the post-elastic deformation caused by wood crushing in the contact zones of bolted connections.
- The proposed material model is incorporated in a nonlinear finite element model developed to predict the post-elastic deformations of single- and double-bolt connections in timber.
- An extensive experimental program is undertaken to measure local and global deformations of connections in glulam tested under static tension up to failure.
- The finite element program gives reasonable agreement as compared to experimental data. Hence, it provides a reliable basis for predicting the post-elastic behavior of bolted connections, which is governed by the inelastic deformation of wood at low load levels.
- The predominant shear-out failure observed in the experiments is caused by combined shear and tensile stresses perpendicular to grain along the sides of a sliding contact zone.
- Variations of load proportions as a function of load are determined in a two-bolt connection and shown to be unequal at the average experimental failure load.
- The double-bolt connection capacity is estimated based on the load sharing and found to be bounded by the European Yield Model and the linear elastic model.

REFERENCES

ADINA R&D Inc., (1995) "Theory and Modeling Guide", Report ARS 95-8, Watertown, MA.

ADINA R&D Inc., (1997) "ADINA User Interface Commend Reference Manual, Vol. 1: ADINA Model Definition", Report ARS 95-8, Watertown, MA.

ADINA R&D Inc., (1997) "ADINA User Interface Commend Reference Manual, Vol. 4: Display Processing", Report ARS 95-8, Watertown, MA.

Agarwal, B. L., (1980). "Static Strength Prediction of Bolted Joints in Composite Materials", *AIAA Journal*, 18(11), 1371-1375.

American Society of Testing and Materials, *Standard Methods of Testing on Small Clear Specimens of Timber, ASTM D143-83*, 1984.

American Society of Testing and Materials, *Standard Methods of Testing Bolted Connections, ASTM D1761-83*, 1984.

Arnold, W. S., Marshall, I. H., and Wood, J., (1990). "Optimum Design Considerations for Mechanically Fastened Composite Joints", *Composite Structures*, 16, 85-101.

Bathe, K.J. and Chaudhary A. "A Solution Method for Planar and Axisymmetric Contact Problems", *International Journal for Numerical Methods in Engineering*, 21, 65-88, 1985.

Bjorhovde, R., and Suddarth, S. K. (1992) "Research Needs for Wood Connectors and Connections", *International Workshop on Wood Connectors, Proceedings of the Meeting*, Nov 9-10, Las Vegas, Forest Products Society, 1992, 147-148.

Bodig, J., and Jayne, B. A., (1982). *Mechanics of wood and Wood Composites*, Van Nostrand Reinhold, New York.

Bouchair, A. (1993). *Modélisation non Linéaire du Comportement Local des Assemblages Bois*, Ph.D. thesis, Department of Civil Engineering, Université Blaise Pascal, France.

Bouchair, A. and Vergne, A., (1995). "An Application of the Tsai Criterion as a Plastic Flow Law for Timber Bolted Joint Modelling", *Wood Science and Technology*, 30, 3-19.

Chang, F. K. and Chang, K. Y., (1987). "Post Failure Analysis of Bolted Composite Joints in Tension and Shear-out Mode of Failure", *Journal of Composite Materials*, 21, 809-833.

Chang, F. K., Scott, R. A., and Springer, G. S.,(1984). "Failure of Composite Laminates Containing Pin-loaded Holes- Method of Solution", *Journal of Composite Materials*, 18, 255-277.

Chen, W. F., and Han, D. J., (1988). *Plasticity for Structural Engineers*, Springer Verlag, New York.

Chiang, Y. J., (1983). *Design of Mechanical Joints in Composites*, Ph.D. thesis, Department of Mechanical Engineering, University of Wisconsin, Madison.

Chui, Y. H. (1991). "Simultaneous Evaluation of Bending and Shear Moduli of Wood and the Influence of Knots on these Parameters", *Wood Science and Technology*, 25, 125-134.

Cramer, C. O. (1968). "Load Distribution in Multiple-Bolt Tension Joints", *Journal of the Structural Division, ASCE*, 94(ST5), Proc. Paper 5939, 1101-1117.

CSA Canadian Standards Association, (1994). Engineering Design in Wood (Limit States Design), National Standard of Canada CAN/CSA-O86.1-M94, Rexdale, Ontario, Canada.

Daudeville, L., Davenne, L., and Yasumara, M. (1996). "Experimental and Numerical Analysis of Failure in Bolted Joints", *Proceedings of the International Wood Engineering Conference*, edited by Gopu, K.A., New Orleans, Louisiana, October 28-31, 153-159.

De Jong, T. (1977). "Stresses Around Pin-loaded Holes in Elastically Orthotropic or Isotropic Plates", *Journal of Composite Materials*, 2, 313-331.

Dinwoodie, J.M. 1989 "Wood: Nature's cellular, polymeric fibre-composite", The Institute of Metals. London, U.K).

Eisenmann, J. R. (1975). "Bolted Joint Static Strength Model for Composite Materials", *3rd Conference on Fibrous Composites in Flight vehicule Design, Part II, NASA TMX-3377*, Williamsburg, Virginia, Nov 4-6, 365-602.

Ericksson, I. (1990). "On the Bearing Strength of Bolted Graphite/Epoxy Laminates", *Journal of Composite Materials*, 24, 1247-1269.

Foliente, G. C. (1998). "Design of timber structures subjected to extreme loads", *Progress in Structural Engineering and Materials*, 1(3), 236-244.

Francois, P. (1992). *Plasticité du Bois en Compression Multiaxiale, Application à l'absorption d'énergie mécanique*, Thèse de Docteur de l'université Bordeaux I, Bordeaux, France.

Gibson, L. J., and Ashby, M. F. (1988). *Cellular Solids - Structure and Properties*, Pergamon Press, Oxford, N.Y. , 357p.

Gotoh, M. (1977). "A Theory of Plastic Anisotropy Based on a Yield Function of Fourth Order (Plane Stress State)", *International Journal of mechanics and Science*, V19, 505-520.

Green, A. E. (1945). "Stresses in Aelotropic Plates", *Proc. Roy. Soc. London*, A184, 288-301.

Griffin, O. H., Hyer, M. W., Cohen, D., Shuart, M. J., Yalamanchili, S. R., and Prasad, C. B. (1994). "Analysis of Multifastener Composite Joints", *Journal of Spacecraft and Rocket*, 31(2), 278-284.

Guan, Z. G., and Rodd, P. D. (1996) "A Simplified FE Model for Double Shear Joints Made with a Hollow Dowel Fastener", *Proceedings of the International Wood*

Engineering Conference, edited by Gopu, K.A., New Orleans, Louisiana, October 28-31, 164-171.

Guan, Z. G., and Rodd, P. D. (1999) "3-D Numerical Modeling of Moment Transmitting Joints Made with Hollow Steel Dowels", *Proceedings Pacific Timber Engineering Conference*, edited by G. B. Walford and D. J. Gaunt, Rotorua, New Zealand, March 14-18, 77-83.

Hahn, H. T., and Tsai, S. W. (1973). "Nonlinear Elastic Behavior of Unidirectional Composite Laminae", *Journal of Composite Materials*, 7, 102-118.

Harding, N. and Fawkes, A. H. R. (1984). "Bolted Timber Joints", *Pacific Timber Engineering conference,* New Zealand, 3, 872-882.

Hill, R. (1950). *The Mathematical Theory of Plasticity*, Oxford University Press, Oxford, N.Y.

Hashin, Z., Bagchi, D., and Rosen, W. (1974). "Non-Linear Behavior of Fiber Composite Laminates", NASA Contractor Report 2313.

Hassan, N. K., Mohamedien, M. A. ,Rizkalla, S. H. (1996). "Finite Element Analysis if Bolted Connections for PFRP Composites", *Composites*, Part B, 27B, 339-349.

Johansen, K. W. "Theory of Timber Connectors", *Inter. Assoc. of Bridge and Structural Engineering*, 249-262, 1949.

Jorissen, A. (1998). *Double Shear timber Connections with Dowel Type Fasteners*, Ph.D. thesis, Deft University of Technology, Netherlands.

Jurf, R. A. and Vinson, J. R. (1990). "Failure Analysis of Bolted Joints in Composite Laminates", *Composite Materials: Testing and Design, ASTM-STP 1059*, 165-190.

Kedward, K. T., and Whitney, J. M. (1990). "Design of Joints", *Delaware Composite Design Encyclopedia*, Vol 5, Technomic Publishing Company, Lancaster, Pennsylvania, 21-43.

Kharouf, N., McClure, G., and Smith, I. (1998). "Stress Analysis of Single and Double bolt Timber Connections", Proceedings World Conference on Timber Engineering, edited by J. Natterer and J. L. Sandoz, Montreux , Switzerland., August 17-20, 329-336.

Kharouf, N., Tan, D., Smith, I., and McClure, G. (1998). "Application of Fracture Theories to Predict the Strength of Bolted Timber Connections", Proceedings World Conference on Timber Engineering, edited by J. Natterer and J. L. Sandoz, Montreux , Switzerland., August 17-20, 814-816.

Kharouf, N., McClure, G., and Smith, I. (1999). "Fracture Modeling of Bolted Connections in Wood and Composites", ASCE *Journal of Materials in Civil Engineering*, 11(4), 345-352.

Lantos, G. (1969). "Load Distribution in a Row of Fasteners Subjected to Lateral Load", *Wood Science,* 1(3), 129-136.

Lekhnitskii, S. G. (1968). , *Theory of Elasticity of an Anisotropic Elastic Body*, Holden-Day, San Francisco, 404p.

Lessard, L. B, and Shokrieh, M. M (1995). "Two-dimensional Modelling of Composite Pinned-joint Failure", *Journal of Composite Materials*, 29, 671-697.

Lourenço, P. B., De Borst, R., and Rots, J. G. (1997). "A Plane Stress Softening plasticity Model For Orthotropic Materials", International Journal for Numerical Methods in Engineering, 40, 4033-4057.

Mangalgiri, P. D., and Dattaguru, B. (1986). "A large Orthotropic Plate with Misfit Pin under Arbitrary Oriented Biaxial Loading", *Computers and Structures*, 6, 271-281.

Marshall, I. H. Arnold, W. S., Wood, J., and Mously, R. F. (1989). "Observations on Bolted Connections in Composite Structures", *Composite Structures*, 13, 316-322.

Masuda, (1998). "Fracture Analysis of Bolted Joints Using the Finite Small Area Criterion", Proceedings World Conference on Timber Engineering, edited by J. Natterer and J. L. Sandoz, Montreux , Switzerland., August 17-20, 321-328.

Matthews, F. L., Wong, C. M., and Chryssafitis, S. (1982). "Stress Distribution Around a Single Bolt in Fiber-reinforced Plastic", *Composites*, 13, 316-322.

Mohammadien, A., Hassan, N. K., and Rizkalla, H. (1996). "Finite Element Analysis of Bolted Connections for PFRP Composites", *Composites*, Part B, 27B, 339-349.

Mohammad, M. A. H. (1997). *Bolted Connection Testing.* Natural Science and Engineering Research Council Collaborative Project on "Failure Mechanisms for Structural Connections in Wood-Fiber Composites", Royal Military College of Canada.

Mohammad, M. A. H., Quenneville, P., and Smith, I. (1997). "Investigation on Failure Mechanism", Proceedings of International Union of Forestry Research Organization: S5.02 Timber Enginnering Group, Copenhagen, Denmark, June 18-20, Technical University of Denmark, Lingby, Denmark, 211-226.

Moss, P. J. (1984). "Plain Stress Analysis of a Bolted Joint in Wood", *Pacific Timber Engineering Conference*, New Zealand, 3, 864-871.

Moses, M. D., Prion, H. G. L. (1999) "Bolted Connections in Structural Composite Lumber: Anisotropic Plasticity Approach", Proceedings Pacific Timber Engineering Conference, edited by G. B. Walford and D. J. Gaunt, Rotorua, New Zealand., March 14-18, 92-99.

Moses, D. (2000). *Constitutive and Analytical Models for Structural Composite Lumber with Application to Bolted Connections*, Ph.D. thesis, University of British Columbia, Vancouver.

Nahas, M. N. (1986). "Survey of Failure and Post-failure Theories of Laminated Fiber-reinforced Composites", *Journal of Composites Technology and Research*, 8, 138-153.

Naik, R. A., and Cruse, J. H. (1986). "Stress Analysis Method for a Clearance Fit Bolt Under Bearing Loads", *AIAA Journal*, 24, 1348-1353.

Nayak, G. C., and Zienkiewicz, O. C. (1972). "Elasto-Plastic Stress Analysis: A Generalization for Various Constitutive Relations Including Strain Softening", *International Journal of Numerical Methods in Engineering*, 15, 113-135.

Patton-Mallory, M., Pellicane, P. J., and Smith, I. W. (1997). "Modelling Bolted Connections in Wood: Review", *Journal of Structural Engineering*, 123, No.8, 1054-1062.

Patton-Mallory, M., Pellicane, P. J., and Smith, I. W. (1997). "Nonlinear Material Models For Analysis of Bolted Wood Connections", *Journal of Structural Engineering*, 123, No.8, 1063-1070.

Petit , P. H., and Waddoups M. E. (1969) "A Method of Predicting the Nonlinear Behavior of Laminated Composites", *Journal of Composite Materials*, 3, 2-99.

Rahman, M. U. (1981). *Stress and Strength Analysis of Double-bolted Mechanical Joints in Orthotropic Materials*, Ph.D. thesis, Department of Mechanical Engineering, University of Wisconsin, Madison, 228p.

Rahman, M. U., Chiang, Y. J., and Rowlands, R. E. (1991). "Stress and Failure Analysis of Double Bolted Joints in Douglas-Fir and Sitka-Spruce", *Wood and Fibre Science*, 23(4), 567-589.

Rahman, M. U., and Rowlands, R. E. (1993). "Finite Element Analysis of Multiple Joints in Orthotropic Plates", *Computers and Structures*, 46, 859-867.

Ramamurthy, T. S. (1989). "Recent Studies of the Behavior of Interference Fit Pins in Composite Plates", *Computers and Structures*, 13, 81-99.

Rizzi , S. A., Leewood, A. R., Doyle, J. F., and Sun, C. T. (1987) "Elastic-Plastic Analysis of Boron/Aluminum Composite under Constrained Plasticity Conditions", *Journal of Composite Materials*, 21, 734-749.

Rodd, P. D. (1973). *The Analysis of Timber Joints made with Circular Dowel Connectors*, Ph.D. thesis, University of Sussex, Brighton, UK.

Rodd, P. D. (1988). "Timber Joints made with Improved Circular Dowel Fasteners", Proceedings of the Timber Engineering Conference, Seattle,WA, Vol1, 26-37.

Rowlands, R. E., Rahaman, M. U., Wilkinson, T. L., and Chiang, Y. J. (1982). "Single and Multiple-bolted Joints in Orthotropic Materials", *Composites*, 13, 273-380.

Sandhu, R. S. (1976). "Non-Linear Behavior of Unidirectional and Angle Ply Laminates", *Journal of Aircraft*, 13(2), 104-111.

Sawaya, M. (1998). "A Critical Review on the Characterization of Wood Material Properties", Project Report for Master of Engineering, McGill University, Montreal, Canada.

Schulz, K. C., Packman, P. F., and Eisenman, J. R. (1995). "A Tension-mode Fracture Model for Bolted Joints in Laminated Composites", *Journal of Composite Materials*, 29, 37-59.

Shih, C. F., and Lee, D. (1978). "Further Developments in Anisotropic Plasticity", *Trans. ASME, J. Engrg. Mat. and Tech.*, 100, 294-302.

Shokrieh, M., and Lessard, L. B. (1996). "Effects of Material Nonlinearity on the Three-dimensional Stress State of Pin-loaded Composite Laminates", *Journal of Composite Materials*, 30(7), 839-861.

Smith, I., (1983) "Coefficient of Friction Values Applicable to Contact Surfaces Between Mild Steel Connectors Such as Bolts and Dry European White Wood", *Journal of the Institute of Wood Science*, 229-234.

Smith, I., and Hu, L. J. (1994). "Fracture Analysis of Bolted Timber Connections", *Proceedings of ASCE Structures Congress*, Atlanta, 912-917.

Smith, I., Daneff, G. , Ni, C., and Chui, Y.H. (1998) "Performance of bolted and nailed timber connections subjected to seismic loading", *In:* Special Publication 7275, Forest Products Society, Madison, WI: 6-17.

Smith, I., Tan, D., Kharouf, N., and McClure, G. (1999) "Modeling Brittle Failure in a Row of Bolts", Proceedings Pacific Timber Engineering Conference, edited by G. B. Walford and D. J. Gaunt, Rotorua, New Zealand., March 14-18, 71-76.

Soni, S. R., (1981). "Failure Analysis of Composite Laminates with a Fastener Hole", *Joining of Composite Materials ASTM STP 749*, 145-164.

Tan, D., and Smith, I., (1999). "Failure in-the-Row Model for Bolted Timber Connections ", ASCE *Journal of Structural Engineering*, 125(7), 713-718.

Vasic, S. and Smith, I., (1996) "The Brittleness of Wood in Tension Perpendicular to the Grain: Micro-mechanical Aspects", *International COST 508 Wood Mechanics Conference*, Stuttgart, Germany, May 14-16, 556-569.

Vasic, S. and Smith, I., (1998). "Bridged Crack Model of Wood Fracture: Experimental Analysis and Numerical Modeling", Proceedings World Conference on Timber Engineering, Lauzanne, Switzerland., August .

Vaziri, R. , Olsen, M. D., and Anderson, D. L. (1992). "A Plasticity-Based Constitutive Model for Fibre-Reinforced Composite Laminates", *Journal of Composite Materials*,25, 512-535.

Vaziri, R. , Olsen, M. D., and Anderson, D. L. (1992). "Finite Element Analysis of Fibrous Composite Structures: A Plasticity Approach", *Computers and Structures*,44, 103-116.

Wazczack, J. P., and Cruse, T. A. (1971). "Failure Mode and Strength Prediction of Anisotropic Bolt Bearing Specimen", *Journal of Composite Materials*, 5, 421-425.

Weibull, W. (1939). "A Statistical Theory of the Strength of Materials", *Proceedings of the Swedish Institute of Engineering Research*, 1-45.

Whang, B. (1969). "Elasto-Plastic Plates and Shells", *Proc. Symp. On Application of Finite Element Method in Civil Engineering*, Vanderbilt University Tennessee, 481-515.

Wilkinson, T. L. (1978). *Stresses in the Neighborhood of Loaded Holes in Wood with Application to Bolted Joints*, Ph.D. thesis, Department of Mechanical Engineering, University of Wisconsin, Madison.

Wilkinson, T. L., and Rowlands, R. E. (1981). "Analysis of Mechanical Joints in Wood", *Experimental Mechanics*, 21, 408-414.

Wilkinson, T. L., Rowlands, R. E., and Cook, R. D. (1981). "An Incremental Finite Element Determination of Stresses Around Loaded Holes in Wood Plates", *Computers and Structures*, 14, 123-128.

Wilkinson, T. L (1986). "Load Distribution among Bolts Parallel to Load", *Journal of the Structural Division, ASCE,* 1. 112 (4), 835-851.

Zanhn, J. J. (1991). "Design Equation for Multiple-Fastener Wood Connections", ASCE *Journal of Structural Engineering*, 117(11), 3477-3486.